Orbital Transfer Trajectory Optimization

by

James K Whiting

Submitted to the Department of Aeronautical and Astronautical Engineering
in partial fulfillment of the requirements for the degree of

Master of Science in Aeronautical and Astronautical Engineering

at the

MASSACHUSETTS INSTITUTE OF TECHNOLOGY

February 2004

Author .....
Department of Aeronautical and Astronautical Engineering
January 30, 2004

Certified by .....
Manuel Martinez-Sanchez
Professor of Aeronautics and Astronautics
Thesis Supervisor

Accepted by .....
Edward M. Greitzer
H.N. Slater Professor of Aeronautics and Astronautics
Chair, Committee on Graduate Students

Orbital Transfer Trajectory Optimization

by

James K Whiting

Submitted to the Department of Aeronautical and Astronautical Engineering
on January 30, 2004, in partial fulfillment of the
requirements for the degree of
Master of Science in Aeronautical and Astronautical Engineering

Abstract

Recent developments in astronautical engineering have led to the adoption of low thrust rocket engines for spacecraft. Optimizing the orbital transfers for low thrust engines is significantly more complicated than optimizing transfers for impulsive engines because a continuous control law must be found and long integrations are necessary to determine whether the control law works or not. Previous work on optimizing low thrust orbital transfers has led to the development of control laws for continuous thrusting including the effects of oblateness, multiple attracting bodies, eclipses, and solar cell degradation. The current work adds to this by developing control laws for optimal coasting and for variable specific impulse at constant power. The Hamiltonian method is used to develop the optimal control laws and physical interpretations are given to each term in the Hamiltonian. Application of the optimal coasting control law to transfers from LEO to GEO indicate that small amounts of coasting can significantly reduce the fuel needed for a transfer.

Thesis Supervisor: Manuel Martinez-Sanchez
Title: Professor of Aeronautics and Astronautics

Acknowledgments

Many thanks to my professor, Manuel Martinez-Sanchez, for all his help while doing this research.

Many more thanks to Meldanya Mira Blumberg, for proofreading and support while writing this thesis.

Many thanks to Kayla Jacobs and Cally Perry for proofreading.

Contents

List of Figures

List of Tables

p	semi-latus rectum
h	modified angular momentum ($\sqrt{p/\mu}$)
e_x	eccentricity in the projected x direction ($e\cos(\omega+\Omega)$)
e_y	eccentricity in the projected y direction ($e\sin(\omega+\Omega)$)
i_x	inclination in the x direction ($\tan(i/2)\cos\Omega$)
i_y	inclination in the y direction ($\tan(i/2)\sin\Omega$)
$\mathbf{X}$	orbit vector ($\mathbf{X}=[h,e_x,e_y,i_x,i_y]^T$)
f	true anomaly
Ω	longitude of the ascending node
ω	argument of perihelion
ϖ	longitude of perihelion ($\Omega+\omega$)
L	true longitude ($f+\varpi$)
δ	thrust modulation
F_{max}	maximum thrust
F	thrust
c	engine effective fuel velocity $I_{sp}g$
P	engine power
m	spacecraft mass
$\mathbf{a}$	acceleration vector ($\|a\|=\delta F/m$)
θ	in-plane thrust angle
ψ	out-of-plane thrust angle
ξ	$1+e_x\cos L+e_y\sin L=p/r$
η	$i_x\sin L-i_y\cos L=\tan i/2\sin(\omega+f)$
ϕ	$1+i_x^2+i_y^2=\sec^2 i/2$
ψ_s	The switching function $b+A/m$

The basis directions are radial, tangential, and normal to the orbital plane. This is effectively a spherical coordinate system.

Table 1: List of Symbols

Chapter 1

Introduction

Orbital dynamics is the study of how objects move under the influence of gravity at large distances. It has been studied since prehistoric times, making it one of the oldest sciences in the world. Many mathematical and physical discoveries have been made by people trying to solve problems in orbital dynamics[1], including most of Newton's development of calculus and analytical physics and Einstein's theory of general relativity. The problems of movement due to gravity alone, such as orbit determination and future position prediction, have been mostly solved over the past 400 years.

In the twentieth century, people began launching rockets into space. Spaceships opened up a whole new series of problems, because they can change their orbits. Merely predicting where a spaceship would go based on its current orbit was no longer sufficient. The problems of determining how to change from one orbit to a different orbit became interesting.

Early spacecraft used high thrust chemical rocket engines to move from one orbit to another. The thrust from these rockets is normally approximated as impulsive, because they produce a large amount of thrust for a relatively short period of time. The orbital transfers are calculated by the patched conics method, where the spacecraft is assumed to instantaneously change from one orbit to another intersecting orbit each time it fires its rockets and coasts along the orbital path between rocket firings.

The law of conservation of momentum requires a rocket to eject fuel in order to produce thrust. The force produced by the rocket is proportional to the velocity at which the fuel is ejected and to the mass flow rate of the fuel. The effective exit velocity is called c, and is proportional to the specific impulse, I_{sp}. Typical impulsive rockets have a specific impulse around 250-400s, with high performance engines having a specific impulse of up to 455s. This leads to c being in the range of $2.4 - 4.6$km/s.

Other than the thrust produced by a rocket, all the important forces in orbital dynamics are proportional to mass. This allows all the calculations to be done without considering the mass of

the rocket. The thrust is divided by the mass to determine the acceleration, which is integrated to determine the total change in velocity (the Δv). The Δv is the same for all spaceships using impulsive thrusting to conduct a given orbital maneuver. The Δv can then be used to determine the mass change of the spacecraft through the rocket equation[1]:

$$\frac{m_f}{m_i} = \mathrm{e}^{-\Delta v/c} \tag{1.1}$$

where m_f is the mass after all the thrusting is done and m_i is the mass before all the thrusting.

The smaller the quantitiy $\Delta v/c$ is, the more mass is left after the orbital maneuvers. The Δv can be reduced by finding a more efficient path between the initial and final orbit, which is the problem of orbital transfer trajectory optimization.

Another option to increase the final mass is to increase the specific impulse. Electric propulsion systems typically have a specific impulse of 800-3,000s, with some in development now that have a specific impulse as high as 10,000s. However, the thrust produced by these engines is much lower than the thrust produced by chemical engines.

Electric propulsion systems do not produce enough thrust to use the impulse approximation, so the orbital transfers have to be done differently. Instead of thrusting briefly between long periods of coasting, the thrusting is continuous for most of the duration of the transfer. The impulsive thrust problem can be solved using only a small number of impulses[7], which limits the complexity of the control problem to finding a small number of thrust directions and magnitudes. With continuous thrusting, the thrust direction and magnitude can be varied continuously, which requires a continuous control function. Finding an optimum function is significantly more difficult than finding a small number of optimal impulses.

A further complication is that the trajectory must be integrated from the beginning to the end. With patched conics, the orbits between thrustings are known, so only a small number of calculations are needed to determine if a given set of firings will produce the desired transfer. With continuous thrusting, the entire trajectory must be integrated, which is significantly more computational work. It is only recently that computers have become fast enough to make it feasible to quickly solve optimal orbit transfer problems with continuous thrusting[2].

1.1 Low Thrust Orbital Transfer Optimization

Finding the lowest Δv transfer between orbits using continuous thrusting will allow significant mass savings for future missions. Launch vehicles capable of putting heavy spacecraft into orbit are more

[1] This equation is only valid for constant specific impulse transfers. If the specific impulse is varied, an averaging integral must be used

[2] Most of the trajectories calculated for this work took between 2 and 50 minutes to calculate on a Pentium IV 2.4 GHz computer, which is still not very fast.

expensive than launch vehicles that can only put light spacecraft into orbit, so reducing the $\Delta v/c$ ratio will allow either cheaper or better missions. Some current plans for electric propulsion missions include raising satellites to geosynchronous orbit (GEO), sending larger spaceships to explore other planets, and colonizing Mars.

The methods used to optimize orbital trajectories are the same for all uses of low-thrust engines. The problem considered in this work is raising satellites to GEO. This problem has the most immediate application and is also the simplest one to solve. Because the entire mission is around Earth, only one central body needs to be considered, whereas the multi-planet missions require considering the Earth, the Sun, and the other planets. After completing work with only one central body, it is possible to extend it to include multiple central bodies, but developing an optimizer for interplanetary missions from scratch would be more difficult than developing it one step at a time.

The calculus of variations is the field of math concerned with finding a function that optimizes a cost function subject to a constraint function. The Hamiltonian method (described in Appendix B) is used to determine the optimal control law for the orbital transfer.

1.1.1 Prior Work

Previous work done by others has established optimal control laws for low-thrust orbital transfers. Previous work includes finding optimal transfers with many second order effects, including J_2 and other oblateness terms, three and more body problems, eclipsing, and solar cell degradation. However, most of the previous work has not optimized the coasting periods analytically, and almost none of the previous work has used constant thrust levels. The new work done here includes optimizing the coasting periods and determining the control law for variable specific impulse optimizations[3]. More emphasis is given to determining the physical meaning of the terms in the optimal control law than in prior work by others.

1.2 Orbital Elements

When determining orbits from observations, it is convenient to describe the orbit using geometrical parameters. All purely gravitational orbits are conic sections, so their shape can be described by a and e, the semi-major axis and the eccentricity of the ellipse (or hyperbola). The orientation of the orbit is described by the longitude of perihelion, ϖ. All orbits are two-dimensional, so the orbital plane can be described by the inclination angle, i, and the longitude of the ascending node, Ω. The longitude of perihelion is often replaced by the argument of perihelion, $\omega = \varpi - \Omega$. This provides the classical orbital elements: a, e, i, Ω, and ω, as shown in figure 1-1

When determining how to modify orbits, it is more convenient to use orbital elements based

[3]The control law is determined analytically, but has not been implemented in an integrator yet.

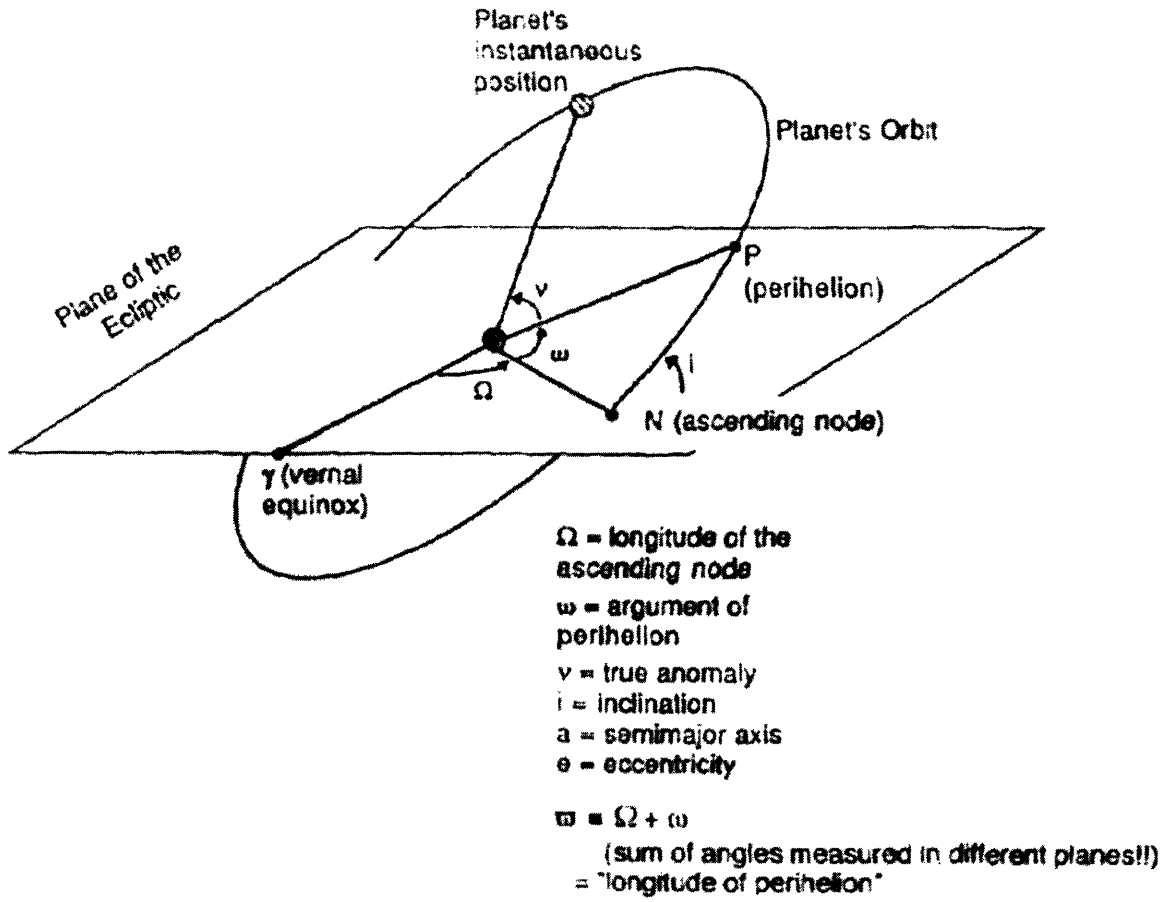

Figure 1-1: Diagram showing the definition of the classical orbital elements

on the physical properties of the orbit. The physical properties of the orbit can be determined from the angular momentum vector, **h**, and the eccentricity vector, **e**. Breaking these vectors down into components and then grouping the components in useful ways produces the equinoctial orbital elements (described in Appendix A) - h, e_x, e_y, i_x, and i_y. It is difficult to show these orbital elements on a diagram, because they describe the physical properties of the orbit rather than the geometrical properties. The following relations exist between the classical elements and the equinoctial elements:

$$e_x = e\cos\varpi \tag{1.2}$$

$$e_y = e\sin\varpi \tag{1.3}$$

$$p = a(1-e^2) \tag{1.4}$$

$$p = \frac{h^2}{\mu} \tag{1.5}$$

$$i_x = \tan(i/2)\cos\Omega \tag{1.6}$$

$$i_y = \tan(i/2)\sin\Omega \tag{1.7}$$

where μ is the gravitational constant of the central body, as defined in Newton's law of gravity

$$\frac{d\mathbf{v}}{dt} = -\frac{\mu}{r^3}\mathbf{r} \tag{1.8}$$

For the present work, h has a modified value. The standard value of h is the angular momentum of the orbit. However, the equations for the equinoctial elements have the term h/μ everywhere that h appears, so it is mathematically convenient to use $h' = h/\mu$ instead. The units of h' are time/length, which is the inverse of velocity, and it is not clear what its physical meaning actually is, but it is proportional to h and can be considered the angular momentum for almost all practical purposes.

Chapter 2

Method

The method used here for solving orbital transfer problems is based on the Hamiltonian method of optimal control theory. The full development of the Hamiltonian method is given for reference in Appendix B. This method uses a cost function which must be minimized along the path integral of the transfer.

The cost function for minimum fuel is

$$\int_0^T \dot{m}dt = \int_0^T -\frac{F}{c}dt = \int_0^T Jdt \tag{2.1}$$

where F is the thrust magnitude and c is the specific impulse. The cost is negative, so it should be maximized in order to minimize the magnitude. The Hamiltonian is formed by adding the product of the state and costate vectors to the cost function.

The state vector includes all of the equinoctial orbital elements (defined in Appendix A), the true longitude, and the mass:

$$\mathbf{X}^T = [h,\ e_x,\ e_y,\ i_x,\ i_y,\ L,\ m] \tag{2.2}$$

It is also useful to define the reduced state vector, $\tilde{\mathbf{X}}$, which contains only the orbital elements.

$$\tilde{\mathbf{X}}^T = [h,\ e_x,\ e_y,\ i_x,\ i_y] \tag{2.3}$$

The costate vector comes from the Hamiltonian method as described in Appendix B. It is

$$\mathbf{p}^T = [p_h,\ p_{e_x},\ p_{e_y},\ p_{i_x},\ p_{i_y},\ p_L,\ p_m] \tag{2.4}$$

$$\tilde{\mathbf{p}}^T = [p_h,\ p_{e_x},\ p_{e_y},\ p_{i_x},\ p_{i_y}] \tag{2.5}$$

The Hamiltonian is

$$H = J + \mathbf{p}^T \frac{d\mathbf{X}}{dt} \tag{2.6}$$

The time rate of change of $\mathbf{X}$ is found from

$$\frac{d\tilde{\mathbf{X}}}{dt} = \nabla_v \tilde{\mathbf{X}} \cdot \mathbf{a} \tag{2.7}$$

$$\frac{dm}{dt} = -\frac{F}{c} \tag{2.8}$$

$$\frac{dL}{dt} = \frac{\xi^2}{\mu h^3} + \nabla_v L \cdot \mathbf{a} \tag{2.9}$$

where $\mathbf{a}$ is the non-gravitational acceleration vector, with magnitude F/m.

Expanding the Hamiltonian produces

$$H = -\frac{F}{c}(1 + p_m) + \frac{\xi^2}{\mu h^3} p_L + (\tilde{\mathbf{p}}^T \nabla_v \tilde{\mathbf{X}} + p_L \nabla_v L) \cdot \mathbf{a} \tag{2.10}$$

The Hamiltonian can be divided into three parts

$$H = Fb + \mathbf{A} \cdot \mathbf{a} + H_L \tag{2.11}$$

where

$$b = -\frac{1 + p_m}{c} \tag{2.12}$$

$$= -\frac{p'_m}{c} \tag{2.13}$$

$$\mathbf{A} = \tilde{\mathbf{p}}^T \nabla_v \tilde{\mathbf{X}} + p_L \nabla_v L \tag{2.14}$$

$$H_L = \frac{\xi^2}{\mu h^3} p_L \tag{2.15}$$

The simplification of using $p'_m = 1 + p_m$ is useful because the only place where p_m occurs is in the combination $1 + p_m$. Because p_m is an unknown function, adding a constant to it does not cause any problems (although the constant does affect the transversality conditions). The derivatives still have to be the same to satisfy the Hamiltonian method, so only constants can be added.

Each of these terms has its own meaning. The term with b shows the cost of using fuel. The term with $\mathbf{A}$ shows how effectively the orbital elements can be changed (with a more in-depth discussion in sections 2.1 and 2.5).

The H_L term comes from the natural orbital motion and has essentially no impact on the optimization. p_L is a periodic function with only small variations in magnitude and is equal to 0 at the beginning and end of the transfer (see Appendix B), so it is set to 0 and ignored for the remainder of this optimization. The value of p_L can be calculated because $H = 0$ at all times if the equations are solved exactly. If p_L is assumed to be zero, then H will not remain zero, but will

instead have a magnitude proportional to p_L. During the integrations, the actual value of H was normally on the order of 10^{-5} or smaller. The other elements of the costate had magnitudes on the order of 0.1-20, so setting p_L to zero should cause errors on the order of 10^{-5}.

2.1 The A Vector

The A vector is defined as[1]

$$\mathbf{A} = \nabla_v \tilde{\mathbf{X}} \cdot \mathbf{p} \tag{2.16}$$

$$A_i = \frac{\partial \tilde{\mathbf{X}}}{\partial v_i} \cdot \mathbf{p} \tag{2.17}$$

With just one orbital element, the A vector would be

$$\mathbf{A} = p \nabla_v X \tag{2.18}$$

which says that the A vector is the gradient of the orbital element with respect to velocity. Thrusting in the direction of the gradient will increase the orbital element at the maximum possible rate. The costate scales the A vector so that it is larger when more of an increase is desired and smaller when less is desired. It can also be negative to show that the orbital element should be decreased.

With multiple orbital elements, the A vector becomes a weighted average of the gradient with respect to velocity of all the orbital elements. The weighting factors are the p's that correspond to each orbital element. This suggests that the optimal thrusting should be in the direction of the A vector.

When the A vector is small, it means either the orbital elements cannot be changed effectively or that different orbital elements need thrust in nearly opposite directions. Either way, the thrusting is not going to be effective for getting to the final orbit. This suggests that the thrust should be reduced where A is small. When A is large, it means that several of the orbital elements can be changed by thrusting in nearly the same direction, so thrusting will be very effective. This suggests that the thrust should be concentrated in the areas where A is large.

A simple control algorithm can be developed based on the definition of the A vector. Consider a control law for just one of the orbital elements (X)

$$\frac{dX}{dt} = \frac{A}{p} \tag{2.19}$$

A is always positive, so for X to reach 0, p must have the opposite sign from X. One way to do this

[1] p_L is assumed to be 0, so the final term is ignored

is

$$p = -X \tag{2.20}$$

If this is done for all of the orbital elements, the resulting control law is

$$\tilde{\mathbf{p}} = -\tilde{\mathbf{X}} \tag{2.21}$$

so that

$$\mathbf{A} = (-\nabla_v \tilde{\mathbf{X}}) \cdot \tilde{\mathbf{X}} \tag{2.22}$$

This control law will necessarily move the orbit towards 0. It is not necessarily an optimal control law, but it will reach 0 eventually.

To reach a final orbit $\tilde{\mathbf{X}}_{final}$ instead of 0, the control law becomes

$$\begin{aligned} \tilde{\mathbf{p}} &= \tilde{\mathbf{X}}_{final} - \tilde{\mathbf{X}} && (2.23) \\ \mathbf{A} &= (-\nabla_v \tilde{\mathbf{X}})(\tilde{\mathbf{X}} - \tilde{\mathbf{X}}_{final}) && (2.24) \end{aligned}$$

As long as $\mathbf{a}$ is controlled to be in the same direction as $\mathbf{A}$, this will cause the orbital elements to change in the direction of their final values:

$$\begin{aligned} \frac{d\tilde{\mathbf{X}}}{dt} &= \nabla_v \tilde{\mathbf{X}} \cdot \mathbf{a} && (2.25) \\ \mathbf{a} &= \frac{a}{A}\mathbf{A} && (2.26) \\ \frac{d\tilde{\mathbf{X}}}{dt} &= -\frac{a}{A}(\nabla_v \tilde{\mathbf{X}})^2(\tilde{\mathbf{X}} - \tilde{\mathbf{X}}_{final}) && (2.27) \\ \frac{d\tilde{\mathbf{X}}}{dt} &\propto -(\tilde{\mathbf{X}} - \tilde{\mathbf{X}}_{final}) && (2.28) \end{aligned}$$

which is the standard form of a linear regulator. This differential equation guarantees that $\tilde{\mathbf{X}}$ will approach $\tilde{\mathbf{X}}_{final}$. Other control laws can be generated that will change the orbit to the desired one as long as the sign of each of the costate elements is opposite to the sign of $(\tilde{\mathbf{X}}_final - \tilde{\mathbf{X}})$. There is no guarantee that the optimal control law will be of this form, and this method does not provide a simple means of calculating how efficient various possible control laws based on this principle are.

2.2 Control Optimization

To find the optimal control law, the Hamiltonian is maximized with respect to all the control variables (in accordance with Pontryagin's maximum principle). There are two sets of control variables: the thrust magnitude and the thrust direction.

2.2.1 Thrust Direction

The only part of the Hamiltonian that is affected by the direction of the thrust is the $\mathbf{A} \cdot \mathbf{a}$ term. As this is a dot product, the maximum value will be found when the two vectors point in the same direction. This means that

$$\mathbf{a} = \frac{a}{A}\mathbf{A} = \frac{F}{mA}\mathbf{A} \tag{2.29}$$

so

$$\mathbf{A} \cdot \mathbf{a} = \frac{FA^2}{mA} = \frac{FA}{m} \tag{2.30}$$

2.2.2 Thrust Magnitude

There are several options for varying the magnitude of the thrust. The simplest one is to have the engine on at constant power the entire time. In this case, there is no control variable for the magnitude of the thrust, so the optimization is complete.

The next simplest thrust magnitude modulation is to switch the engine on and off without changing the level of thrust. The Hamiltonian is

$$H = F[b + A/m] + H_L = F[A/m - p'_m/c] + H_L \tag{2.31}$$

The way to maximize this when F can only be 0 or F_{max} is to turn the engine off when $b + A/m$ is negative and on when it is positive (the optimization cannot determine whether the engine should be on or not when $b + A/m$ is 0, but this should only happen for brief time periods as it changes sign). A and m are always positive, so only b can make the quantity negative. Whenever p'_m is positive, b will be negative.

The next simplest control method is constant power and efficiency with variable thrust and specific impulse. In this case

$$\eta_{prop}P = \frac{1}{2}\dot{m}c^2 \tag{2.32}$$

$$\dot{m} = \frac{2\eta_{prop}P}{c^2} \tag{2.33}$$

$$F = \dot{m}c = \frac{2\eta_{prop}P}{c} \tag{2.34}$$

$$H = -\frac{2\eta_{prop}P}{c^2}p'_m + \frac{2\eta_{prop}P}{mc}A + H_f \tag{2.35}$$

$$\frac{\partial H}{\partial c} = \frac{4\eta_{prop}P}{c^3}p'_m - \frac{2\eta_{prop}P}{mc^2}A = 0 \tag{2.36}$$

$$2mp'_m = Ac \tag{2.37}$$

$$c = \frac{2mp'_m}{A} \tag{2.38}$$

$$F = \frac{\eta_{prop}PA}{mp'_m} \tag{2.39}$$

$$\mathbf{F} = \frac{\eta_{prop} P}{m p'_m} \mathbf{A} \tag{2.40}$$

Real engines will not have constant efficiency as the specific impulse and thrust magnitude change, but variable efficiency adds significantly more complexity to the problem without providing any significant general mathematical insight. Variable efficiency can be analyzed for a specific engine if desired, but there is no general solution because different efficiency curves will produce different solutions.

Variable power problems cannot be solved with this formulation because the Hamiltonian is linearly proportional to the power in all terms that depend on it, so the Hamiltonian will always be maximized by having either no power or by having the maximum amount of power possible. This is then equivalent to the on/off control described above. It might be possible to solve variable power problems with another method that allows more explicit time constraints or that has power in the cost function. It is also possible to have variable power constraints in the problem.

With constant power, there is a tradeoff between the time the transfer takes and the amount of power used. For a given transfer, the Δv will be approximately constant for a wide range of powers as long as the thrust is kept low. More power will allow a faster transfer, but will generally require a heavier power system. Increasing c will reduce the amount of fuel needed, but will slow down the transfer. The power and specific impulse can be optimized after the orbital trajectory is found, as long as the thrust is kept low.

2.2.3 Eclipse Control

One particular case where the power could be constrained is eclipse control. For eclipse control, the engine is turned off whenever the spacecraft is in the Earth's shadow, allowing the engine to be powered by the solar panels alone, saving the batteries for use after the orbital transfer is completed.

The optimization is the same for all the parts of the transfer where the spacecraft is outside the shadow. While inside the shadow, the spacecraft coasts and none of the orbital elements change. This will produce the optimal transfer with respect to the constraints. The initial value of the costate will be different, which will change the thrusting pattern, but the final equations of motion are the same.

2.2.4 Engine Switching

Another option for varying the magnitude of the thrust is to use multiple engines and switch between them based on which one is most effective at each point in the transfer. The most useful combination is a high thrust chemical engine and a low thrust electrical engine.

The switching function is still based on maximizing the Hamiltonian. However, instead of optimizing a function, there are four possible states (both engines off, both engines on, chemical engine

on, electrical engine on). Having both engines on is not generally going to be useful, because the low thrust engine will have almost no impact compared to the high thrust engine. This leaves three possible states.

The Hamiltonian can be one of

$$H_c = -\frac{F_c p_m}{c_c} + \frac{F_c}{m} A + H_L \tag{2.41}$$

$$H_e = -\frac{F_e p_m}{c_e} + \frac{F_e}{m} A + H_L \tag{2.42}$$

$$H_o = H_L \tag{2.43}$$

where the subscript c is used for when just the chemical engine is on, the subscript e is used for when just the electrical engine is on, and the subscript o is used when both engines are off. The control function is to choose the maximum of these three options and set the engines to the corresponding state.

The largest difficulty with using chemical engines with the general method developed here is that the large thrust causes small errors to lead to large changes in the orbit, which means that the initial values must be determined with high precision. When switching between high and low thrust engines, this problem is magnified. As such, the integrator must be accurate to determine the proper values of the control variables. The solutions are also much less stable. Only a few trajectories have been succesfully found using the current integrator. Similar methods have been used to optimize purely impulsive thrusting[7], so it should be possible to combine both methods.

The engine switching algorithm could also be used to provide control over a single engine that has multiple throttle points. This provides a discrete approximation to the problem of continuously varying the thrust level. It could be used as an approximation to variable power or variable efficiency engines, and might be easier to solve than the continuously variable thrust problem discussed above. As long as no high thrust engines are used, the algorithm should converge with no further modifications.

2.3 Optimal Equations of Motion

The optimal equations of motion come from the Hamiltonian:

$$\frac{d\mathbf{X}}{dt} = \frac{\partial H}{\partial \mathbf{p}} = \frac{F}{m}\left[\frac{1}{A}\left(A_t \frac{\partial A_t}{\partial \mathbf{p}} + A_r \frac{\partial A_r}{\partial \mathbf{p}} + A_n \frac{\partial A_n}{\partial \mathbf{p}}\right)\right] \tag{2.44}$$

$$\frac{d\mathbf{p}}{dt} = \frac{\partial H}{\partial \mathbf{X}} = -\frac{F}{m}\left[\frac{1}{A}\left(A_t \frac{\partial A_t}{\partial \mathbf{X}} + A_r \frac{\partial A_r}{\partial \mathbf{X}} + A_n \frac{\partial A_n}{\partial \mathbf{X}}\right)\right] \tag{2.45}$$

The resulting equations are:

$$\frac{dh}{dt} = \frac{FA_t}{mA}\frac{h^2}{\xi} \tag{2.46}$$

$$\frac{de_x}{dt} = \frac{Fh}{mA\xi}\left[A_r\xi\sin L - A_n\eta e_y + A_t\{(\xi+1)\cos L + e_x\}\right] \tag{2.47}$$

$$\frac{de_y}{dt} = \frac{Fh}{mA\xi}\left[-A_r\xi\cos L + A_n\eta e_x + A_t\{(\xi+1)\sin L + e_y\}\right] \tag{2.48}$$

$$\frac{di_x}{dt} = \frac{FA_nh\phi}{2mA\xi}\cos L \tag{2.49}$$

$$\frac{di_y}{dt} = \frac{FA_nh\phi}{2mA\xi}\sin L \tag{2.50}$$

$$\frac{dm}{dt} = -\frac{F}{c} \tag{2.51}$$

$$\frac{dp_h}{dt} = -\frac{F}{m}\left[\frac{A}{h} + \frac{A_thp_h}{\xi}\right] \tag{2.52}$$

$$\frac{dp_{e_x}}{dt} = -\frac{F}{mA\xi}\left[h(p_{e_x} + p_{e_x}\cos^2 L + p_{e_y}\cos L\sin L)A_t + h\eta p_{e_y}A_n - (A_t^2 + A_n^2)\cos L\right] \tag{2.53}$$

$$\frac{dp_{e_y}}{dt} = -\frac{F}{mA\xi}\left[h(p_{e_y} + p_{e_y}\sin^2 L + p_{e_x}\cos L\sin L)A_t - h\eta p_{e_x}A_n - (A_t^2 + A_n^2)\sin L\right] \tag{2.54}$$

$$\frac{dp_{i_x}}{dt} = -\frac{FhA_n}{mA\xi}[(e_xp_{e_y} - e_yp_{e_x})\sin L + i_x(p_{i_x}\cos L + p_{i_y}\sin L)] \tag{2.55}$$

$$\frac{dp_{i_y}}{dt} = -\frac{FhA_n}{mA\xi}[-(e_xp_{e_y} - e_yp_{e_x})\cos L + i_y(p_{i_x}\cos L + p_{i_y}\sin L)] \tag{2.56}$$

$$\frac{dp_m}{dt} = \frac{FA}{m^2} \tag{2.57}$$

$$\frac{dp'_m}{dt} = \frac{FA}{m^2} \tag{2.58}$$

It is important to remember to use the instantaneous values of all the variables, including F and c if the thrust magnitude is being varied. If the engine is being switched on and off, then none of the variables will change during the coasting periods. If the thrust level is being varied, then equations 2.38 and 2.39 can be used to substitute in the varying values of c and F in the equations of motion.

2.4 Extensions

This method is fairly general, and can be extended to include a number of non-idealities. If there is a disturbing acceleration $\mathbf{a}_d$, this can be included in the optimization. The Hamiltonian is then

$$H = Fb + \mathbf{A}\cdot\mathbf{a} + \mathbf{A}\cdot\mathbf{a}_d + H_L \tag{2.59}$$

The control laws will be exactly the same, because the only term that has been added has no control variables. The actual thrust directions and magnitudes will be different, because the optimal

value of the costate (p_h, p_{e_x}, p_{e_y}, p_{i_x}, p_{i_y}, and p_m) will be different, but the method does not change. The optimal equations of motion will change for most of the variables (both the orbital elements and the costate).

This will work with any disturbing acceleration. It will be easier if the disturbing acceleration can be easily calculated from the orbital elements and if it easily breaks down into the tangential, radial, and normal directions, but any arbitrary function could be used.

2.5 The A Vector Revisited

Prior to determining the optimal control equations, it was stated that the thrust should be concentrated in the areas where the A vector is largest. The control laws have now been developed, so it is possible to compare the actual control laws with the assumed principle.

When the thrust magnitude is held constant, the thrust must be equally spread throughout the orbit. In this case, the thrust is not concentrated anywhere. The thrust direction does point in the direction of the A vector, as expected.

For on/off thrust control, the engine is turned on whenever $b + A/m$ is positive. This will be whenever $A > -bm$. In this case, the thrust is only applied if the effectiveness of thrusting is high enough. The exact threshold for what is considered high enough is set by b (which relates to how important conserving fuel is).

With engine switching, low values of A will favor the engine with a higher specific impulse because the size of p'_m/c matters more when A/m is smaller. When A is large, the engine with a higher thrust will be favored because p'_m/c will be relatively less important, so multiplying A by a large F will maximize H.

A further consideration for engine switching is that p'_m always increases throughout the mission, while m always decreases. This means that the relative value of A/m as compared to p'_m/c always decreases. This suggests that at the beginning of the mission, the optimal control will favor the impulsive engine, while towards the end of the mission, it will favor the high specific impulse engine.

2.6 Boundary Conditions

The boundary conditions for a Hamiltonian optimization are derived in Appendix B, and are often called the transversality conditions. For each of the free elements of the state at the terminal time, the corresponding costate element must be 0. Additionally, the value of the Hamiltonian must be 0 at the terminal time. The only free elements of the state are L and m. This means that H, p_m, and p_L are all 0 at t_f. Because p_L has already been assumed as 0, this is expected for p_L.

The condition on p_m provides almost no useful information for the optimization, because with a

slight modification, the costate vector can be multiplied by an arbitrary constant without changing anything about the optimization. The slight modification is replacing p_m with $p'_m = 1 + p_m$. With this replacement, all the equations involve a ratio of two elements of the costate vector, so it can be scaled by a constant with no effect. The transversality condition provides the scaling constant.

With $p_L = 0$, the Hamiltonian is

$$H = F(A/m - p'_m/c) \tag{2.60}$$

It is possible to remove p'_m from this equation, because it is equal to 1 (at the final time). However, doing so requires that A is scaled by the same amount, which leads to

$$H = F\left(\frac{A/p'_m}{m} - \frac{1}{c}\right) \tag{2.61}$$

This equation is not any easier to work with, so there is no advantage to actually scaling the costate in this manner.

Equation 2.60 is always equal to zero for the variable thrust optimization, so the transversality condition adds no information.

The orbital elements do not change significantly during the final orbit, and the errors in the numerical methods used will generally be too large to allow the exact final time to be determined. As a result, the stopping point can be chosen arbitrarily almost anywhere in the final orbit.

For on-off thrust control, the Hamiltonian is equal to zero at the times when the engine is switched on or off. As long as the mission is longer than the minimum time, there will be some coasting during the final orbit, so the transversality condition for on-off control is met naturally by turning the engine off at the beginning of one of the coasting arcs.

For the minimum time problem, the value of p'_m has no impact on the optimization. Choosing p'_m such that equation 2.60 will satisfy the transversality condition on the Hamiltonian. Then the transversality condition on p_m will provide a scaling factor which will correct the value of the rest of the costate.

Chapter 3

The Two Point Boundary Value Problem

Optimal orbital transfers can be calculated with the optimal equations of motion as determined in section 2.3. However, these equations specify the optimal transfers using both the state and the costate vectors. For a given initial orbit and costate vector, a path through orbit space is determined. This path will not necessarily go to the desired final orbit.

In order to find the proper initial values of the costate, a gradient-based method is used. An initial guess is made at the proper value of the costate. The transfer that results from the initial guess is compared to the desired transfer in order to improve the guess.

One difficulty is determining when to stop integrating the transfer. It is unlikely that the initial guess will ever get to the desired orbit, so the stopping point of the integration cannot be the final orbit. The orbital elements do not always vary monotonically, so integrating until they have all gotten at least as far as they are supposed to is also not generally possible.

The only orbital element that always varies monotonically is the inclination. Any reasonable guess will cause the inclination to change in the proper direction, which means that the final inclination will eventually be reached, and it is never necessary to overshoot on the inclination. This means that the desired inclination will be reached exactly once for any initial value of the costate.

Once the desired inclination is reached, all the other orbital elements can be compared to their desired values to determine how to improve the guess. The costate is then changed based on how the orbit needs to be modified.

It is possible to compute a multidimensional gradient of the costate with respect to all the orbital elements. However, the final orbit is a nonlinear function of the costate, so varying all the elements of the costate simultaneously causes many complications. While this method does often converge quickly (frequently in fewer than 10 iterations), it sometimes gets stuck in a loop where it is circling

around the correct solution. Detecting such loops and then correcting them is difficult.

A more stable method of improving the guess is to vary one element of the costate at a time. While all of the orbital elements are affected by every element of the costate, each orbital element is most strongly affected by the element of the costate that corresponds to it. This leads to an algorithm that compares all of the orbital elements to their desired values and modifies the costate element corresponding to the orbital element that is the furthest from the desired value. With the minor modifications described in section 3.1, this method converges for all orbits and normally converges reasonably quickly.

Another difficulty with determining the initial value of the costate is that all the differential equations only involve ratios of the costate. This means that multiplying all of them by the same amount will have no effect on anything. The transversality conditions provide the necessary conditions for determining the correct value to scale the costate by, but any other value can be used without causing problems. The easiest method to implement is fixing the initial value of one element of the costate. Any costate element that is not equal to zero can have its value set arbitrarily, and the rest of the costate will be scaled appropriately.

For this project, Ω had an arbitrary value because the orientation of the coordinate axis can be chosen freely (other than the z direction), so it was set to 0. This means that i_x is always the only contributor to the initial inclination. For all the non-flat orbits, p_{i_x} was set to $-i$ and the values for the rest of the costate were found iteratively.

3.1 Implementation

The method based on varying the costate element associated with the orbital element that has the largest error mostly works, but it is sometimes impossible to reduce the error in one of the orbital elements just by modifying the corresponding costate element. To fix this problem, a count is kept of how many times in a row each costate element has been adjusted. When the count gets too high, other costate elements are modified as well.

In order to determine how much to modify each costate element, a gradient method is used.

$$\frac{dp}{dX} = \frac{p_{saved} - p}{X_{saved} - X} \tag{3.1}$$

$$p_{new} = p + \frac{dp}{dX}(X_{desired} - X) \tag{3.2}$$

Where X_{saved} and p_{saved} are the values that were recorded when this element of the costate was last modified, X and p are the current values, $X_{desired}$ is the desired final value of the orbital element, and p_{new} is the new value of the costate element. Once the error in a speecific orbital

element is reduced enough, other costate elements are modified. This often increases the error in the orbital element, so the saved values of p and X do not just show the impact of changing p, which means that the slope will not generally be correct on the first iteration. The slope should almost always be positive[1], so on the first iteration on each multiplier, the sign is corrected to be positive. After the first iteration, the slope as calculated is the best estimate of how the multiplier and the final value of the orbital element are related. The value of the slope is always left unchanged, because there is no way of determining a better value, even on the first iteration.

Because the relationship between the multipliers and the final values of the orbital elements is not actually linear, the slope sometimes overestimates the amount that the multiplier should be modified by quite a lot. In order to prevent this from being a problem, limits are placed on the amount that the multipliers can change. These limits are scaled based on the value of the fixed multiplier. To prevent the multiplier from oscillating back and forth between two points, the limits are modulated slightly by a random number on each iteration.

A sample of the MATLAB code used to modify the multipliers is shown in table 3.1. The code for the other multipliers is essentially the same.

3.2 Fixed-Time Problems

The fixed-time, optimal coasting problems are significantly more difficult to compute. Due to the nature of the switching function, changing p_m significantly changes the trajectory. As a result, far more iterations are required to reach the proper values of the multipliers.

A further complication comes from the extreme non-linearity of the dependance of t on p_m. A sample graph showing t as a function of p_m is shown in figure 3.2. For very low values of p_m, the time is constant because psi_s is always positive. There is a maximum useful value of p_m, above which psi_s is always negative and the engine never turns on. As p_m approaches that value, t increases in a hyperbolic manner. The minimum and maximum useful values of p_m depend on the values of all the other multipliers, so it is not worth computing them every time the other multipliers change. It is also impossible to compute where on the curve a given multiplier and time are without computing many trajectories, which would be computationally inefficient.

A better method is to pretend the graph is linear and use a gradient method. This can be augmented by reducing the slope when it is likely to be overestimated (when $t < t_{desired}$).

Storing the maximum value of p_m that has underestimated the correct value and the minimum value that has overestimated the correct value reduces the time wasted searching far from the correct value. To account for the possibility that the correct value of p_m will be outside of the previous

[1]The slope should be positive for reasons outlined in section 2.1. The only time it is negative is when there are interactions between the orbital elements causing the integration to end earlier as the multiplier is increased. To allow for this, the sign is free after the first iteration on each multiplier.

variable name	meaning
doex	should p_{e_x} be modified
dpex	the change in p_{e_x}
pex1	the saved initial value of p_{e_x}
pex0	the current initial value of p_{e_x}
dex	the change in e_x
ex1	the saved final value of e_x
ex	the current final value of e_x
exslope	the slope dpex/dex
excount	the number of time that pex0 has been modified in a row
pix0	the initial value of p_{i_x}
exs	the desired final value of e_x
doh	should p_h be modified

```
if (doex)
  dpex=pex1-pex0;
  dex=ex1-ex;
  pex1=pex0;
  ex1=ex;
  if (isfinite(exslope)&&dex!=0)
    exslope=dpex/dex;
    if excount==0
      exslope=abs(exslope)*-1;
    end
    pex0=pex0+min(pix0/3*(rand()/10+.95),\\
                  max(-pix0/3*(rand()/10+.95),exslope*(exs-ex)));
  else
    pex0=pex0+rand()*2-1;
  end
  if rem(excount,15)==14
    doh=1;
  end
  excount=excount+1;
end
```

Table 3.1: Sample code for modifying the costate

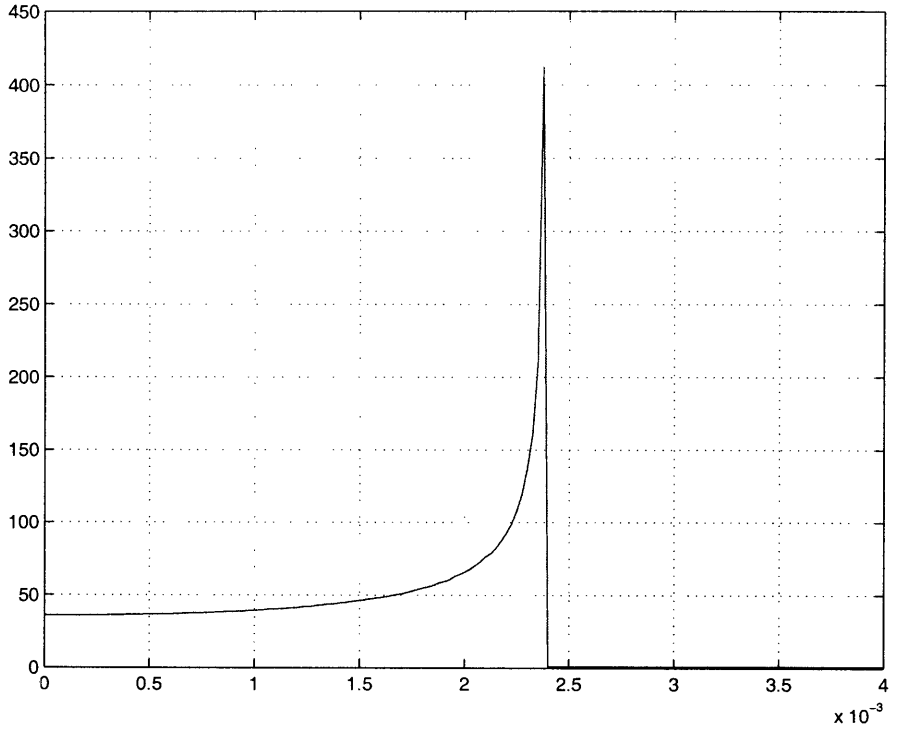

Figure 3-1: t as a function of p_m

range when the other multipliers change, the range should be increased when the other multipliers are modified.

A further complication with fixed-time is that there can be more than one solution to the optimal transfer problem[8]. The cause of this is that thrusting at a higher radius is generally more effective, so for some orbital transfers, increasing certain orbital elements beyond both the initial and final values reduces the total Δv. A well-known example of this is the bi-elliptic transfer, which uses less fuel than the Hohmann transfer for large changes in the orbital radius. In general, having a large eccentricity during the transfer will reduce the cost of changing the other orbital elements. As a result, whenever the eccentricity can be increased towards the beginning of the transfer and decreased at the end of the transfer for less fuel than the amount saved by having the high eccentricity in the middle, there will be two paths. One of the paths will be the global minimum and will have the large eccentricity in the middle (called the e-solution), and the other one will be a local minimum without the large eccentricity in the middle (called the c-solution).

The characteristic that shows something as a c-solution is that the eccentricity goes through 0 during the transfer and then the eccentricity switches directions. This can be seen in plots of the apogee and perigee radius because the two lines intersect and appear to cross. This is clearly not going to be the optimal transfer, because changing the direction of the eccentricity does not in any way benefit the transfer (except for transfers with both initial and final eccentricities where the

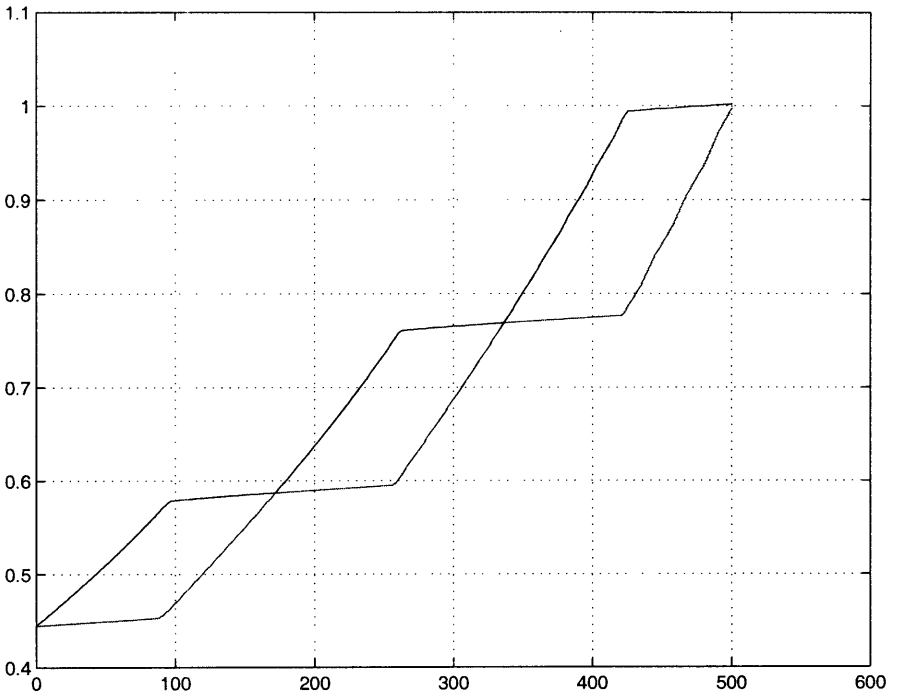

Figure 3-2: Transfer between circular, coplanar orbits from $h = 2/3$ to $h = 1$. Apogee and perigee radius are shown, normalized to GEO=1.

eccentricity must change direction), but it does use fuel.

The minimum time problem will never generate a c-solution, because changing the direction of the eccentricity wastes time. However, it can happen in the fixed-time problem because the wasted time is not a problem. An example of a c-solution is shown in figure 3.2, which is a fixed-time transfer between two coplanar circular orbits. The minimum transfer time for this transfer is 124.5 days, so the 500 day transfer is very stretched out, and has essentially become an impulsive transfer. However, instead of being a 2 thrust Hohmann transfer, it is a 4 thrust triple-Hohmann transfer (going through 2 intermediate circular orbits before reaching the final one).

The thrusting pattern is shown in figure 3.2. For the first part of the transfer, the thrusting only occurs in a small arc near what becomes the perigee. For the second part, all the thrusting occurs in a small arc near what switches from apogee to perigee. The third part is the same as the second part, although the thrusting is in the same place as it was for the first part. The fourth part of the transfer circularizes the orbit by thrusting around apogee. During this transfer, three Hohmann-like transfers take place. The Δv for the transfer is 1531.8m/s, while for a Hohmann transfer it would be 1476.3m/s.

Because the c-solutions are valid solutions to the equations of motion, it is difficult to remove them automatically. Fortunately, they will rarely be generated except when the initial and final orbits are both circular. Circular-to-circular transfers are difficult because the eccentricity can be

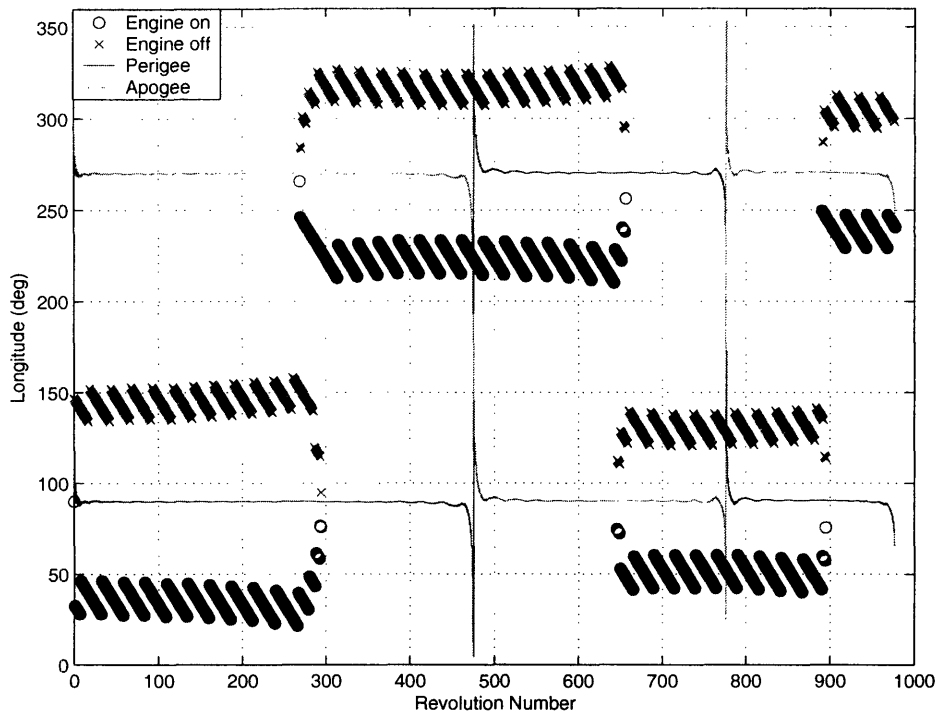

Figure 3-3: Engine turn-on and turn-off points for a transfer between circular, coplanar orbits from $h = 2/3$ to $h = 1$.

left near zero for the entire transfer. With either initial or final eccentricity, the solution is much less likely to go through zero eccentricity in the middle. Changes in inclination also make the c-solution less likely to appear.

One important point is noticing that for a fixed-time solution, the final time must be correct when the orbital elements are modified. The reason for this is that the intermediate eccentricity and other elements are not even close to the final values. This means that p_m must be corrected every time any of the other multipliers change, so the convergence rate for p_m has a very large impact on how quickly the solution as a whole converges.

Chapter 4

Results

The method described here was used to write an orbit integrator to determine the optimal trajectories for various orbital transfers. The integrator was specifically made to integrate orbits from LEO (low earth orbit) to GEO (geosynchronous orbit), however it could be modified to work for any starting or ending orbit, around any central body without much more work.

There are a large number of possible orbits from which to start. Showing the results for all of them is not practical and would not be very useful. Data for a small selection of orbits has been generated to make a few comparisons.

The general trends are that it takes more fuel when the line of nodes and the line of apses are initially misaligned, when the starting orbit is smaller, or when the inclination is larger. The eccentricity does not have a general impact on the fuel usage. When the line of nodes and the line of apses are aligned, a larger eccentricity decreases the fuel requirement at high inclinations and increases it at low inclinations. When the line of nodes and the line of apses are perpendicular, a larger eccentricity increases the fuel requirement. The impact of the eccentricity is larger when the inclination is larger.

For all the orbits described in this chapter, h is normalized so that it equals one at GEO. The initial value of Ω is 0, which corresponds to having i_y be 0. The line of nodes can be chosen arbitrarily because the reference direction for x and y is not set by outside constraints.

4.1 Comparison of Algorithms

Several different control alorithms were used. As a comparison, the results from all the integrators for $h = 0.8$, $i = 5°$ are shown here. The graphs show the contours of time or Δv associated with the trajectory starting from the orbits on the graph. The graphs only show the eccentricity, because all the other orbital elements are fixed. The magnitude of the eccentricity is shown by the distance from the center, and the direction of perigee is shown by the direction from the center. The ascending

node is in the positive x direction.

There are also graphs showing the Δv and the time for transfers starting with the line of nodes and line of apses in the same direction. These graphs are based on the semimajor axis (a) and the eccentricity (e). The semimajor axis is normalized with respect to GEO ($a_{GEO} = 1$).

In all cases, the spacecraft uses an engine with a specific impulse of 1500s and a thrust of 0.68N (10kW of thrust power). The initial spacecraft mass is 5000kg. All the trajectories go from LEO to GEO. The averaged trajectories were integrated backwards, but all the other trajectories were integrated forwards. This leads to the times being longer for the averaged case because the final mass for the orbit-averaged trajectories is 5000kg, while all the other trajectories have an initial mass of 5000kg. The integration direction does not significantly affect the Δv calculations.

4.1.1 Averaged Trajectories

These trajectories use the optimal control algorithm with always-on thrusting. The derivatives are averaged over one orbit to allow larger time steps.

4.1.2 Non-Averaged Trajectories

These trajectories use the optimal control algorithm with always-on thrusting, but without averaging.

4.1.3 Eclipse Control

These trajectories use the eclipse control algorithm as described in section 2.2.3. The spacecraft starts the transfer at the vernal equinox, with the x direction pointing from the Sun to the Earth.

4.1.4 Fixed-time Trajectories

These trajectories use the optimal coasting control algorithm with a specified transfer time. The fixed times are 125, 150, 200, and 250 days. Only the Δv's are plotted. The maximum time that any of the trajectories take with the engine always on is 100 days.

4.1.5 Non-optimal Trajectories

These trajectories are provided for comparison. They were generated using the algorithm developed at the end of section 2.1. They are provided for comparison, as this algorithm is the simplest one that is guaranteed to work.

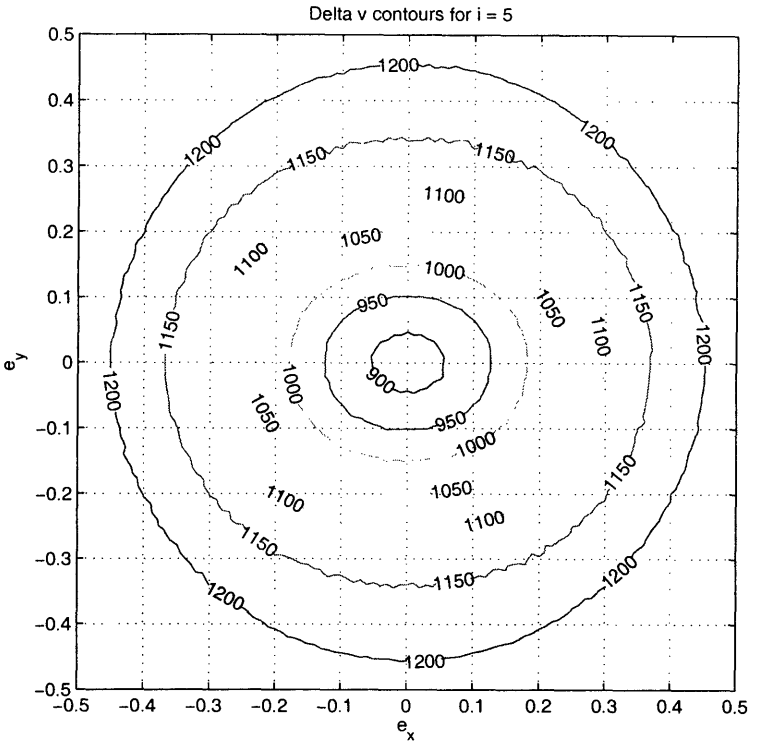

Figure 4-1: Δv contours (m/s) for averaged trajectories

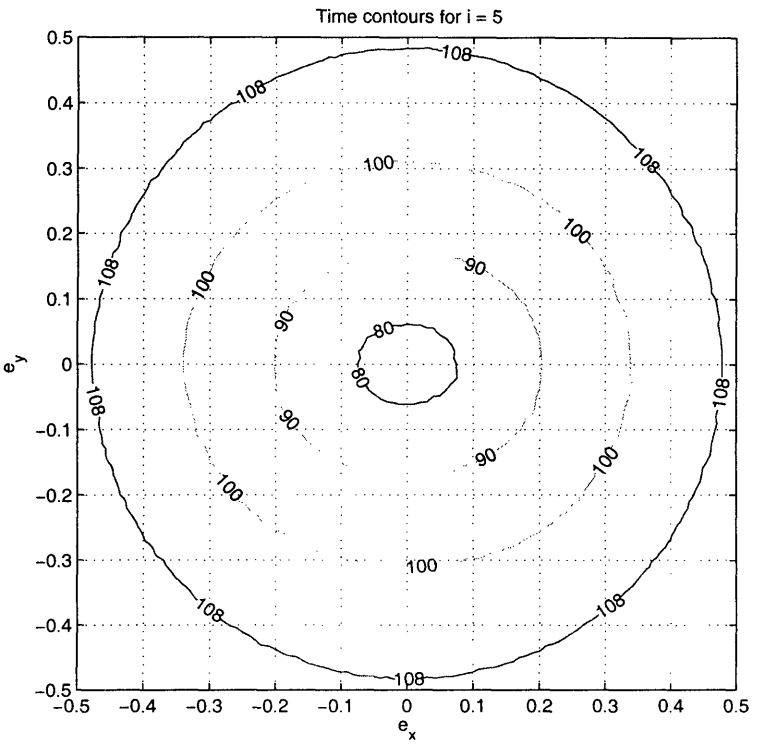

Figure 4-2: Time contours (days) for averaged trajectories

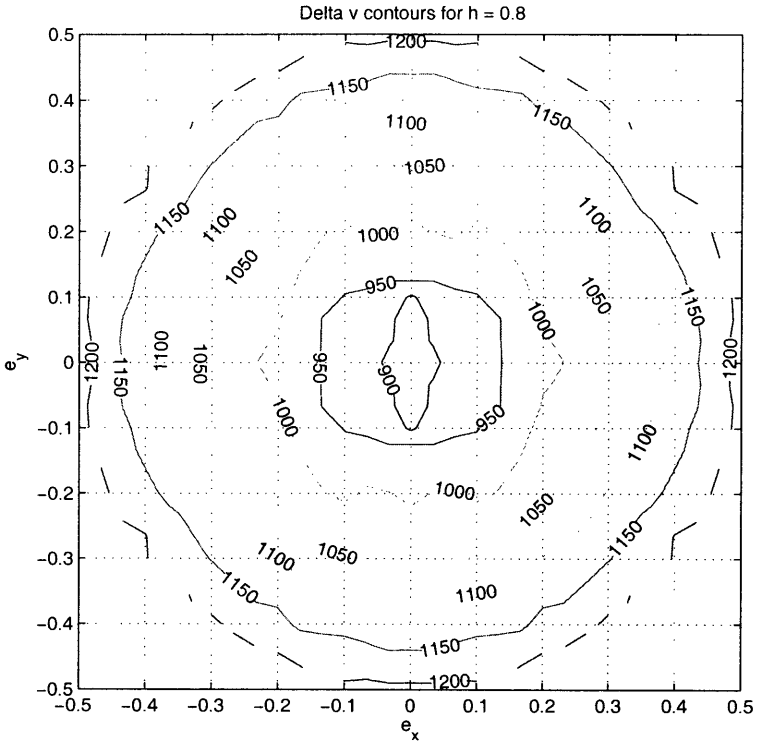

Figure 4-3: Δv contours (m/s) for non-averaged trajectories

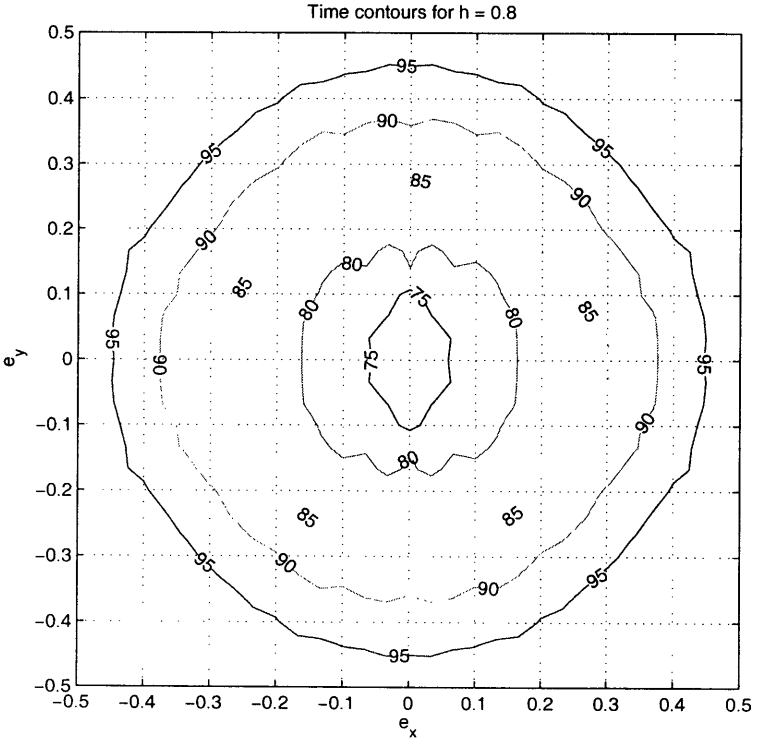

Figure 4-4: Time contours (days) for non-averaged trajectories

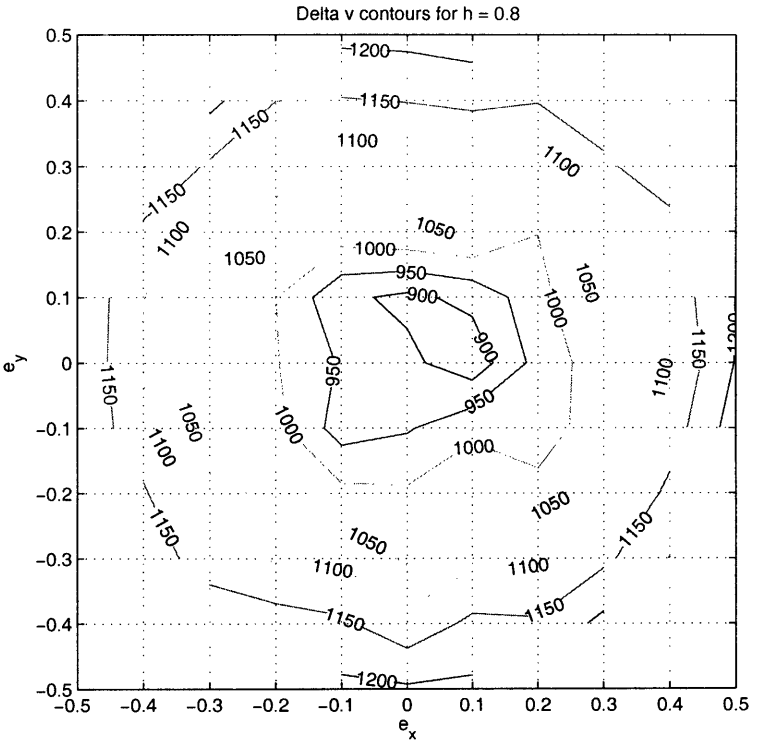

Figure 4-5: Δv contours (m/s) for eclipse control trajectories

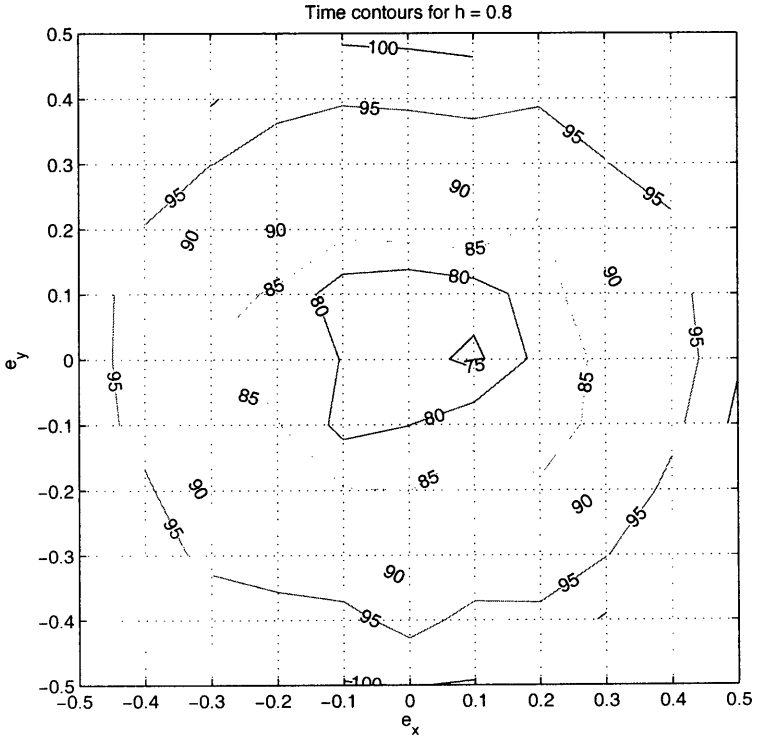

Figure 4-6: Time contours (days) for eclipse control trajectories

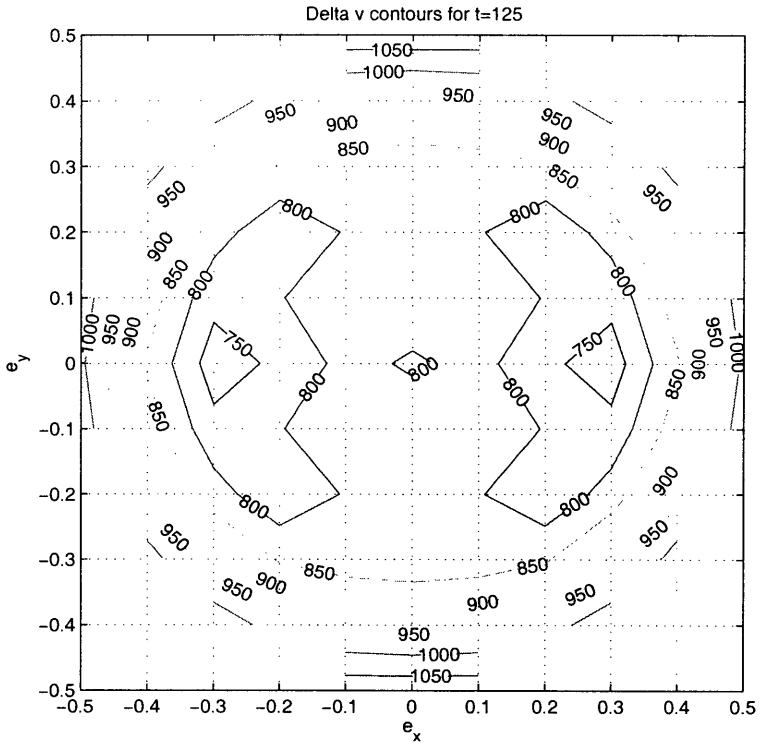

Figure 4-7: Δv contours (m/s) for 125 day trajectories

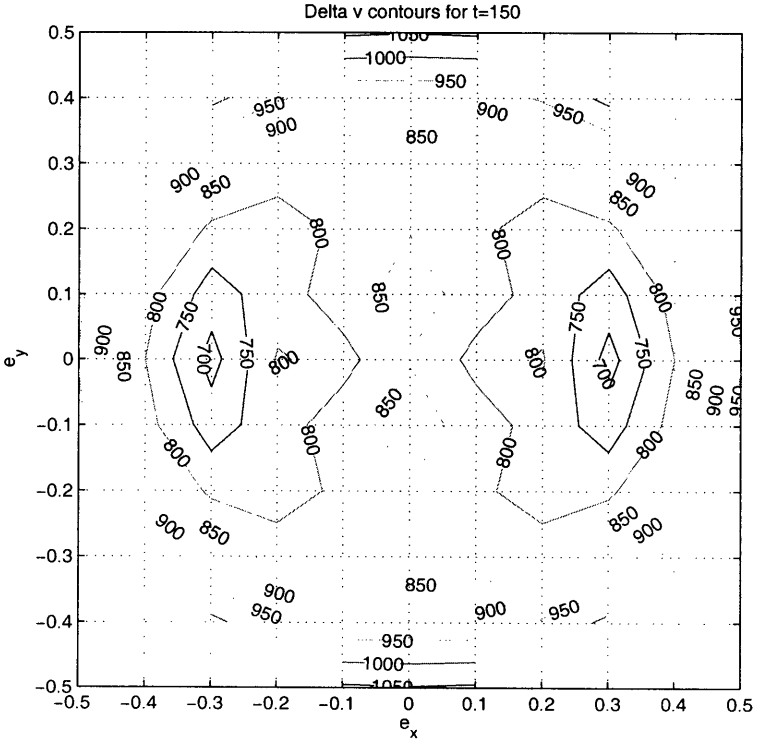

Figure 4-8: Δv contours (m/s) for 150 day trajectories

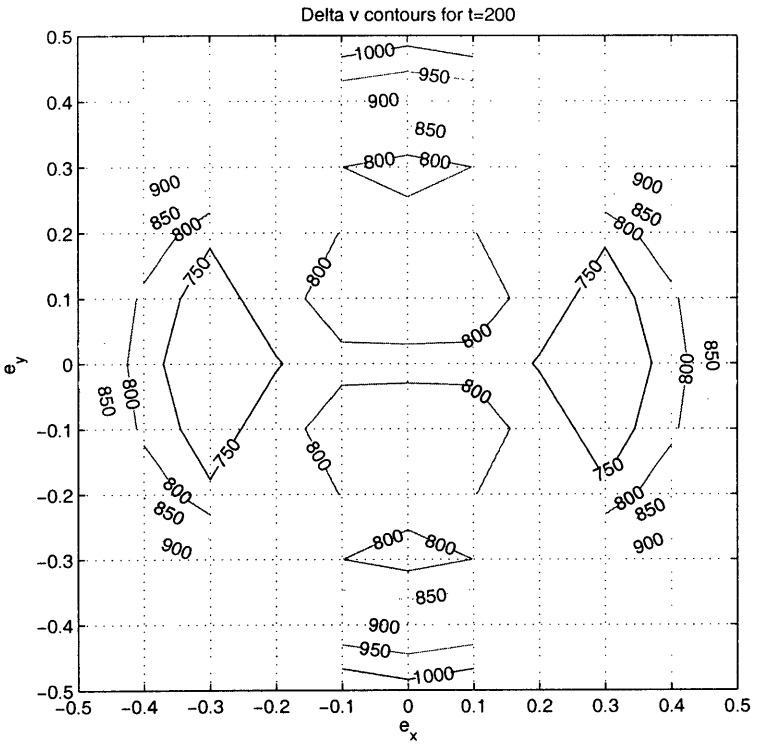

Figure 4-9: Δv contours (m/s) for 200 day trajectories

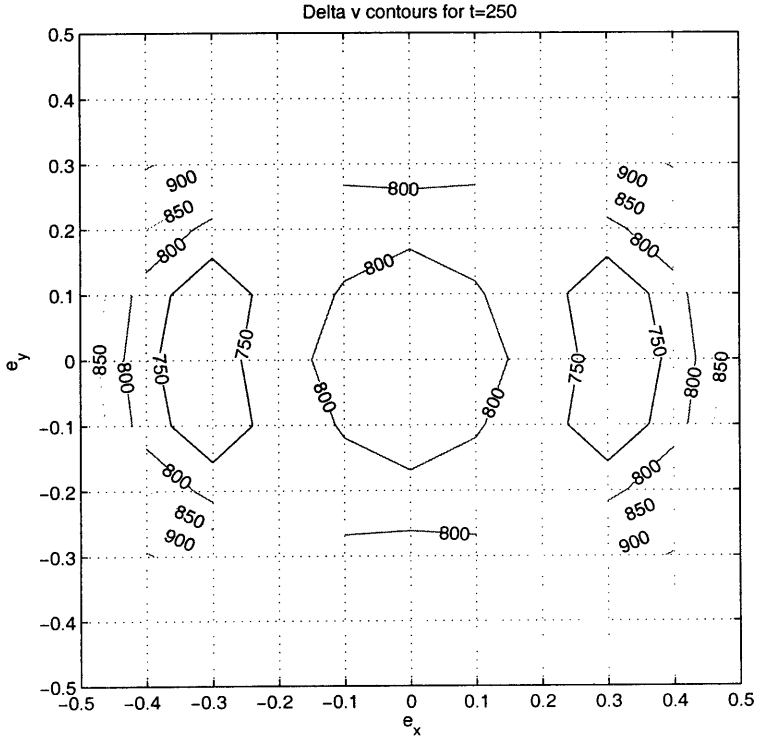

Figure 4-10: Δv contours (m/s) for 250 day trajectories

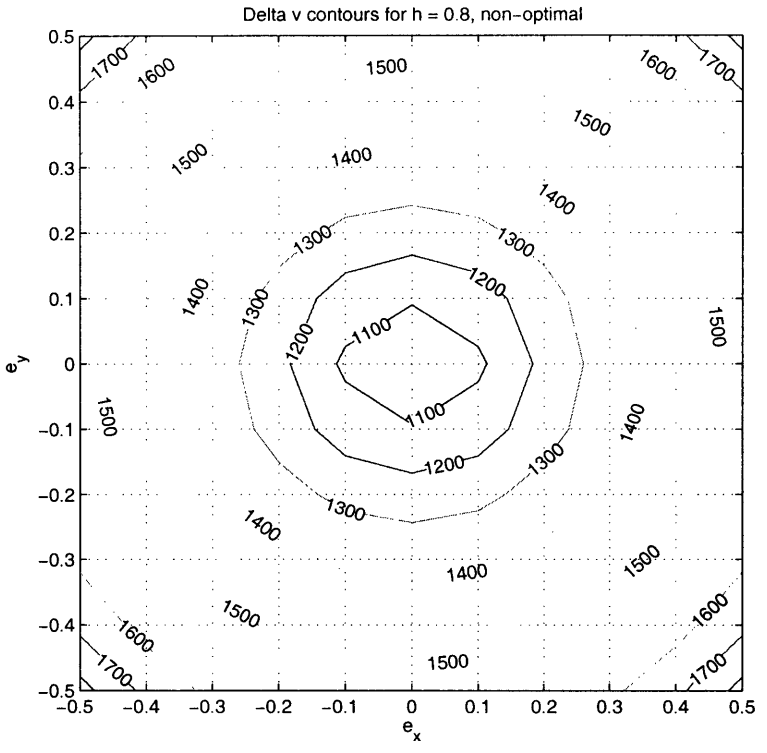

Figure 4-11: Δv contours (m/s) for non-optimal trajectories

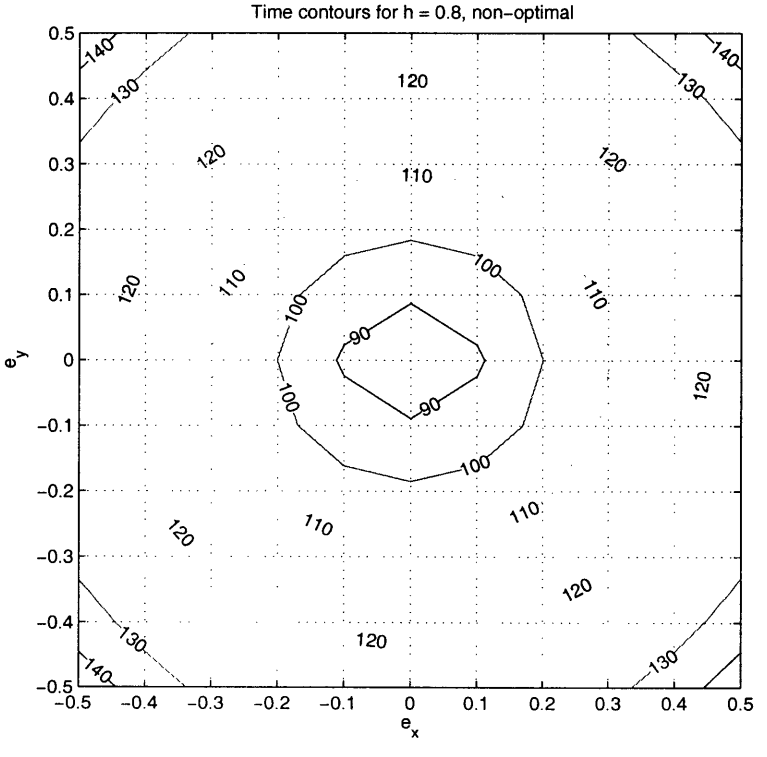

Figure 4-12: Time contours (days) for non-optimal trajectories

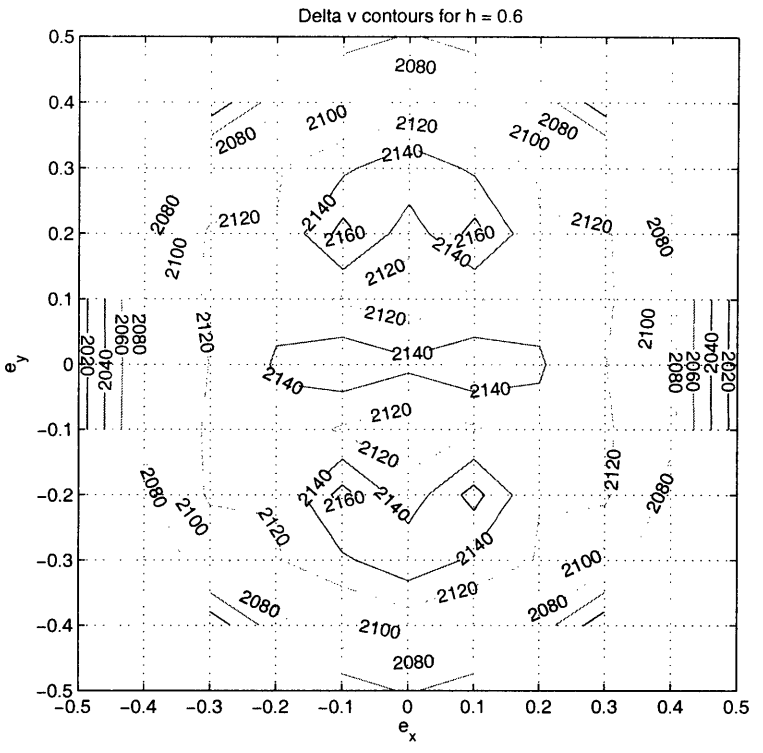

Figure 4-13: Δv contours (m/s) for non-averaged trajectories (h=0.6)

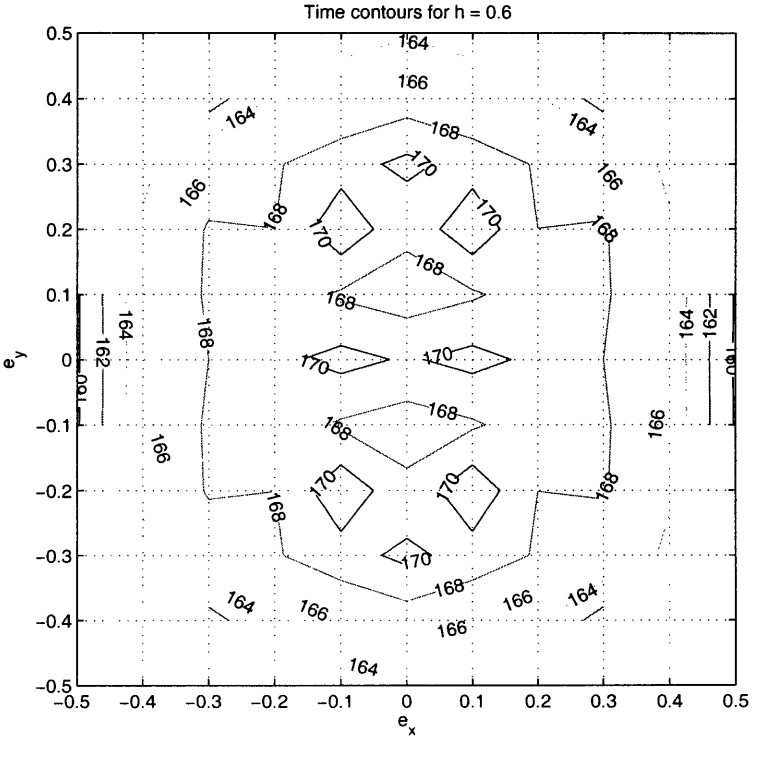

Figure 4-14: Time contours (days) for non-averaged trajectories (h=0.6)

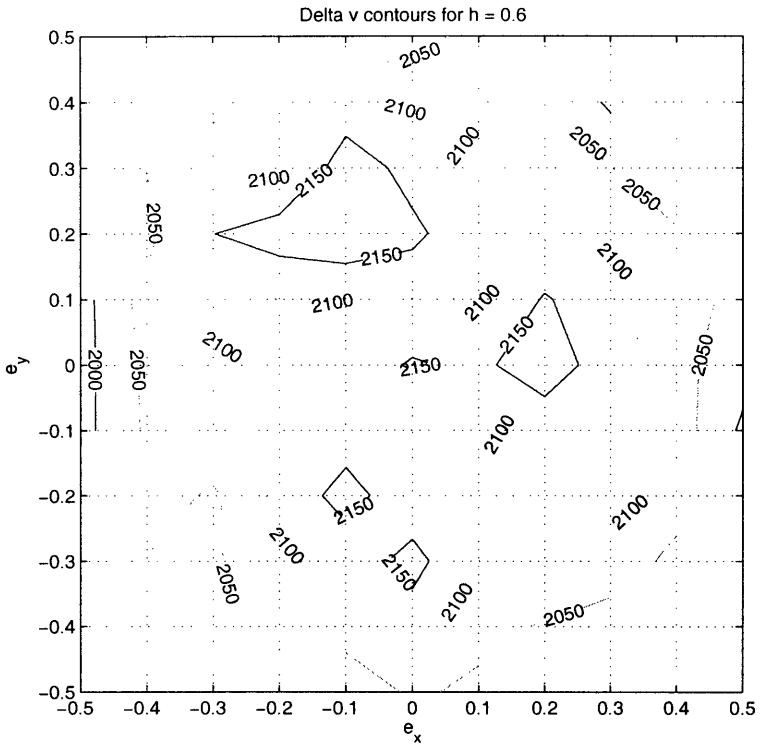

Figure 4-15: Δv contours (m/s) for eclipse control trajectories (h=0.6)

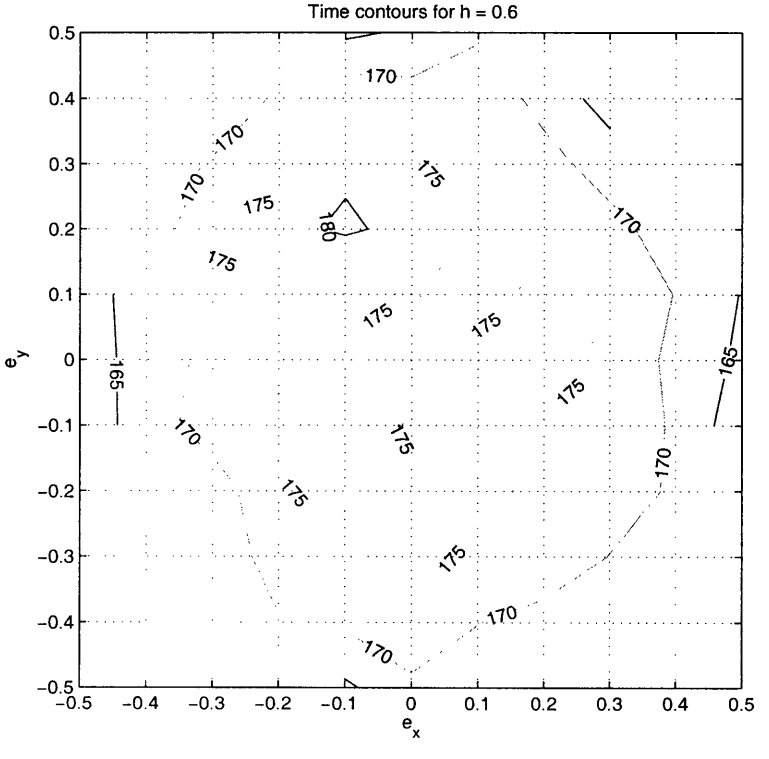

Figure 4-16: Time contours (days) for eclipse control trajectories (h=0.6)

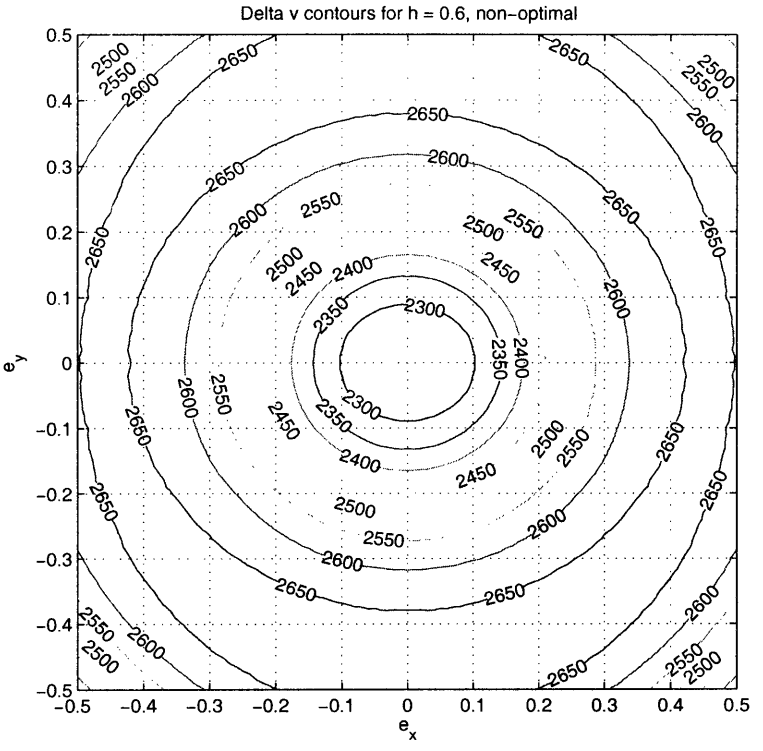

Figure 4-17: Δv contours (m/s) for non-optimal trajectories (h=0.6)

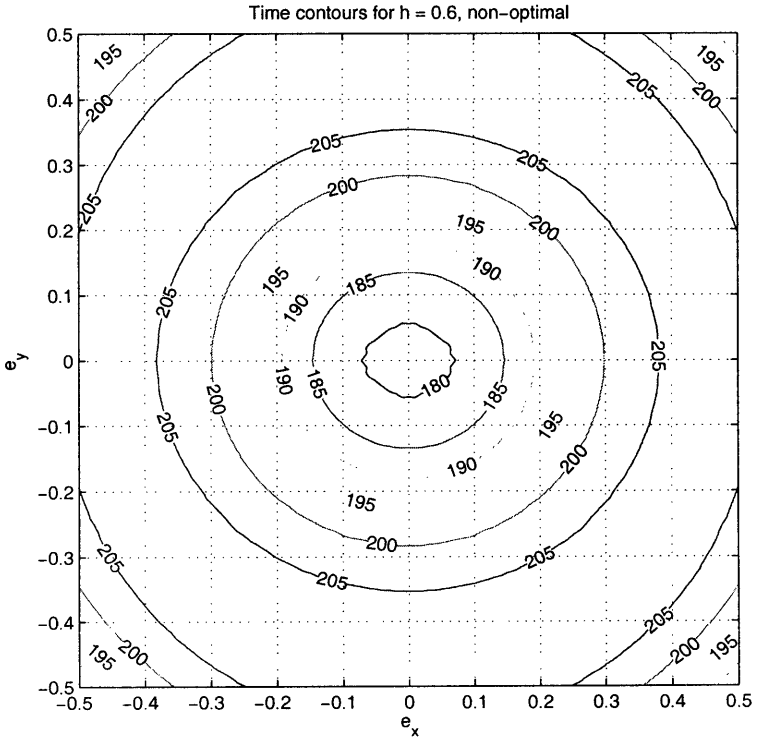

Figure 4-18: Time contours (days) for non-optimal trajectories (h=0.6)

4.1.6 Conclusions

As expected, the non-optimal trajectories take longer and use more fuel than all the other trajectories. This check is useful because the Hamiltonian is a first order optimization method, so it is capable of producing both minimums and maximums. Comparing to a different case proves that the trajectories found here are minimum fuel trajectories.

The averaged trajectories are more stable and therefore produce better graphs, although the results are essentially the same as the non-averaged trajectories. Most of the apparent roughness in the non-averaged graphs comes from the graphing method, and is not real. The interpolation function used to produce the contour plots does not work very well when there is any noise in the data, which is why the graphs appear as rough as they do. The graphing method also means that the Δv's from the graphs are less precise than they appear to be.

The time for the averaged and non-averaged trajectories cannot be directly compared because the integration direction is different. However, the time is proportional to the amount of fuel used because the engine is always on with constant thrust and specific impulse, so the mass flow rate is constant.

At the high starting radius used for most of the results ($h = 0.8$, $p = 0.64 r_{GEO}$), the eclipse periods are small. As a result, the eclipse control has almost no impact on the Δv or time of the transfer. A lower starting radius ($h = 0.6$, $p = 0.36 r_{GEO}$) is used to provide a better comparison. At this lower radius, it is clear that the eclipse control is slower. It is interesting that the eclipse control often uses less fuel. This is surprising because the engine is turned off at odd times that would not generally be expected to reduce the total Δv. The reason that the Δv's are lowered cannot be determined from these graphs, because they do not have enough detail. Examining the trajectories closely provides more information about why the eclipse control provides more fuel efficient trajectories (see section 4.2.2).

Allowing the spacecraft to coast saves large amounts of fuel. The Δv's for the many of the 125 day trajectories are much lower than for the minimum time trajectories. Beyond 125 days, the Δv's do not decrease significantly, which suggests that only a small amount of coasting is necessary to save a lot of fuel. This becomes more clear with some of the trajectory analysis.

4.2 Trajectory Analysis

A small number of selected trajectories have been chosen to show how the orbits change during the transfers.

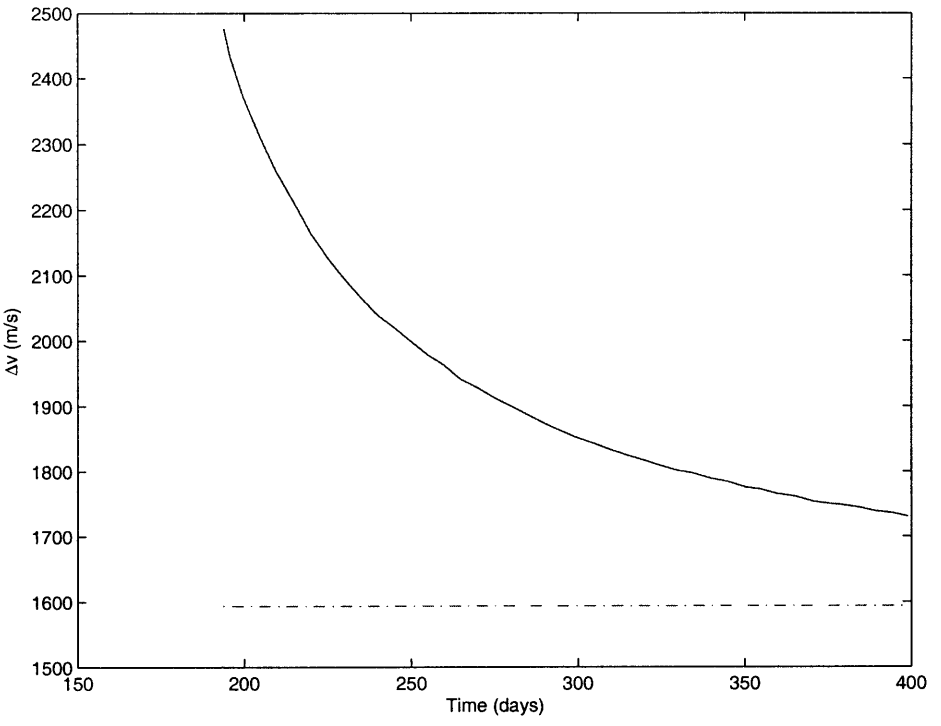

Figure 4-19: Δv as a function of time.

4.2.1 Time Variations

It is interesting to see how the trajectories change as more time is allowed for the transfer. For the minimum time problem, the engine is always on, but as the time is allowed to increase the engine is on for smaller and smaller arcs. As the time is allowed to approach infinity, the arcs eventually become points and the trajectory becomes an impulsive transfer (an infinite time is used to generate the impulses instead of an infinite thrust level). This can be seen in figure 4-19. This graph shows the Δv as a function of time. The line towards the bottom of the graph shows the value of the impulsive Δv.

The graph shows that small amounts of optimal coasting can significantly decrease the fuel requirement for an orbital transfer. About 1/3 of the Δv difference between the minimum time transfer and the impulsive transfer comes from a 10% increase in the transfer time, and about 1/2 of it comes from a 20% increase in transfer time.

A series of transfers are used to show the effect of varying the time. All of these transfers start from what is essentially a geo-transfer orbit (GTO). The initial inclination is 28.7°, which is typical for a launch from Cape Kennedy. The initial apogee is 42,243km, which is the radius needed for GEO. The initial perigee is 12,756km (twice the radius of the Earth), which is above the inner radiation belt, so it should be a good place to start the low-thrust transfer. The alignment between the line of nodes and the line of apses, ω, is varied between 0 and 90 degrees.

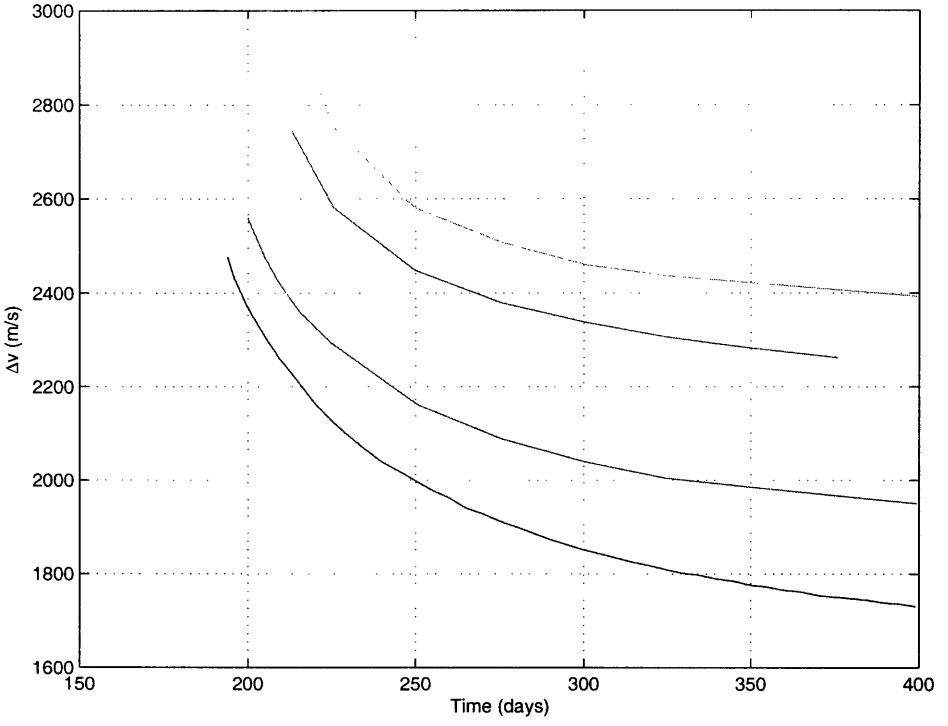

Figure 4-20: Δv as a function of time for GTO like orbits with $\omega = 0$ for the lowest line and in order of increasing Δv, $\omega = 30°$, $\omega = 60°$, and $\omega = 90°$

The Δv as a function of the transfer time is shown in figure 4-20. The bottom line corresponds to $\omega = 0$, and the other lines going up correspond to $\omega = 30°$, $\omega = 60°$, and $\omega = 90°$. As expected, a misalignment of the line of nodes and the line of apses leads to an increase in the Δv. The shape of all the lines is essentially the same. What is interesting is that most of the drop in Δv comes quickly. This means that significant decreases in Δv can be obtained with relatively small coasting periods. The general trend is that the total Δv drops about 10% for a 10% increase in transfer time. The impulsive Δv is only about a 30% decrease for the $\omega = 0$ case, which means that 1/3 of the possible Δv savings is obtained with only a 10% increase in transfer time.

The trajectory for the minimum time, $\omega = 0$, problem is shown in figures 4-21 and 4-22. The minimum time to complete the transfer is 193.88 days.

The trajectory for a 400 day, $\omega = 0$ transfer is shown in figures 4-23 and 4-24. This is a fairly long transfer, and the trajectory is beginning to take on the shape of the impulsive transfer[1].

Figure 4-25 shows several of the trajectories overlapped. The timescale has been normalized for each trajectory to go from 0 to 1. This shows that the perigee increases at about the same normalized rate regardless of how slowly the transfer is done. The peak in the apogee radius decreases as more time is taken, approaching the flat apogee line of the impulsive transfer trajectory. This is a general

[1]For the impulsive transfer, the apogee radius is constant while the inclination decreases and the perigee radius increases

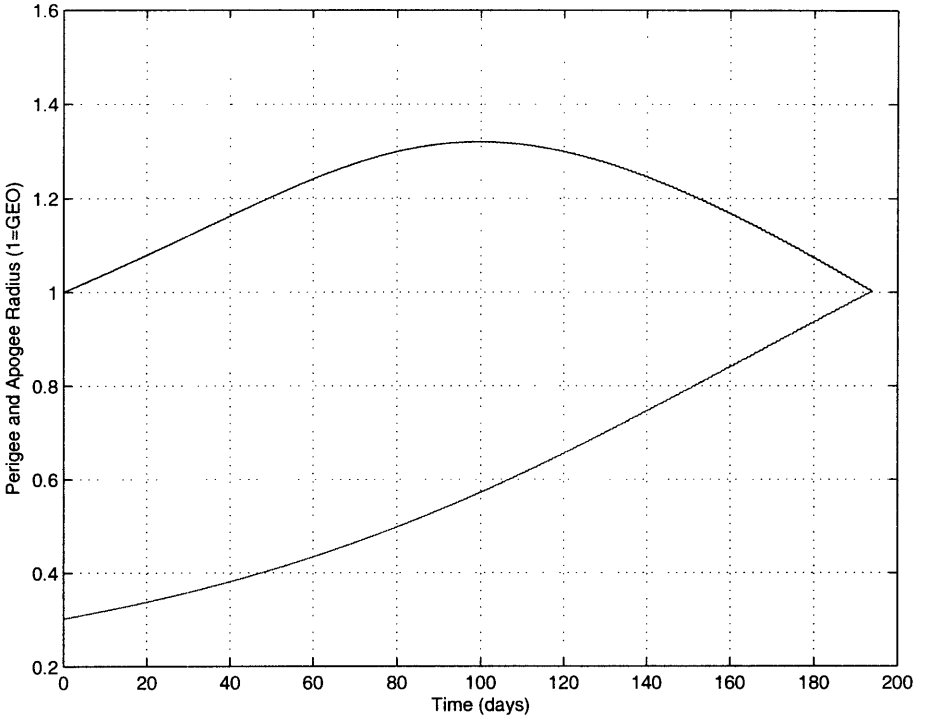

Figure 4-21: Perigee and apogee during the minimum time transfer

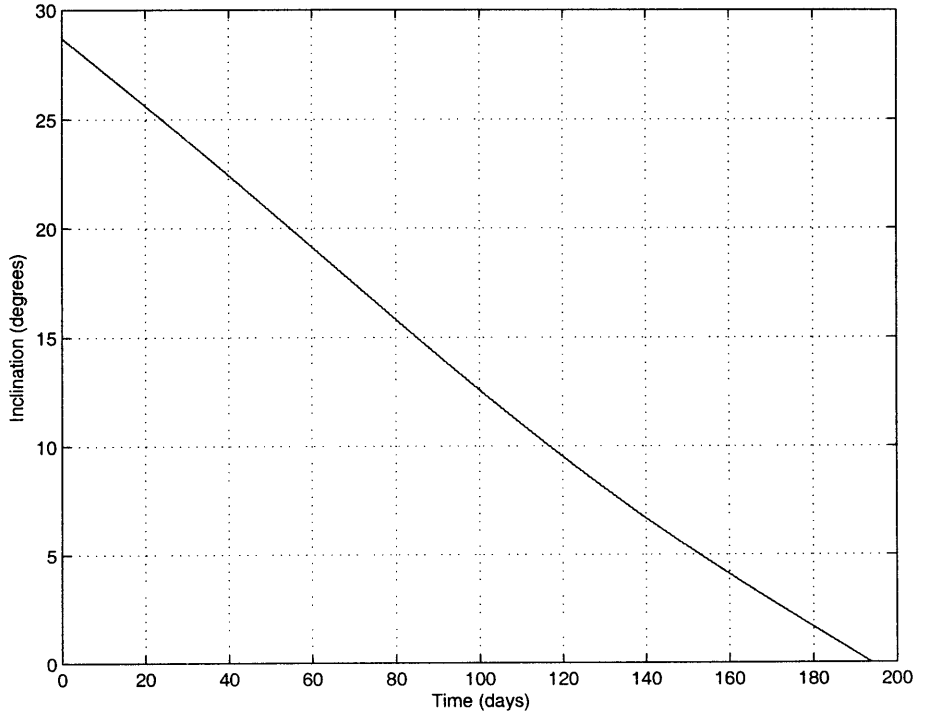

Figure 4-22: Inclination during the minimum time transfer

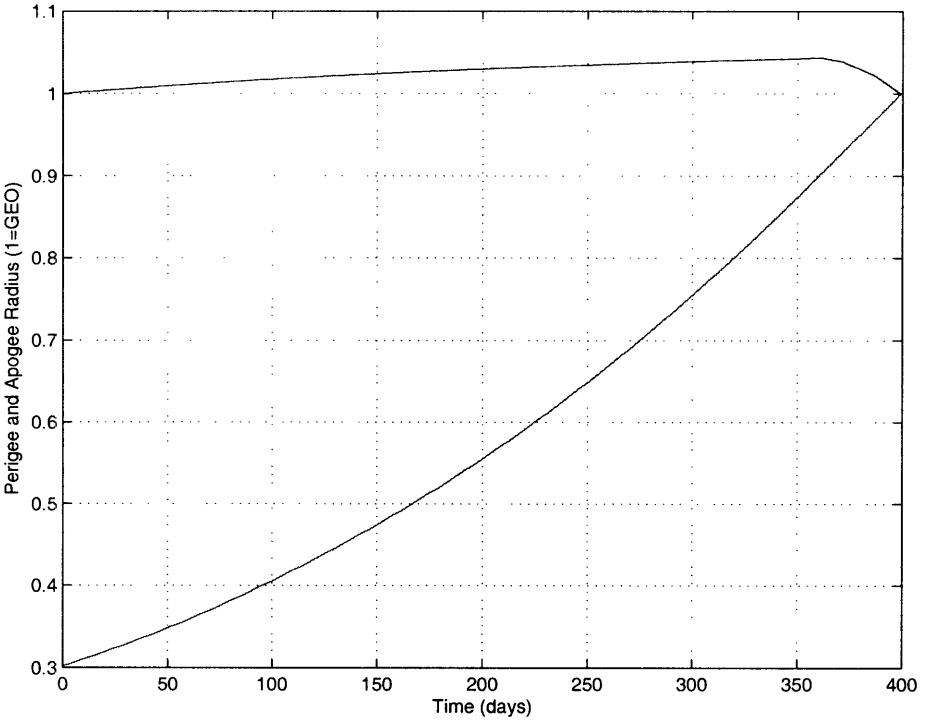

Figure 4-23: Perigee and apogee during the 400 day transfer

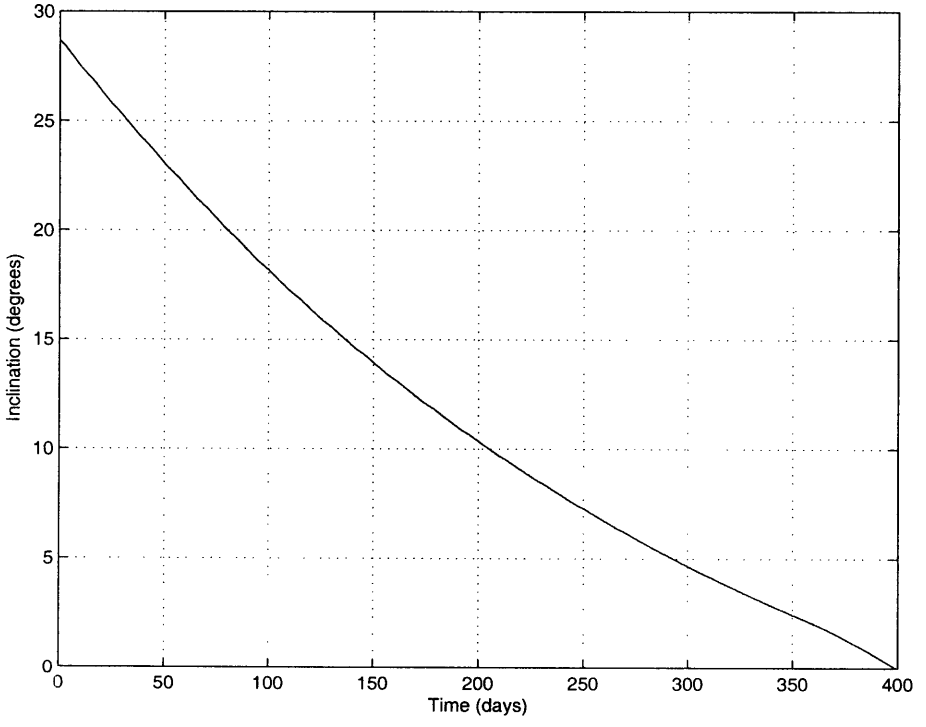

Figure 4-24: Inclination during the 400 day transfer

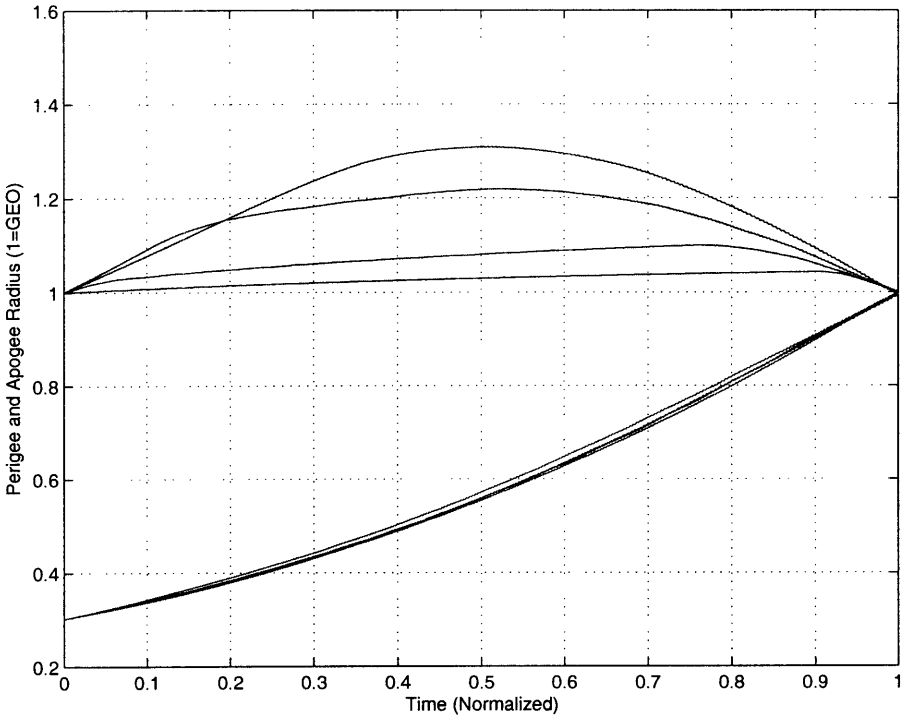

Figure 4-25: Perigee and apogee during several transfers

trend which is also seen in other transfers. For transfers that start with apogee below GEO, the apogee radius is increased quickly to GEO at the beginning of the transfer regardless of the transfer time. After the apogee is raised to the final radius, it continues to rise in a somewhat similar manner to that which is seen in figure 4-25, with more peaking for faster transfers.

It is also interesting to loook at how ϖ and Ω vary if the line of nodes and line of apses are initially misaligned. For this purpose, another family of initial orbits was analyzed. These orbits are similar to the GTO orbits, except that the apogee radius is 0.8GEO instead of GEO. They will be referred to as medium orbits.

The graphs showing ϖ and Ω require some explanation, as they are not common graphs. There are two lines on each graph. One of the lines shows the magnitude and direction of the eccentricity vector (e_x, e_y). The other line shows the magnitude and direction of the inclination vector (i_x, i_y). The lines approach the origin because all of the transfers are going to GEO, which has no eccentricity or inclination. The time scale cannot be determined from these graphs. This method is preferred over graphing the angles ϖ and Ω directly because the angles become meaningless as the magnitude of the vectors approach 0, which cannot be seen on a plot of just the angles. In these plots, ϖ is the angle from the origin to the eccentricity line, and Ω is the angle from the origin to the inclination line. The inclination line always starts with i_x positive and $i_y = 0$, which corresponds to $\Omega = 0$.

For the minimum time transfers, ϖ remains almost unchanged. It moves slightly towards 0,

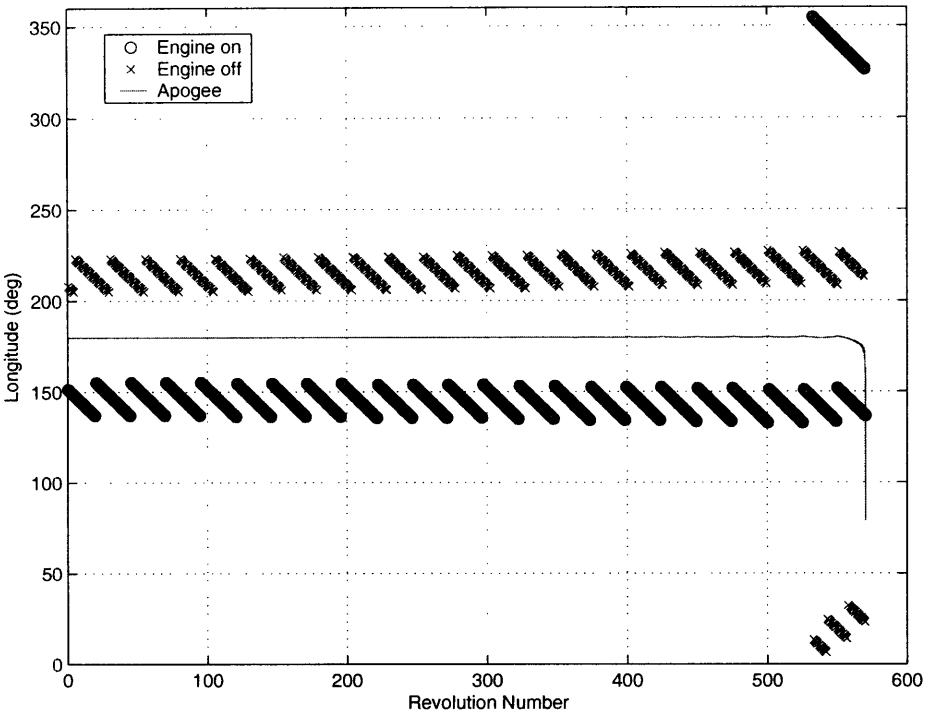

Figure 4-26: Engine turn-on and turn-off points for the GTO orbit with $\omega = 0$, 400 day transfer time. Engine is on for a narrow band around apogee for most of the transfer, then it also turns at perigee at the end of the transfer.

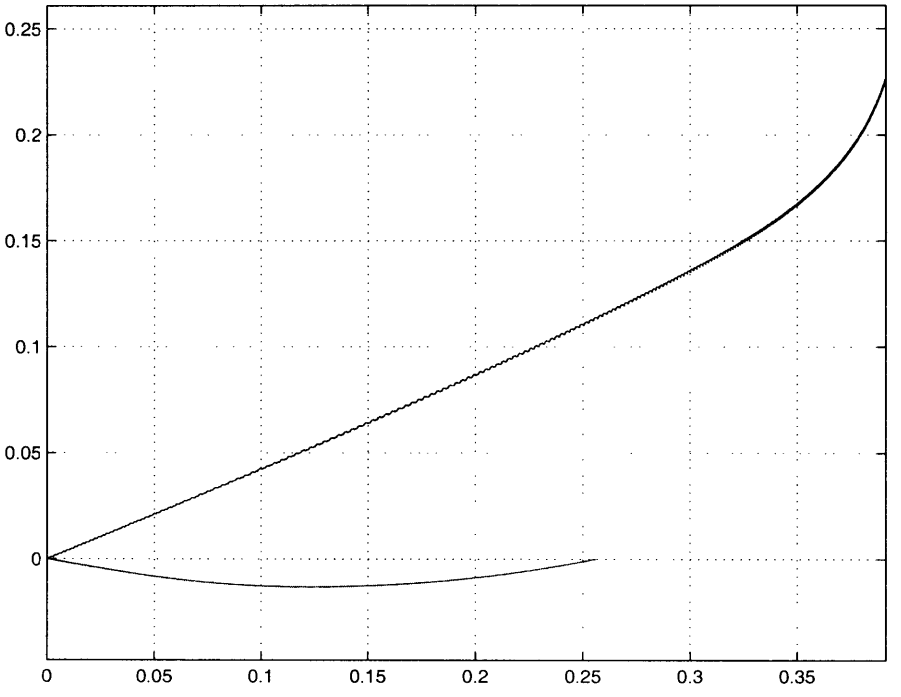

Figure 4-27: Graph of the eccentricity and inclination vectors for a minimum time (215 day) transfer with $\omega_0 = 30°$. Top line is eccentricity, bottom line is inclination.

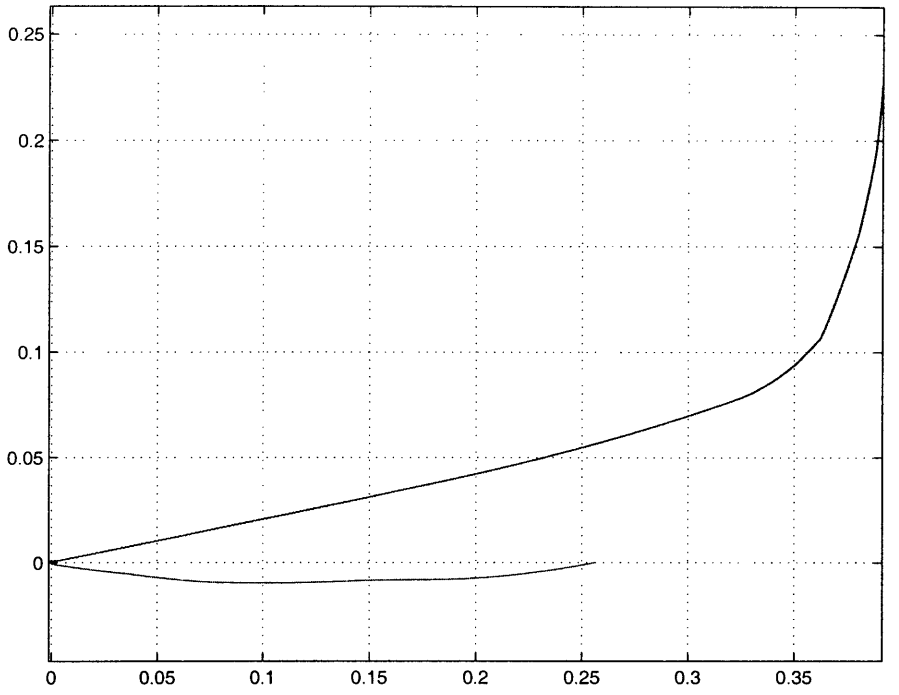

Figure 4-28: Graph of the eccentricity and inclination vectors for a 300 day transfer with $\omega_0 = 30°$. Top line is eccentricity, bottom line is inclination.

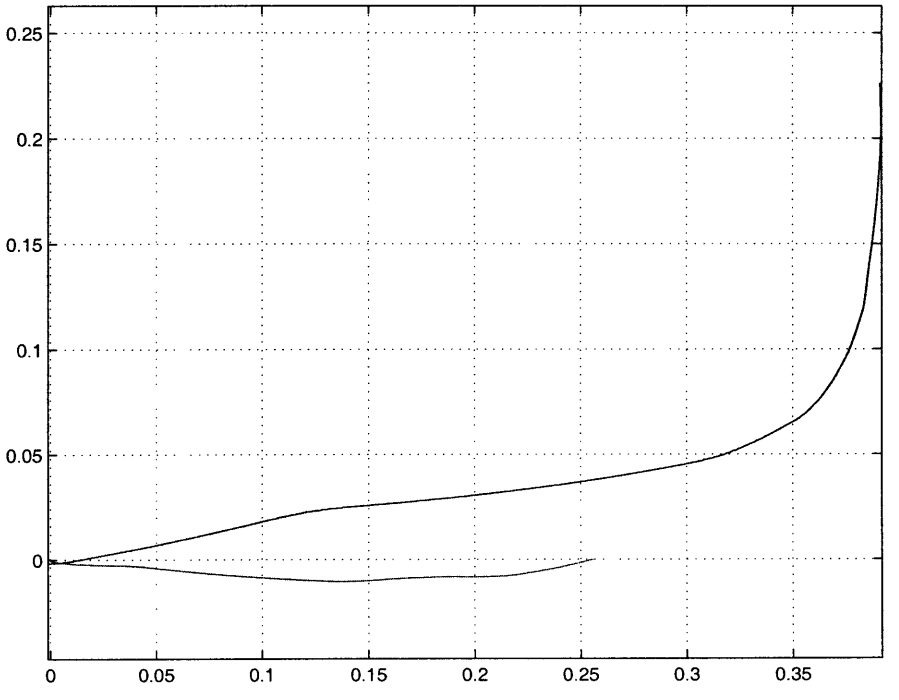

Figure 4-29: Graph of the eccentricity and inclination vectors for a 400 day transfer with $\omega_0 = 30°$. Top line is eccentricity, bottom line is inclination.

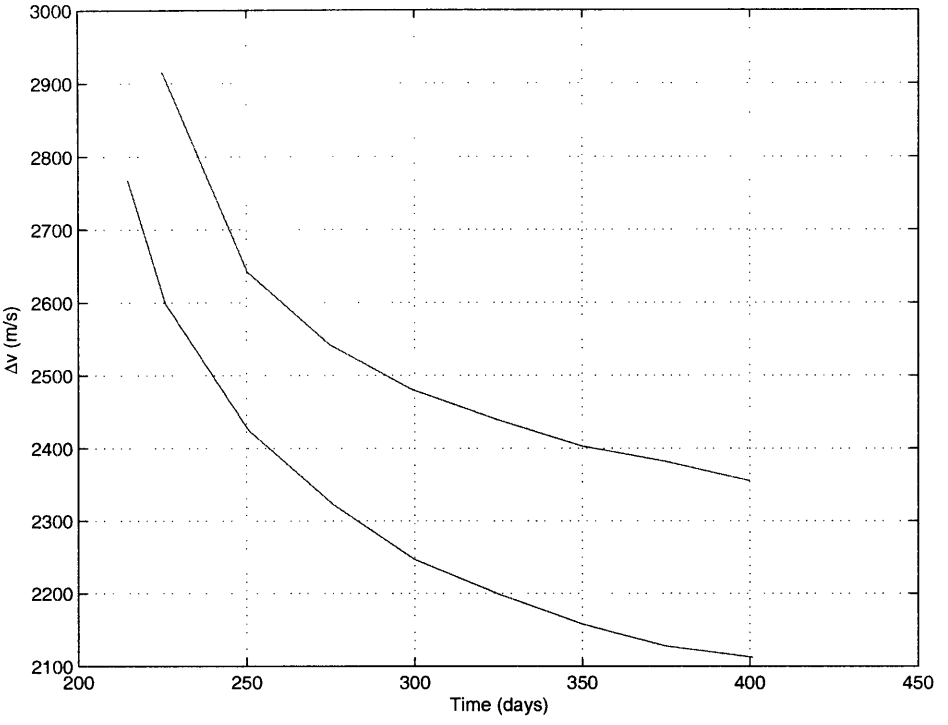

Figure 4-30: Δv vs. time for $h = 0.66$, $e = .45$. Bottom line is $\omega = 30°$. Top line is $\omega = 60°$

which indicates that the direction to perigee is rotating towards the line of nodes, but does not change significantly. This is shown in figure 4-27.

As the time increases, the line of apses moves closer and closer to the line of nodes. This can be seen by looking at figures 4-28 and 4-29, which show 300 and 400 day transfers. This implies that bringing the two vectors into alignment allows enough fuel savings to justify rotating the line of apses.

The Δv vs time graph for these orbits is shown in figure 4-30

It is also useful to examine the coasting periods of these orbits. The GTO orbits did not need their apogees raised, so they could coast through perigee without any problems. The medium orbits need their apogees raised and their inclination lowered. These competing goals lead to rather different coasting periods. The Δv graph shows that the Δv drops slightly faster for the medium orbits than for the GTO orbits. The faster drop is due to the competing requests for thrust. The competing requests will cause the components of A to point in different directions for some parts of the orbit, which reduces the effectiveness of the thrusting. This means that short coasting periods will have a large impact on the total Δv.

The coasting profile graphs have step changes in the coasting angles due to the integration method used. If the steps sizes were infinitely small, the on/off transitions would be smooth lines. The apparent steps are not real. The graphs show where the engine turns on and off, as well as ϖ,

the direction to perigee. The vertical axis shows the angle within each orbit, and the horizontal axis shows the number of orbits that have been completed, which is a measure of how much time has been put into the transfer.

The coasting profile for $\omega_0 = 30°$ with a 300 day transfer is shown in figure 4-31. There is a brief coasting period after perigee in the early phase of the mission. This band expands backwards to include apogee until there is only thrusting for a narrow band around apogee. At the end, thrusting at perigee is done again.

The coasting profile for $\omega_0 = 30°$ with a 400 day transfer is shown in figure 4-32. There is a coasting period after perigee in the early phase of the mission. Then a small amount of coasting is added after apogee. The coasting period near perigee expands backwards to include apogee until there is only thrusting for a narrow band around apogee. At the end, a small amount of thrusting at perigee is done again.

The coasting profile for $\omega_0 = 60°$ with a 300 day transfer is shown in figure 4-33. The spacecraft coasts from a little before perigee until about halfway between perigee and apogee for the early phase of the mission. A brief coasting period is added after apogee about halfway through. The perigee coasting period moves with perigee, but does not grow or shrink significantly. The apogee coasting period grows as the mission continues.

The coasting profile for $\omega_0 = 60°$ with a 400 day transfer is shown in figure 4-34. The spacecraft is coasting from a little before perigee until about halfway to apogee towards the beginning of the transfer. Then a small coasting period is added shortly after apogee, which expands as the mission continues and eventually combines with the perigee coasting period. The perigee coasting period shrinks towards the end of the mission and does not include perigee at the end of the mission.

All of these mission plans have a few things in common. They all start coasting near perigee early in the mission, and continue to coast near perigee for almost the entire mission. This is because thrusting at a low radius is inefficient, so the optimization removes the low-radius thrusting around perigee first. The maximum inclination change comes from thrusting at the line of nodes, which is around 0° and 180° for all these missions. This contributes to moving the thrust away from perigee and apogee and towards the line of nodes. Thrusting in alignment with the line of nodes instead of the line of apses spins the line of apses towards the line of nodes.

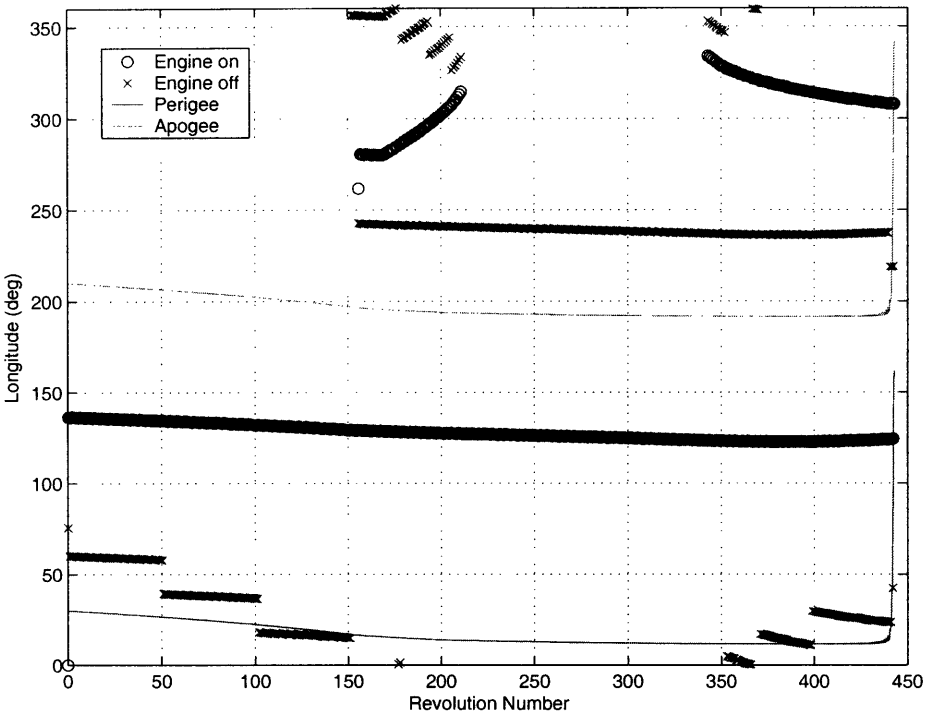

Figure 4-31: Engine turn-on and turn-off points for $h = 0.66$, $e = .45$, $\omega = 30$ with 300 day transfer time.

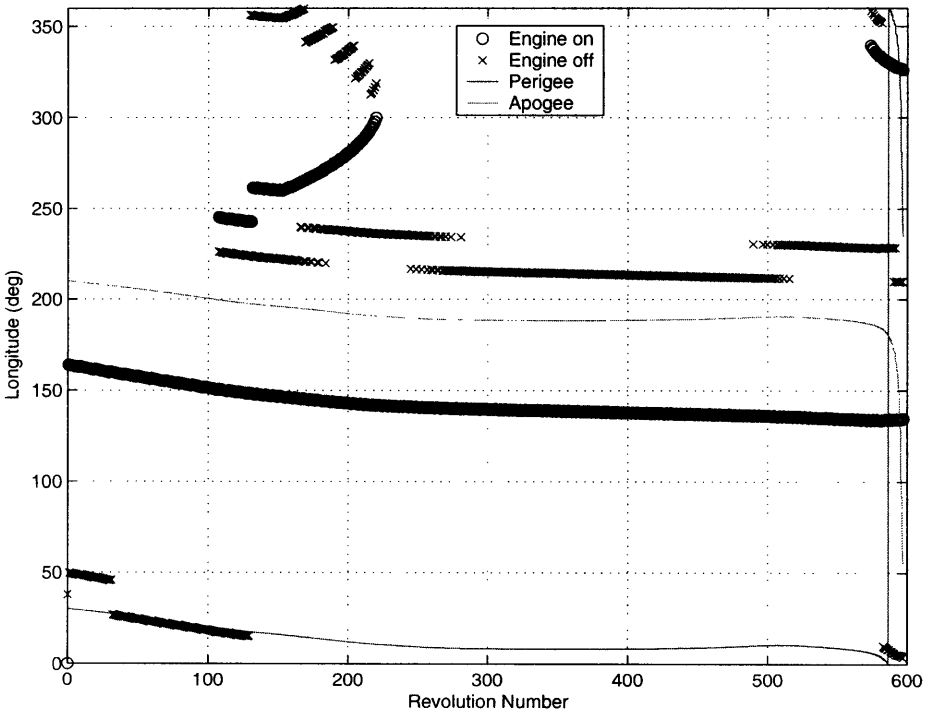

Figure 4-32: Engine turn-on and turn-off points for $h = 0.66$, $e = .45$, $\omega = 30$ with 400 day transfer time.

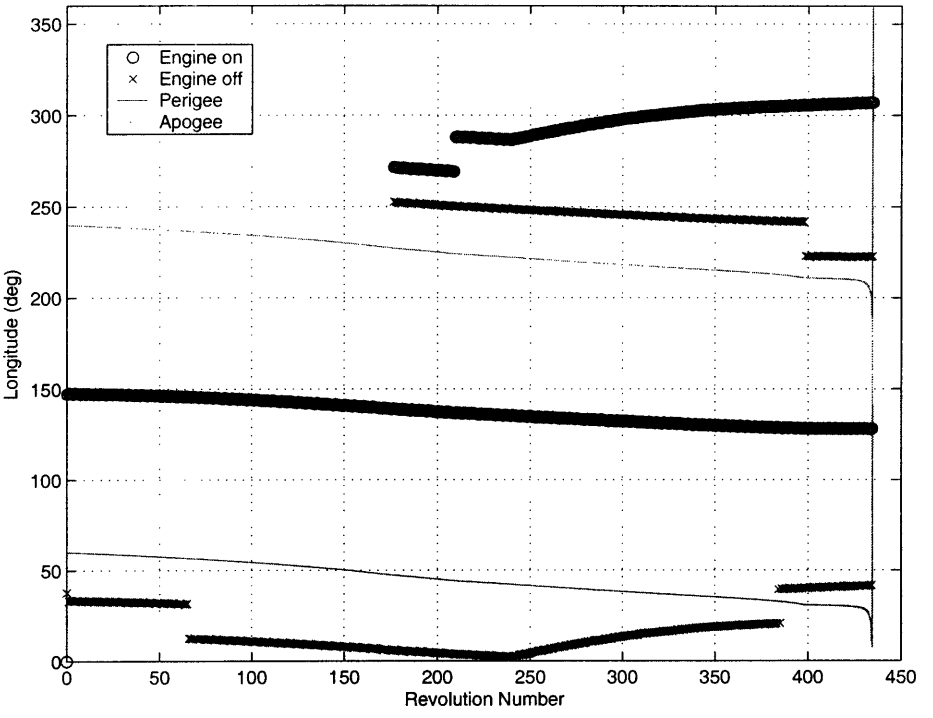

Figure 4-33: Engine turn-on and turn-off points for $h = 0.66$, $e = .45$, $\omega = 60$ with 300 day transfer time.

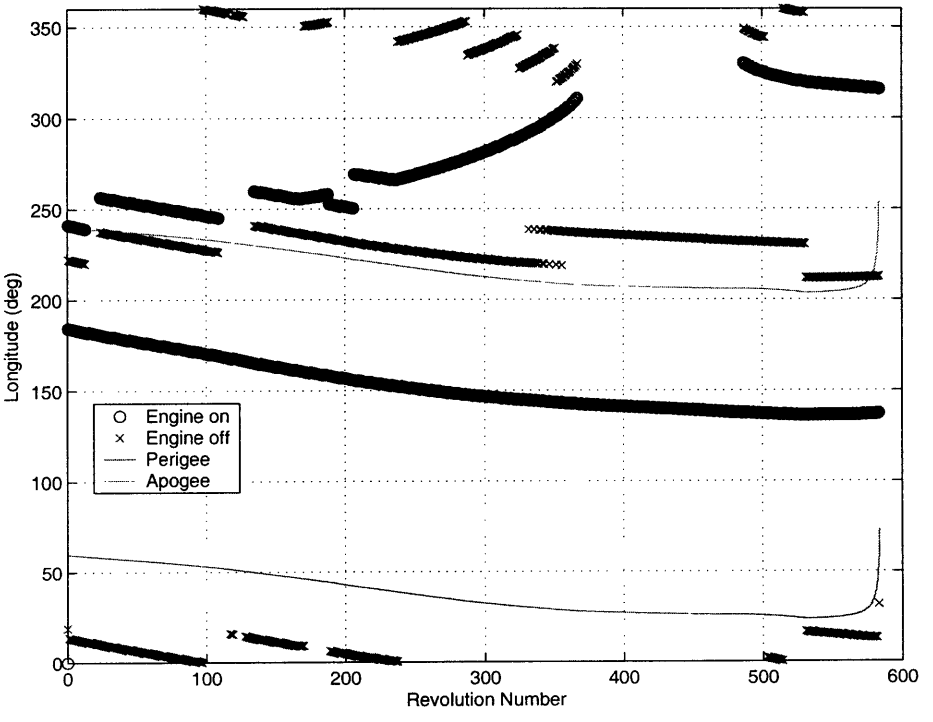

Figure 4-34: Engine turn-on and turn-off points for $h = 0.66$, $e = .45$, $\omega = 60$ with 400 day transfer time.

4.2.2 Eclipse Control

By comparing figures 4-13 and 4-14 to figures 4-15 and 4-16, it can be seen that using eclipse control reduces the Δv in almost all cases and always takes longer. Three orbital transfers were selected to show the impact of using eclipse control. The initial orbits are described in table 4.1. In all cases, $i_y = 0$, so the longitude of the ascending node is at 0°. The sun starts in the $-x$ direction (the x direction goes from the Sun to the Earth), and the transfer starts at vernal equinox.

In order to provide a useful comparison, the transfers from the selected orbits were calculated for the minimum-time case and for the optimal coasting with the same total transfer time as the eclipse control case. Table 4.2 shows the total Δv and transfer tiem for all three control methods and all three orbits.

For the first orbit, the Δv actually increases due to eclipse control by 1.3%. The transfer time also increases by about 5.1%. With the same time increase, optimal coasting leads to an 8% decrease in Δv. Looking at the engine turn-on and turn-off times in figures 4-35 and 4-36 suggest that the reason that the Δv increases is that the eclipse periods are towards the beginning of the transfer and near apogee, while the optimal coasting periods are towards the end of the transfer and near perigee. Comparing the evolution of the orbital elements shows that all three control methods go through about the same orbital trajectory. The trajectory is included in figure 4-41. All three control methods are shown, but there is not a significant difference between them.

For the second orbit, the Δv decreases due to eclipse control by 0.9%. The transfer time increases by about 1.3%. This is clearly a much better case for eclipse control, as the time increases much less and the Δv actually decreases. However, the decrease in Δv is still not as good as with optimal coasting for the same time increase, which decreases the Δv by 3.5%. Looking at the engine turn-on and turn-off times in figures 4-37 and 4-38 suggest that the reason that the Δv decreases is that the eclipse periods are towards the beginning of the transfer near perigee, and there is almost a small amount of overlap between the final eclipse periods and the initial optimal coasting periods. Comparing the evolution of the orbital elements shows that all three control methods go through about the same orbital trajectory. The trajectory is included in figure 4-42. All three control methods are shown, but there is not a significant difference between them.

For the third orbit, the Δv decreases due to eclipse control by 0.3%. The transfer time increases by about 1.3%. The Δv still decreases, but not by as much as in the second case, despite the similar increases in time. Furthermore, with optimal coasting, the Δv decreases by 6.9%, which is more than the decrease for the second orbit. This means that eclipse control is actually much worse for the third orbit than the second one. Looking at the engine turn-on and turn-off times in figures 4-37 and 4-38 suggest that the reason that the Δv decreases is that the eclipse periods are towards the beginning of the transfer near perigee, and there is almost a small amount of overlap between the final eclipse periods and the initial optimal coasting periods. The reason it is not as good as the

number	h	e_x	e_y	i
1	0.6	-0.2	0.2	5°
2	0.6	-0.5	0	5°
3	0.6	-0.35	-0.35	5°

Table 4.1: Orbits selected to show the impact of eclipse control

	Δv (km/s)				Transfer Time (days)		
number	min-time	eclipse	eclipse-time	number	min-time	eclipse	eclipse-time
1	2.1411	2.1697	1.9712	1	169	178	178
2	2.0366	2.0174	1.9640	2	162	164	164
3	2.0410	2.0353	1.9213	3	162	166	166

Table 4.2: Δv's and transfer times for the transfers using minimum time, eclipse control, and optimal coasting with time equal to the eclipse control time.

second case is that the eclipse periods are not as close to being centered around perigee. Comparing the evolution of the orbital elements shows that all three control methods go through about the same orbital trajectory. The trajectory is included in figure 4-43. All three control methods are shown, but there is not a significant difference between them.

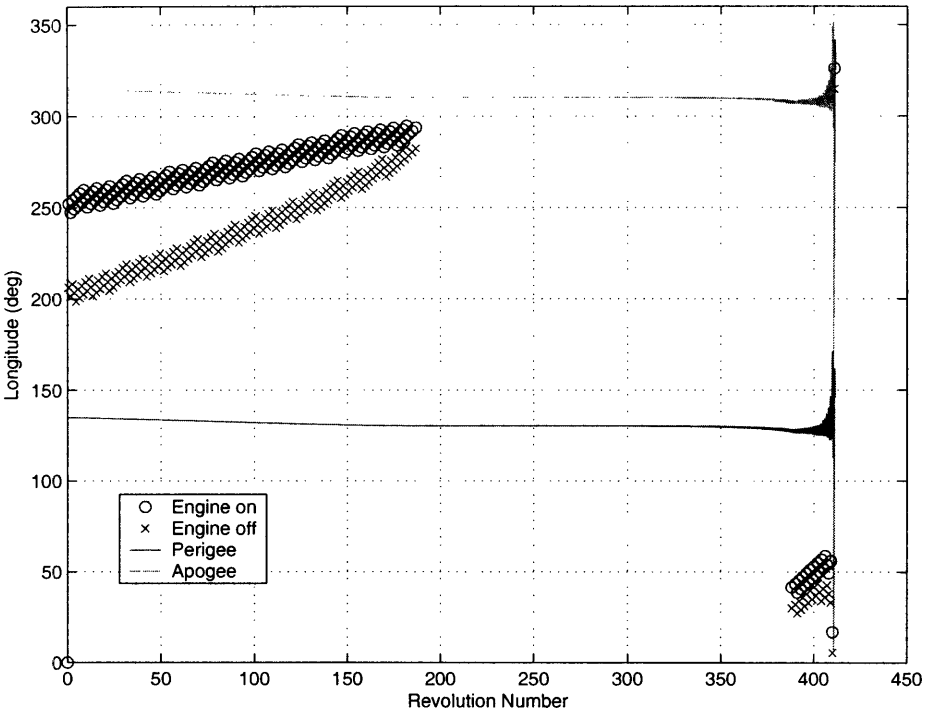

Figure 4-35: Engine turn-on and turn-off points for the first orbit, eclipse control case. The engine is off between the two bands. Perigee is at 135° at the beginning of the transfer.

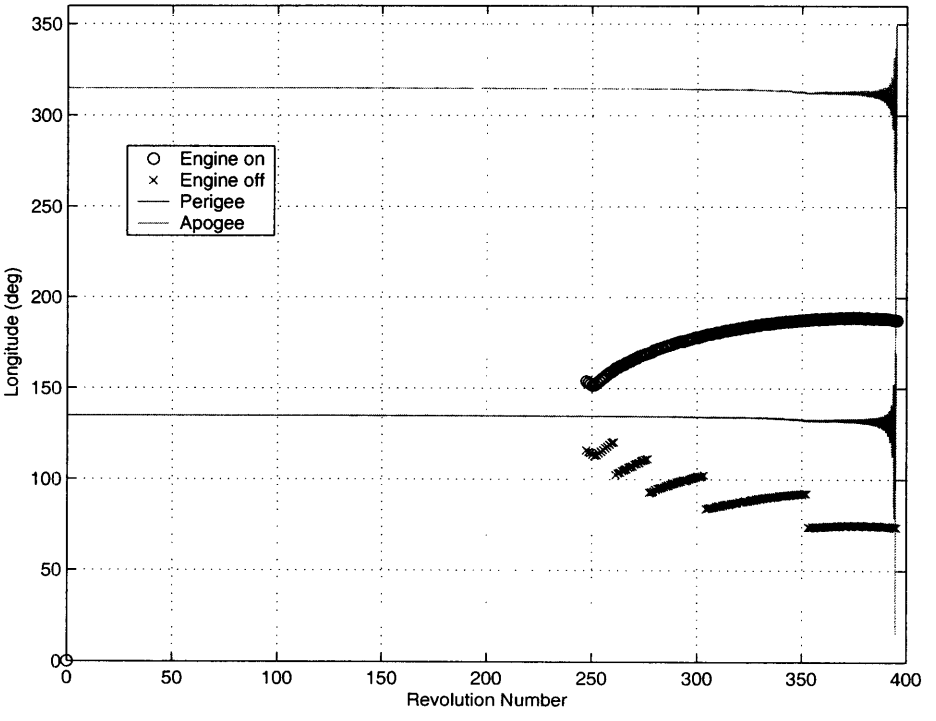

Figure 4-36: Engine turn-on and turn-off points for the first orbit, optimal coasting control case. The engine is off around perigee at the end of the transfer. Perigee is at 135° at the beginning of the transfer.

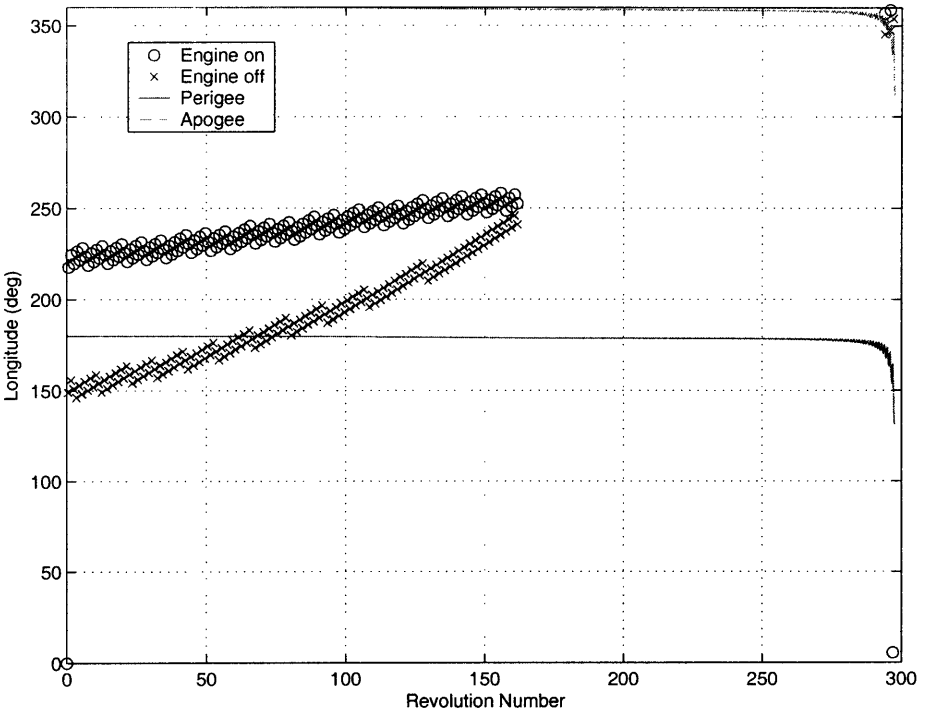

Figure 4-37: Engine turn-on and turn-off points for the second orbit, eclipse control case. The engine is off between the two bands. Perigee is at 180° at the beginning of the transfer.

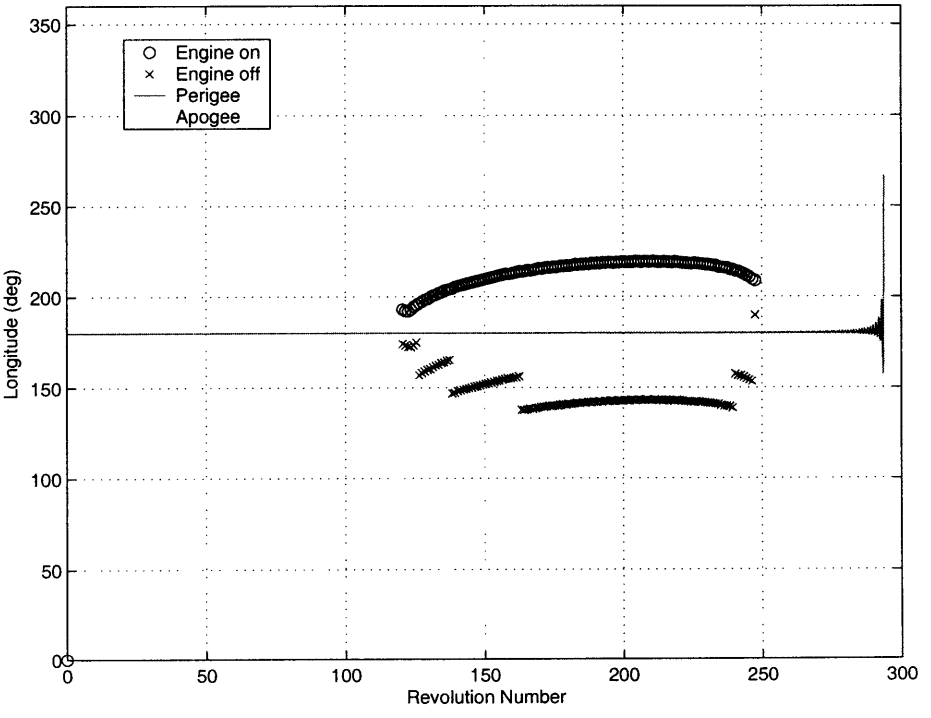

Figure 4-38: Engine turn-on and turn-off points for the second orbit, optimal coasting control case. The engine is off around perigee towards the late part of the transfer, but not all the way to the end. Perigee is at 180° at the beginning of the transfer.

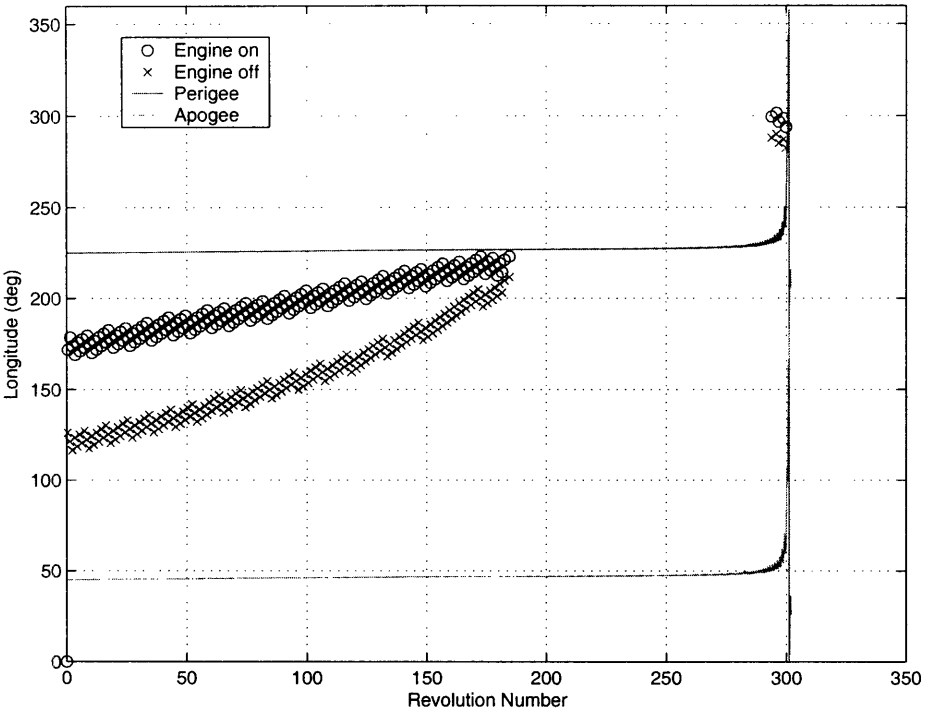

Figure 4-39: Engine turn-on and turn-off points for the third orbit, eclipse control case. The engine is off between the two bands. Perigee is at 225° at the beginning of the transfer.

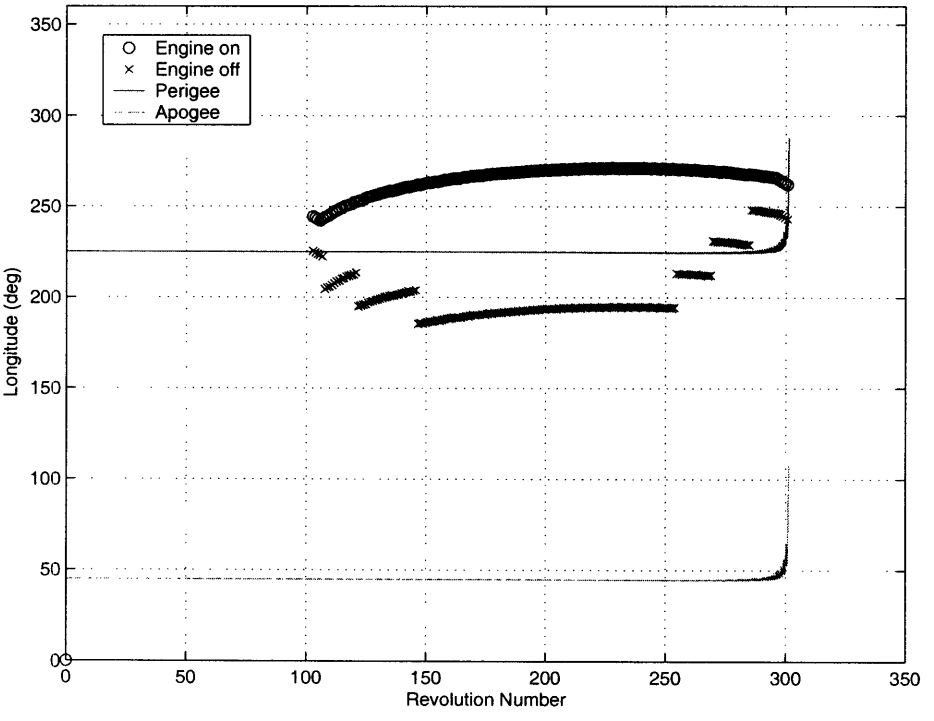

Figure 4-40: Engine turn-on and turn-off points for the third orbit, optimal coasting control case. The engine is off around perigee towards the end of the transfer. Perigee is at 225° at the beginning of the transfer.

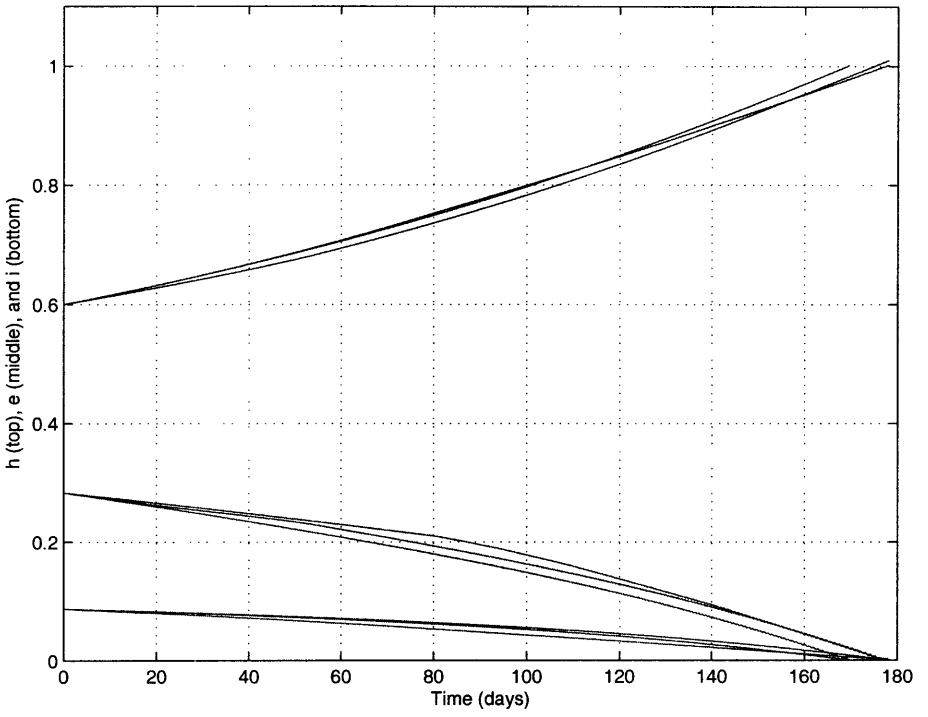

Figure 4-41: Trajectories for the first orbital transfer. The top set of lines is h, the middle set is e, and the bottom set is i.

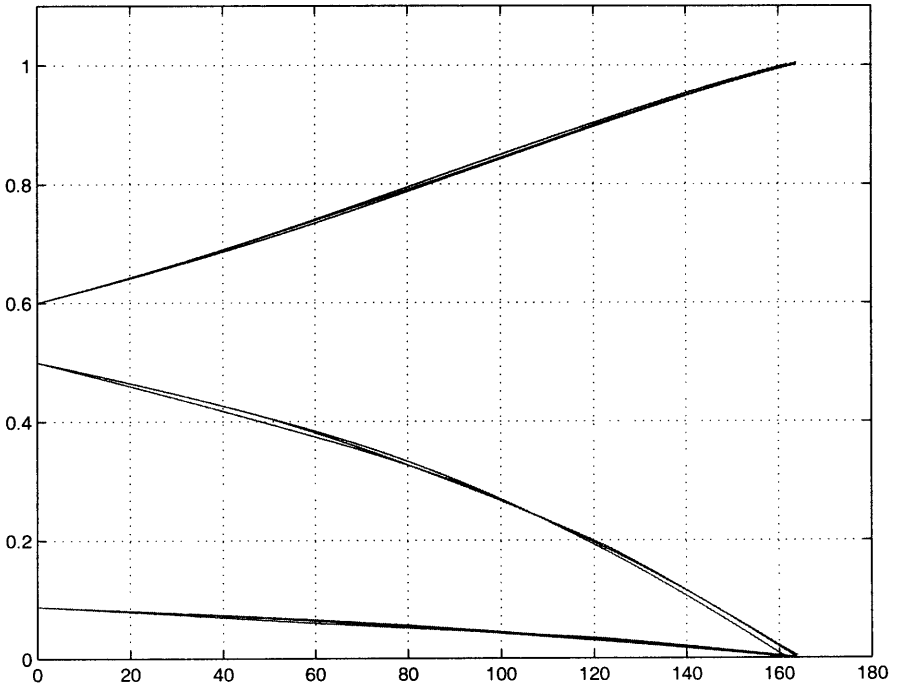

Figure 4-42: Trajectories for the second orbital transfer. The top set of lines is h, the middle set is e, and the bottom set is i.

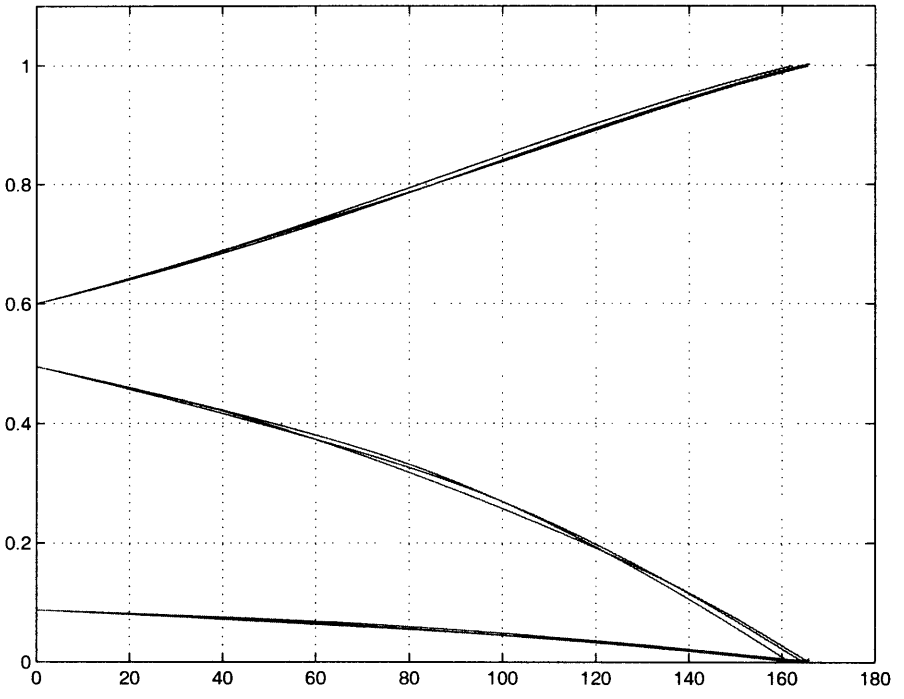

Figure 4-43: Trajectories for the third orbital transfer. The top set of lines is h, the middle set is e, and the bottom set is i.

Appendix A

Derivation of Equinoctial Orbital Elements

This appendix is provided for reference only. The equations derived here are the standard equations for the equinoctial elements, and are derived in many texts on orbital dynamics

A.1 Notation

The notation in this appendix differs in some ways from the notation used in the rest of this thesis. In this appendix, the following symbols have these meanings:

h'	The modified angular momentum $\sqrt{p/\mu}$
h	The standard angular momentum $\sqrt{\mu p}$
e'_x	The eccentricity in the projected x direction $(e\cos(\omega+\Omega))$
e'_y	The eccentricity in the projected y direction $(e\sin(\omega+\Omega))$
e_x, e_y, and e_z	The eccentricity vector in the absolute x, y, and z directions

A.2 Basic Theory

The basic equation of orbital motion is

$$\frac{d\mathbf{v}}{dt} = -\frac{\mu}{r^3}\mathbf{r} \tag{A.1}$$

some manipulation on this shows that

$$\frac{d}{dt}(\mathbf{r}\times\mathbf{v}) = \frac{d\mathbf{r}}{dt}\times\mathbf{v} + \mathbf{r}\times\frac{d\mathbf{v}}{dt} \tag{A.2}$$

$$= \mathbf{v} \times \mathbf{v} + \mathbf{r} \times \frac{d\mathbf{v}}{dt} \tag{A.3}$$

$$= \mathbf{r} \times \frac{d\mathbf{v}}{dt} \tag{A.4}$$

$$= \mathbf{r} \times \left(-\frac{\mu}{r^3}\right)\mathbf{r} \tag{A.5}$$

$$= 0 \tag{A.6}$$

which means that $\mathbf{r} \times \mathbf{v}$ is a constant until thrust or other disturbing forces are applied. This provides a convenient vector which defines part of the orbit. The vector defined by this term is the massless angular momentum, so the symbol $\mathbf{h}$ is used.

$$\mathbf{h} = \mathbf{r} \times \mathbf{v} \tag{A.7}$$

The position and velocity vectors are always in the plane perpendicular to the angular momentum vector. The most common way to break the angular momentum vector into components is to use spherical coordinates. This provides the inclination, i, the longitude of the ascending node, Ω, and the angular momentum, h.

Taking the cross product of equation A.1 with the angular momentum vector produces:

$$\frac{d\mathbf{v}}{dt} = -\frac{\mu}{r^3}\mathbf{r} \times \mathbf{h} \tag{A.8}$$

$$= \frac{\mu h}{r^2}\mathbf{i}_\theta \tag{A.9}$$

$$= \mu\frac{d\theta}{dt}\mathbf{i}_\theta \tag{A.10}$$

$$= \mu\frac{d\mathbf{i}_r}{dt} \tag{A.11}$$

$$\frac{d\mathbf{v}}{dt} \times \mathbf{h} = \frac{d}{dt}(\mathbf{v} \times \mathbf{h}) \tag{A.12}$$

$$\frac{d}{dt}(\mathbf{v} \times \mathbf{h}) = \mu\frac{d}{dt}\mathbf{i}_r \tag{A.13}$$

Integrating A.13 leads to

$$\mathbf{v} \times \mathbf{h} = \mu\mathbf{i}_r + \mathbf{C} \tag{A.14}$$

The constant of integration is called the eccentricity vector and is defined by

$$\mu\mathbf{e} = \mathbf{v} \times \mathbf{h} - \frac{\mu}{r}\mathbf{r} \tag{A.15}$$

The eccentricity vector shows how misaligned the velocity and position are. The magnitude of the eccentricity vector is equal to the eccentricity of the orbit and it points in the direction of the periapse.

The two vectors $\mathbf{h}$ and $\mathbf{e}$ define the orbit. Because they are always perpendicular, this provides

five orbital elements. The two elements added by the eccentricity vector are often broken down as e (the magnitude of the vector) and ω (the angle between the ascending node and the periapse in the plane of the orbit).

A.2.1 Derived Elements

Other orbital elements can be derived from these basic ones. Various manipulations of the vector equations can produce other constants associated with the orbit. The most common ones are:

$$p = \frac{h^2}{\mu} \tag{A.16}$$

$$a = \frac{p}{1-e^2} \tag{A.17}$$

These orbital elements also have a geometrical meaning with respect to elliptical orbits. a is the semi-major axis of the ellipse and p is the parameter of the ellipse. a is useful for calculating the period of the ellipse and is associated with the amount of energy the orbit has. However, these elements have little physical meaning, so they are difficult to work with when deriving basic equations of orbital transfers.

Other orbital elements can be derived based on the direction of the angular momentum vector, $\mathbf{h}$. To do this, the vector must be broken down into its components:

$$\mathbf{h} = h_x\mathbf{i}_x + h_y\mathbf{i}_y + h_z\mathbf{i}_z \tag{A.18}$$

where $\mathbf{i}_x$, $\mathbf{i}_y$, and $\mathbf{i}_z$ form an orthonormal basis with a fixed orientation.

The orbital elements chosen for the derivation given here are

$$i_x = \frac{-h_y}{h+h_z} \tag{A.19}$$

$$i_y = \frac{h_x}{h+h_z} \tag{A.20}$$

The reasons for using these elements is obscured by the math used in deriving them, however, they lead to fairly simple equations and are therefore convenient to use. They are the components of a vector pointing in the direction $\mathbf{i}_z \times \mathbf{i}_h$ with magnitude $\sqrt{h_x^2+h_y^2}/(h+h_z)$.

It is also convenient to define a term that is created by combining these elements together

$$\phi = 1 + \frac{h_y^2}{(h+h_z)^2} + \frac{h_x^2}{(h+h_z)^2} \tag{A.21}$$

$$= 1 + \frac{h^2-h_z^2}{(h+h_z)^2} \tag{A.22}$$

$$= \frac{2h}{h + h_z} \tag{A.23}$$

$$= \frac{2}{1 + \cos i} \tag{A.24}$$

$$= \sec^2 \frac{i}{2} \tag{A.25}$$

so that

$$i_x = -\frac{\phi}{2}\frac{h_y}{h} \tag{A.26}$$

$$i_y = \frac{\phi}{2}\frac{h_x}{h} \tag{A.27}$$

The eccentricity vector is broken into two components. When the angular momentum is in the $\mathbf{i}_z$ direction, the components are in the $\mathbf{i}_x$ and $\mathbf{i}_y$ directions. Those directions are the standard reference for everything in the orbital plane. Because the position, velocity, and eccentricity vectors are always perpendicular to the angular momentum vector, the simplest thing to do is rotate the entire plane with the angular momentum vector.

It is desirable to preserve the angles between $\mathbf{i}'_x$ and $\mathbf{e}$ when rotating the orbital plane. The angle from $\mathbf{i}_x$ to $\mathbf{e}$ is $\varpi = \Omega + \omega$, so the angle between $\mathbf{i}'_x$ and $\mathbf{e}$ should also be ϖ. Because Ω is measured between $\mathbf{i}_n$ (the line of nodes) and $\mathbf{i}'_x$ and ω is measured between $\mathbf{i}_n$ and $\mathbf{e}$, the only way to preserve both of these angles is to rotate around the line of nodes. Rotating the plane any other way would preserve ϖ but would remove all meaning from the angles ω and Ω. After the rotation, the sum $\varpi = \Omega + \omega$ seems to be adding angles in two different planes, but is actually adding the angles in the orbital plane. The meaning of this is that $\mathbf{i}'_x$ is in the orbital plane and rotated $-\Omega$ from the line of nodes.

The vector that the rotation is being done around is

$$\mathbf{i}_n = \cos\Omega\mathbf{i}_x + \sin\Omega\mathbf{i}_y \tag{A.28}$$

$$= \frac{-h_y}{\sqrt{h_x^2 + h_y^2}}\mathbf{i}_x + \frac{h_x}{\sqrt{h_x^2 + h_y^2}}\mathbf{i}_y \tag{A.29}$$

$$= \frac{i_x}{\sqrt{i_x^2 + i_y^2}}\mathbf{i}_x + \frac{i_y}{\sqrt{i_x^2 + i_y^2}}\mathbf{i}_y \tag{A.30}$$

The rotation angle is i. The Euler parameters of the rotation are

$$\alpha = \cos\Omega \sin\frac{i}{2} \tag{A.31}$$

$$\beta = \sin\Omega \sin\frac{i}{2} \tag{A.32}$$

$$\gamma = 0 \tag{A.33}$$

$$\delta = \cos\frac{i}{2} \tag{A.34}$$

$$\sin\frac{i}{2} = \sqrt{\frac{1-\cos i}{2}} \tag{A.35}$$

$$= \sqrt{\frac{h-h_z}{2h}} \tag{A.36}$$

$$\cos\frac{i}{2} = \sqrt{\frac{1+\cos i}{2}} \tag{A.37}$$

$$= \sqrt{\frac{h+h_z}{2h}} \tag{A.38}$$

$$\alpha = -\sqrt{\frac{h-h_z}{2(h_x^2+h_y^2)h}}h_y \tag{A.39}$$

$$\beta = \sqrt{\frac{h-h_z}{2(h_x^2+h_y^2)h}}h_x \tag{A.40}$$

$$\delta = \sqrt{\frac{h+h_z}{2h}} \tag{A.41}$$

The rotation matrix is

$$\mathbf{R} = \begin{bmatrix} 1-2(\beta^2+\gamma^2) & 2(\alpha\beta-\gamma\delta) & 2(\alpha\gamma+\beta\delta) \\ 2(\alpha\beta+\gamma\delta) & 1-2(\alpha^2+\gamma^2) & 2(\beta\gamma-\alpha\delta) \\ 2(\alpha\gamma-\beta\delta) & 2(\beta\gamma+\alpha\delta) & 1-2(\alpha^2+\beta^2) \end{bmatrix} \tag{A.42}$$

$$= \begin{bmatrix} 1-2\frac{(h-h_z)h_x^2}{2(h_x^2+h_y^2)h} & -2\frac{(h-h_z)h_xh_y}{2(h_x^2+h_y^2)h} & 2\frac{h_x\sqrt{h_x^2+h_y^2}}{2h\sqrt{h_x^2+h_y^2}} \\ -2\frac{(h-h_z)h_xh_y}{2(h_x^2+h_y^2)h} & 1-2\frac{(h-h_z)h_y^2}{2(h_x^2+h_y^2)h} & 2\frac{h_y\sqrt{h_x^2+h_y^2}}{2h\sqrt{h_x^2+h_y^2}} \\ -2\frac{h_x\sqrt{h_x^2+h_y^2}}{2h\sqrt{h_x^2+h_y^2}} & -2\frac{h_y\sqrt{h_x^2+h_y^2}}{2h\sqrt{h_x^2+h_y^2}} & 1-2\frac{(h-h_z)(h_x^2+h_y^2)}{2(h_x^2+h_y^2)h} \end{bmatrix} \tag{A.43}$$

$$= \begin{bmatrix} \frac{(h+h_z)h-h_x^2}{(h+h_z)h} & \frac{-h_xh_y}{(h+h_z)h} & \frac{h_x}{h} \\ \frac{-h_xh_y}{(h+h_z)h} & \frac{(h+h_z)h-h_y^2}{(h+h_z)h} & \frac{h_y}{h} \\ \frac{-h_x}{h} & \frac{-h_y}{h} & \frac{h_z}{h} \end{bmatrix} \tag{A.44}$$

The columns of the rotation matrix provide a set of orthonormal basis vectors:

$$\mathbf{i}_x' = \frac{(h+h_z)h-h_x^2}{(h+h_z)h}\mathbf{i}_x - \frac{h_xh_y}{(h+h_z)h}\mathbf{i}_y - \frac{h_x}{h}\mathbf{i}_z \tag{A.45}$$

$$= \mathbf{i}_x - \frac{h_x}{h}(i_y\mathbf{i}_x - i_x\mathbf{i}_y + \mathbf{i}_z) \tag{A.46}$$

$$\mathbf{i}_y' = \frac{-h_xh_y}{(h+h_z)h}\mathbf{i}_x + \frac{(h+h_z)h-h_y^2}{(h+h_z)h}\mathbf{i}_y - \frac{h_y}{h}\mathbf{i}_z \tag{A.47}$$

$$= \mathbf{i}_y - \frac{h_y}{h}(i_y\mathbf{i}_x - i_x\mathbf{i}_y + \mathbf{i}_z) \tag{A.48}$$

$$\mathbf{i}_h = \frac{h_x}{h}\mathbf{i}_x + \frac{h_y}{h}\mathbf{i}_y + \frac{h_z}{h}\mathbf{i}_z \tag{A.49}$$

$\mathbf{i}'_x$ and $\mathbf{i}'_y$ form a useful set of basis vectors for the orbital plane. These three vectors are independent of the magnitude of $\mathbf{h}$, and will only change if the direction of that vector changes (because all the terms involving components of h only have ratios of those components).

The eccentricity vector is broken down into components along these directions to provide the final two orbital elements, $e'_x = \mathbf{e} \cdot \mathbf{i}'_x$ and $e'_y = \mathbf{e} \cdot \mathbf{i}'_y$.

$$\mathbf{e} = e_x\mathbf{i}_x + e_y\mathbf{i}_y + e_z\mathbf{i}_z \tag{A.50}$$

$$e'_x = \mathbf{e} \cdot \mathbf{i}'_x \tag{A.51}$$

$$= e_x - \frac{h_x}{h}(i_y e_x - i_x e_y + e_z) \tag{A.52}$$

$$= e_x - \frac{h_x}{h}\left(\frac{h_x e_x}{h+h_z} + \frac{h_y e_y}{h+h_z} + \frac{h_z e_z}{h+h_z} + \frac{h e_z}{h+h_z}\right) \tag{A.53}$$

$$= e_x - \frac{h_x}{h+h_z}e_z \tag{A.54}$$

$$= e_x - i_y e_z \tag{A.55}$$

$$e'_y = \mathbf{e} \cdot \mathbf{i}'_y \tag{A.56}$$

$$= e_y - \frac{h_y}{h}(i_y e_x - i_x e_y + e_z) \tag{A.57}$$

$$= e_y - \frac{h_y}{h}\left(\frac{h_x e_x}{h+h_z} + \frac{h_y e_y}{h+h_z} + \frac{h_z e_z}{h+h_z} + \frac{h e_z}{h+h_z}\right) \tag{A.58}$$

$$= e_y - \frac{h_y}{h+h_z}e_z \tag{A.59}$$

$$= e_y + i_x e_z \tag{A.60}$$

Two other useful vectors are $\mathbf{i}_r$, the unit vector in the radial direction, and $\mathbf{i}_t$, the unit vector in the tangential direction ($\mathbf{i}_t = \mathbf{i}_h \times \mathbf{i}_r$)

$$\mathbf{i}_r = \cos L\mathbf{i}'_x + \sin L\mathbf{i}'_y \tag{A.61}$$

$$= \left(\frac{(h+h_z)h - h_x^2}{(h+h_z)h}\cos L - \frac{h_x h_y}{(h+h_z)h}\sin L\right)\mathbf{i}_x + \left(\frac{-h_x h_y}{(h+h_z)h}\cos L + \frac{(h+h_z)h - h_y^2}{(h+h_z)h}\sin L\right)\mathbf{i}_y - \left(\frac{h_x}{h}\cos L + \frac{h_y}{h}\sin L\right)\mathbf{i}_z \tag{A.62}$$

$$\mathbf{i}_t = -\sin L\mathbf{i}'_x + \cos L\mathbf{i}'_y \tag{A.63}$$

$$
\begin{aligned}
&= -\left(\frac{(h+h_z)h - h_x^2}{(h+h_z)h}\sin L + \frac{h_x h_y}{(h+h_z)h}\cos L\right)\mathbf{i}_x \\
&\quad + \left(\frac{h_x h_y}{(h+h_z)h}\sin L + \frac{(h+h_z)h - h_y^2}{(h+h_z)h}\cos L\right)\mathbf{i}_y \\
&\quad + \left(\frac{h_x}{h}\sin L - \frac{h_y}{h}\cos L\right)\mathbf{i}_z
\end{aligned} \tag{A.64}
$$

A.3 The Effect of Thrusting

The angular momentum vector is

$$\mathbf{h} = \mathbf{r} \times \mathbf{v} \tag{A.65}$$

The standard assumption when applying thrust is that the position of the spacecraft does not change while the thrust is being applied. In general, the position vector is changing at a very slow rate compared to the velocity vector, so integrations can be done with sufficiently small time steps that this is a good assumption. Using this assumption,

$$d\mathbf{h} = \mathbf{r} \times \mathbf{dv} \tag{A.66}$$

where the symbol **dv** is used to denote the change in velocity due to the thrusting (ignoring the change due to the orbital motion, which has no effect on the angular momentum vector). This equation states that the change in the angular momentum is the torque applied to the spacecraft, as should be expected.

More information can be determined by breaking the thrust vector into components. The most useful components are dv_r (thrust in the direction of the radius vector), dv_h (thrust in the direction of the h vector), and dv_t (thrust in the tangential direction, $\mathbf{h} \times \mathbf{r}$).

$$d\mathbf{h} = dv_r \mathbf{r} \times \mathbf{i}_r + dv_t \mathbf{r} \times \mathbf{i}_t + dv_h \mathbf{r} \times \mathbf{i}_h \tag{A.67}$$

$$= 0 + r dv_t \mathbf{i}_h - r dv_h \mathbf{i}_t \tag{A.68}$$

The direction for $\mathbf{i}_t$ is

$$
\begin{aligned}
\mathbf{i}_t &= \left[\frac{-h_x h_y}{h_x^2 + h_y^2}\frac{h - h_z}{h}\cos L - \left(\frac{h_x^2}{h_x^2 + h_y^2}\frac{h_z}{h} + \frac{h_y^2}{h_x^2 + h_y^2}\right)\sin L\right]\mathbf{i}_x \\
&\quad + \left[\frac{h_x h_y}{h_x^2 + h_y^2}\frac{h - h_z}{h}\sin L + \left(\frac{h_y^2}{h_x^2 + h_y^2}\frac{h_z}{h} + \frac{h_x^2}{h_x^2 + h_y^2}\right)\cos L\right]\mathbf{i}_y \\
&\quad + \left[\frac{-h_y}{h}\cos L + \frac{h_x}{h}\sin L\right]\mathbf{i}_z
\end{aligned} \tag{A.69}
$$

This means that

$$\frac{dh_x}{dv_h} = -r\left[\frac{-h_x h_y}{h_x^2+h_y^2}\frac{h-h_z}{h}\cos L - \left(\frac{h_x^2}{h_x^2+h_y^2}\frac{h_z}{h}+\frac{h_y^2}{h_x^2+h_y^2}\right)\sin L\right] \tag{A.70}$$

$$\frac{dh_x}{dv_t} = r\frac{h_x}{h} \tag{A.71}$$

$$\frac{dh_y}{dv_h} = -r\left[\frac{h_x h_y}{h_x^2+h_y^2}\frac{h-h_z}{h}\sin L + \left(\frac{h_y^2}{h_x^2+h_y^2}\frac{h_z}{h}+\frac{h_x^2}{h_x^2+h_y^2}\right)\cos L\right] \tag{A.72}$$

$$\frac{dh_y}{dv_t} = r\frac{h_y}{h} \tag{A.73}$$

$$\frac{dh_z}{dv_h} = -r\left[\frac{-h_y}{h}\cos L + \frac{h_x}{h}\sin L\right] \tag{A.74}$$

$$\frac{dh_z}{dv_t} = r\frac{h_z}{h} \tag{A.75}$$

Calculating the change in the magnitude of h from thrusting in the i_h direction:

$$h^2 = h_x^2+h_y^2+h_z^2 \tag{A.76}$$

$$2hdh = 2h_x dh_x + 2h_y dh_y + 2h_z dh_z \tag{A.77}$$

$$\frac{-h}{r}\frac{dh}{dv_h} = h_x dh_x + h_y dh_y + h_z dh_z \tag{A.78}$$

$$\begin{aligned} &= \left[\frac{-h_x^2 h_y(h-h_z)}{(h_x^2+h_y^2)h} + \frac{h_y^3 h_z}{(h_x^2+h_y^2)h} + \frac{h_x^2 h_y}{h_x^2+h_y^2} - \frac{h_y h_z}{h}\right]\cos L \\ &\quad + \left[\frac{h_x h_y^2(h-h_z)}{(h_x^2+h_y^2)h} - \frac{h_x^3 h_z}{(h_x^2+h_y^2)h} - \frac{h_x h_y^2}{h_x^2+h_y^2} + \frac{h_x h_z}{h}\right]\sin L \end{aligned} \tag{A.79}$$

$$\begin{aligned} &= \frac{1}{(h_x^2+h_y^2)h}\left[-h_x^2 h_y h + h_x^2 h_y h_z + h_y^3 h_z + h_x^2 h_y h - h_x^2 h_y h_z - h_y^3 h_z\right]\cos L \\ &\quad + \frac{1}{(h_x^2+h_y^2)h}\left[h_x h_y^2 h - h_x h_y^2 h_z - h_x^3 h_z - h_x h_y^2 h + h_x h_y^2 h_z + h_x^3 h_z\right]\sin L \end{aligned} \tag{A.80}$$

$$= 0 \tag{A.81}$$

$$\frac{dh}{dv_h} = 0 \tag{A.82}$$

This means that the magnitude of $\mathbf{h}$ is only changed by thrusting in the tangential direction:

$$\frac{dh}{dv_t} = r \tag{A.83}$$

The change in i_x due to thrusting is:

$$\frac{di_x}{dv_t} = -\frac{dh_y/dv_t}{h+h_z} + \frac{h_y dh/dv_t}{(h+h_z)^2} + \frac{h_y dh_z/dv_t}{(h+h_z)^2} \tag{A.84}$$

$$= -\frac{rh_y}{h(h+h_z)} + \frac{rh_y}{(h+h_z)^2} + \frac{rh_y h_z}{h(h+h_z)^2} \tag{A.85}$$

$$= -\frac{rh_y(h+h_z)}{h(h+h_z)^2} + \frac{rh_y h}{h(h+h_z)^2} + \frac{rh_y h_z}{h(h+h_z)^2} \tag{A.86}$$

$$= 0 \tag{A.87}$$

$$\frac{di_x}{dv_h} = -\frac{dh_y/dv_h}{h+h_z} + \frac{h_y dh/dv_h}{(h+h_z)^2} + \frac{h_y dh_z/dv_h}{(h+h_z)^2} \tag{A.88}$$

$$= -r\left[\frac{-h_x h_y}{(h+h_z)^2 h}\sin L - \frac{h_y^2 h_z + h_x^2 h}{(h-h_z)(h+h_z)^2 h}\cos L\right]$$

$$-r\left[\frac{-h_y^2}{(h+h_z)^2 h}\cos L + \frac{h_x h_y}{(h+h_z)^2 h}\sin L\right] \tag{A.89}$$

$$= r\cos L\frac{h_y^2 h_z + h_x^2 h + h_y^2(h-h_z)}{(h-h_z)(h+h_z)^2 h} \tag{A.90}$$

$$= r\cos L\frac{(h_x^2+h_y^2)h}{(h_x^2+h_y^2)(h+h_z)h} \tag{A.91}$$

$$= \frac{r\cos L}{h+h_z} \tag{A.92}$$

The derivation for i_y is similar and leads to:

$$\frac{di_y}{dv_t} = \frac{dh_x/dv_t}{h+h_z} - \frac{h_x dh/dv_t}{(h+h_z)^2} - \frac{h_x dh_z/dv_t}{(h+h_z)^2} \tag{A.93}$$

$$= \frac{rh_x}{h(h+h_z)} - \frac{rh_x}{(h+h_z)^2} - \frac{rh_x h_z}{h(h+h_z)^2} \tag{A.94}$$

$$= \frac{rh_x(h+h_z)}{h(h+h_z)^2} - \frac{rh_x h}{h(h+h_z)^2} - \frac{rh_x h_z}{h(h+h_z)^2} \tag{A.95}$$

$$= 0 \tag{A.96}$$

$$\frac{di_y}{dv_h} = \frac{dh_x/dv_h}{h+h_z} - \frac{h_x dh/dv_h}{(h+h_z)^2} - \frac{h_x dh_z/dv_h}{(h+h_z)^2} \tag{A.97}$$

$$= -r\left[\frac{-h_x h_y}{(h+h_z)^2 h}\cos L - \frac{h_x^2 h_z + h_y^2 h}{(h-h_z)(h+h_z)^2 h}\sin L\right]$$

$$+r\left[\frac{-h_x h_y}{(h+h_z)^2 h}\cos L + \frac{h_x^2}{(h+h_z)^2 h}\sin L\right] \tag{A.98}$$

$$= r\sin L\frac{h_x^2 h_z + h_y^2 h + h_x^2(h-h_z)}{(h-h_z)(h+h_z)^2 h} \tag{A.99}$$

$$= r\sin L\frac{(h_x^2+h_y^2)h}{(h_x^2+h_y^2)(h+h_z)h} \tag{A.100}$$

$$= \frac{r\sin L}{h+h_z} \tag{A.101}$$

All that is left is finding the differential equations for e'_x and e'_y. The eccentricity vector is

$$\mu\mathbf{e} = \mathbf{v}\times\mathbf{h} - \frac{\mu}{r}\mathbf{r} \tag{A.102}$$

so the change in the eccentricity vector due to thrusting is

$$\mu d\mathbf{e} = \mathbf{dv} \times \mathbf{h} + \mathbf{v} \times d\mathbf{h} \tag{A.103}$$

$$= \mathbf{dv} \times (\mathbf{r} \times \mathbf{v}) + \mathbf{v} \times (\mathbf{r} \times \mathbf{dv}) \tag{A.104}$$

$$= (\mathbf{dv} \cdot \mathbf{v})\mathbf{r} - (\mathbf{dv} \cdot \mathbf{r})\mathbf{v} + (\mathbf{v} \cdot \mathbf{dv})\mathbf{r} - (\mathbf{v} \cdot \mathbf{r})\mathbf{dv} \tag{A.105}$$

$$= 2(\mathbf{dv} \cdot \mathbf{v})\mathbf{r} - (\mathbf{dv} \cdot \mathbf{r})\mathbf{v} - (\mathbf{v} \cdot \mathbf{r})\mathbf{dv} \tag{A.106}$$

$$= 2(v_r dv_r + v_t dv_t) r\mathbf{i}_r - r dv_r (v_r \mathbf{i}_r + v_t \mathbf{i}_t) - r v_r (dv_r \mathbf{i}_r + dv_t \mathbf{i}_t + dv_h \mathbf{i}_h) \tag{A.107}$$

$$= 2 v_t dv_t r\mathbf{i}_r - r dv_r v_t \mathbf{i}_t - r v_r (dv_t \mathbf{i}_t + dv_h \mathbf{i}_h) \tag{A.108}$$

$$= 2 v_t dv_t r\mathbf{i}_r - (r v_t dv_r + r v_r dv_t)\mathbf{i}_t - r v_r dv_h \mathbf{i}_h \tag{A.109}$$

$$= 2 h dv_t \mathbf{i}_r - (h dv_r + r v_r dv_t)\mathbf{i}_t - r v_r dv_h \mathbf{i}_h \tag{A.110}$$

$$\begin{aligned} \mu de_x = {} & 2h dv_t \left(\frac{(h+h_z)h - h_x^2}{(h+h_z)h} \cos L - \frac{h_x h_y}{(h+h_z)h} \sin L \right) \\ & + (h dv_r + r v_r dv_t) \left(\frac{(h+h_z)h - h_x^2}{(h+h_z)h} \sin L + \frac{h_x h_y}{(h+h_z)h} \cos L \right) \\ & - r v_r dv_h \frac{h_x}{h} \end{aligned} \tag{A.111}$$

$$\begin{aligned} = {} & \frac{(h+h_z)h - h_x^2}{(h+h_z)h} [2h dv_t \cos L + (h dv_r + r v_r dv_t) \sin L] \\ & + \frac{h_x h_y}{(h+h_z)h} [(h dv_r + r v_r dv_t) \cos L - 2h dv_t \sin L] - r v_r dv_h \frac{h_x}{h} \end{aligned} \tag{A.112}$$

$$\begin{aligned} = {} & \left[\left(h - \frac{h_x^2}{h+h_z} \right) \sin L + \frac{h_x h_y}{h+h_z} \cos L \right] dv_r \\ & + \left[\left(1 - \frac{h_x^2}{(h+h_z)h} \right) (2h \cos L + r v_r \sin L) + \frac{h_x h_y}{(h+h_z)h} (r v_r \cos L - 2h \sin L) \right] dv_t \\ & - \frac{h_x r v_r}{h} dv_h \end{aligned} \tag{A.113}$$

$$\begin{aligned} \mu de_y = {} & 2h dv_t \left(\frac{(h+h_z)h - h_y^2}{(h+h_z)h} \sin L - \frac{h_x h_y}{(h+h_z)h} \cos L \right) \\ & - (h dv_r + r v_r dv_t) \left(\frac{(h+h_z)h - h_y^2}{(h+h_z)h} \cos L + \frac{h_x h_y}{(h+h_z)h} \sin L \right) \\ & - r v_r dv_h \frac{h_y}{h} \end{aligned} \tag{A.114}$$

$$\begin{aligned} = {} & \frac{-h_x h_y}{(h+h_z)h} [(h dv_r + r v_r dv_t) \sin L + 2h dv_t \cos L] \\ & + \frac{(h+h_z)h - h_y^2}{(h+h_z)h} [2h dv_t - (h dv_r + r v_r dv_t) \cos L] - r v_r dv_h \frac{h_y}{h} \end{aligned} \tag{A.115}$$

$$\begin{aligned} = {} & \frac{-1}{h+h_z} \left[(h^2 + h h_z - h_y^2) \cos L + h_x h_y \sin L \right] dv_r \\ & + \frac{1}{(h+h_z)h} \left[(h^2 + h h_z - h_y^2)(2h \sin L - r v_r \cos L) - h_x h_y (2h \cos L + r v_r \sin L) \right] dv_t \\ & - \frac{h_y r v_r}{h} dv_h \end{aligned} \tag{A.116}$$

$$\mu de_z = -2hdv_t\left(\frac{h_x}{h}\cos L + \frac{h_y}{h}\sin L\right) - (hdv_r + rv_r dv_t)\left(\frac{h_x}{h}\sin L - \frac{h_y}{h}\cos L\right)$$
$$-rv_r dv_h \frac{h_z}{h} \tag{A.117}$$

$$= \frac{-h_x}{h}[2hdv_t\cos L + (hdv_r + rv_r dv_t)\sin L]$$
$$+\frac{h_y}{h}[(hdv_r + rv_r dv_t)\cos L - 2hdv_t \sin L] - \frac{h_z}{h}rv_r dv_h \tag{A.118}$$

$$= (h_y\cos L - h_x \sin L)dv_r - \frac{h_z r v_r}{h}dv_h$$
$$-\left[h_x\left(2\cos L + \frac{rv_r}{h}\sin L\right) + h_y\left(2\sin L - \frac{rv_r}{h}\cos L\right)\right]dv_t \tag{A.119}$$

This provides all the changes in the components of the eccentricity vector along the standard directions, however, the orbital elements are based on a different set of components. In order to find the full derivatives of the components e'_x and e'_y, a few more derivatives are necessary:

$$d(h_x/h) = \frac{dh_x}{h} - \frac{h_x dh}{h^2} \tag{A.120}$$

$$= \frac{hdh_x - h_x dh}{h^2} \tag{A.121}$$

$$\frac{d(h_x/h)}{dv_t} = \frac{h(rh_x/h) - h_x r}{h^2} \tag{A.122}$$

$$= 0 \tag{A.123}$$

$$\frac{d(h_x/h)}{dv_h} = -\frac{r}{h}\left[\frac{-h_x h_y}{h_x^2 + h_y^2}\frac{h - h_z}{h}\cos L - \left(\frac{h_x^2}{h_x^2 + h_y^2}\frac{h_z}{h} + \frac{h_y^2}{h_x^2 + h_y^2}\right)\sin L\right] \tag{A.124}$$

$$d(h_y/h) = \frac{dh_y}{h} - \frac{h_y dh}{h^2} \tag{A.125}$$

$$= \frac{hdh_y - h_y dh}{h^2} \tag{A.126}$$

$$\frac{d(h_y/h)}{dv_t} = \frac{h(rh_y/h) - h_y r}{h^2} \tag{A.127}$$

$$= 0 \tag{A.128}$$

$$\frac{d(h_y/h)}{dv_h} = -\frac{r}{h}\left[\frac{h_x h_y}{h_x^2 + h_y^2}\frac{h - h_z}{h}\sin L + \left(\frac{h_y^2}{h_x^2 + h_y^2}\frac{h_z}{h} + \frac{h_x^2}{h_x^2 + h_y^2}\right)\cos L\right] \tag{A.129}$$

$$d(h_z/h) = \frac{dh_z}{h} - \frac{h_z dh}{h^2} \tag{A.130}$$

$$= \frac{hdh_z - h_z dh}{h^2} \tag{A.131}$$

$$\frac{d(h_z/h)}{dv_t} = \frac{h(rh_z/h) - h_z r}{h^2} \tag{A.132}$$

$$= 0 \tag{A.133}$$

$$\frac{d(h_z/h)}{dv_h} = -\frac{r}{h^2}(-h_y\cos L + h_x \sin L) \tag{A.134}$$

$$\mathbf{e} = e_x\mathbf{i}_x + e_y\mathbf{i}_y + e_z\mathbf{i}_z \tag{A.135}$$

$$e'_x = e_x - \frac{h_x/h}{1+h_z/h}e_z \tag{A.136}$$

$$e'_y = e_y - \frac{h_y/h}{1+h_z/h}e_z \tag{A.137}$$

The derivatives are

$$de'_x = de_x - \left(\frac{d(h_x/h)}{1+h_z/h} - \frac{(h_x/h)d(h_z/h)}{(1+h_z/h)^2}\right)e_z - \frac{h_x}{h+h_z}de_z \tag{A.138}$$

$$de'_y = de_y - \left(\frac{d(h_y/h)}{1+h_z/h} - \frac{(h_y/h)d(h_z/h)}{(1+h_z/h)^2}\right)e_z - \frac{h_y}{h+h_z}de_z \tag{A.139}$$

It is convenient that all the terms involving $d(h_x/h)$, $d(h_y/h)$, and $d(h_z/h)$ are zero for $dv_h = 0$. The derivatives with respect to various thrusting directions are:

$$\mu\frac{de'_x}{dv_r} = \left[\left(h - \frac{h_x^2}{h+h_z}\right)\sin L + \frac{h_xh_y}{h+h_z}\cos L\right] - \frac{h_x}{h+h_z}(h_y\cos L - h_x\sin L) \tag{A.140}$$

$$= \left[h - \frac{h_x^2}{h+h_z} + \frac{h_x^2}{h+h_z}\right]\sin L + \left[\frac{h_xh_y}{h+h_z} - \frac{h_xh_y}{h+h_z}\right]\cos L \tag{A.141}$$

$$= h\sin L \tag{A.142}$$

$$\mu\frac{de'_x}{dv_t} = \left(1 - \frac{h_x^2}{(h+h_z)h}\right)(2h\cos L + rv_r\sin L) + \frac{h_xh_y}{(h+h_z)h}(rv_r\cos L - 2h\sin L)$$
$$+\frac{h_x}{h+h_z}\left[2h_x\cos L + 2h_y\sin L + \frac{rv_rh_x}{h}\sin L - \frac{rv_rh_y}{h}\cos L\right] \tag{A.143}$$

$$= \left[2h - \frac{2h_x^2}{h+h_z} + \frac{h_xh_yrv_r}{h(h+h_z)} + \frac{2h_x^2}{h+h_z} - \frac{h_xh_yrv_r}{h(h+h_z)}\right]\cos L$$
$$+\left[rv_r - \frac{h_x^2rv_r}{h(h+h_z)} - \frac{2h_xh_y}{h+h_z} + \frac{2h_xh_y}{h+h_z} + \frac{h_x^2rv_r}{h(h+h_z)}\right]\sin L \tag{A.144}$$

$$= 2h\cos L + rv_r\sin L \tag{A.145}$$

$$v_r = \frac{\mu}{h}(e'_x\sin L - e'_y\cos L) \tag{A.146}$$

$$\mu\frac{de'_x}{dv_t} = 2h\cos L + \frac{\mu r}{h}(e'_x\sin^2 L - e'_y\cos L\sin L) \tag{A.147}$$

$$= 2h\cos L + \frac{\mu r}{h}(e'_x - e'_x\cos^2 L - e'_y\cos L\sin L) \tag{A.148}$$

$$= \frac{\mu r}{h}\left(\frac{2h^2/\mu}{r} - e'_x\cos L - e'_y\sin L\right)\cos L + \frac{\mu r}{h}e'_x \tag{A.149}$$

$$= \frac{\mu r}{h}\left[2(1 + e'_x\cos L + e'_y\sin L) - e'_x\cos L - e'_y\sin L\right]\cos L + \frac{\mu r}{h}e'_x \tag{A.150}$$

$$= \frac{\mu r}{h}\left[1 + 1 + e'_x\cos L + e'_y\sin L\right]\cos L + \frac{\mu r}{h}e'_x \tag{A.151}$$

$$\mu\frac{de'_x}{dv_h} = -\frac{\mu re_z}{h+h_z}\left(\frac{h_xh_y}{h(h+h_z)}\cos L + \frac{h^2+hh_z-h_x^2}{h(h+h_z)}\sin L\right)$$

$$+\frac{\mu r h_x e_z}{h(h+h_z)^2}(h_y\cos L - h_x\sin L) - \frac{h_x r v_r}{h} + \frac{h_x h_z r v_r}{h(h+h_z)} \tag{A.152}$$

$$= \left[\frac{-\mu(h^2+hh_z-h_x^2)re_z}{h(h+h_z)^2} - \frac{\mu h_x^2 r e_z}{h(h+h_z)^2}\right]\sin L$$

$$+\left[\frac{-\mu h_x h_y r e_z}{h(h+h_z)^2} + \frac{\mu h_x h_y r e_z}{h(h+h_z)}\right]\cos L - \frac{h_x r v_r}{h+h_z} \tag{A.153}$$

$$= \frac{-\mu r e_z}{h+h_z}\sin L - \frac{h_x r v_r}{h+h_z} \tag{A.154}$$

$$v_r = \frac{\mu}{h}(e'_x\sin L - e'_y\cos L) \tag{A.155}$$

$$\frac{de'_x}{dv_h} = \frac{-re_z}{h+h_z}\sin L - \frac{h_x r}{h(h+h_z)}(e'_x\sin L - e'_y\cos L) \tag{A.156}$$

$$= \frac{h_x r e'_y}{h(h+h_z)}\cos L - \frac{hre_z + h_x r e'_x}{h(h+h_z)}\sin L \tag{A.157}$$

$$= \frac{h_x r e'_y}{h(h+h_z)}\cos L - \frac{h^2 re_z + hh_z re_z + hh_x re_x + h_x h_z re_x - h_x^2 re_z}{h(h+h_z)^2}\sin L \tag{A.158}$$

$$= \frac{h_x r e'_y}{h(h+h_z)}\cos L - \frac{r(h+h_z)(h_z e_z + h_x e_x) + h_y^2 re_z}{h(h+h_z)^2}\sin L \tag{A.159}$$

$$= \frac{h_x r e'_y}{h(h+h_z)}\cos L + \frac{r(h+h_z)h_y e_y - h_y^2 re_z}{h(h+h_z)^2}\sin L \tag{A.160}$$

$$= \frac{h_x r e'_y}{h(h+h_z)}\cos L + \frac{h_y r e'_y}{h(h+h_z)}\sin L \tag{A.161}$$

$$\tag{A.162}$$

One thing that is noticeable is that the derivatives for de'_x with respect to in plane thrusting (dv_r and dv_t) are identical to the derivatives for de_x with $h_x = 0$ and $h_y = 0$. This is expected, because it should reduce to that case when the inclination is 0. The same result will be obtained for de'_y.

$$\mu\frac{de'_y}{dv_r} = \left(\frac{h_y^2}{h+h_z} - h\right)\cos L - \frac{h_x h_y}{h+h_z}\sin L + \frac{h_y}{h+h_z}(h_x\sin L - h_y\cos L) \tag{A.163}$$

$$= -h\cos L \tag{A.164}$$

$$\mu\frac{de'_y}{dv_t} = \left(1 - \frac{h_y^2}{h(h+h_z)}\right)(2h\sin L - rv_r\cos L) - \frac{h_x h_y}{h(h+h_z)}(2h\cos L + rv_r\sin L)$$

$$+\frac{h_y}{h+h_z}\left[h_x\left(2\cos L + \frac{rv_r}{h}\sin L\right) + h_y\left(2\sin L - \frac{rv_r}{h}\cos L\right)\right] \tag{A.165}$$

$$= 2h\sin L - rv_r\cos L \tag{A.166}$$

$$\mu\frac{de'_y}{dv_h} = \frac{\mu r e_z}{h+h_z}\left(\frac{h_x h_y}{h(h+h_z)}\sin L + \frac{h^2+hh_z-h_y^2}{h(h+h_z)}\cos L\right)$$

$$+\frac{\mu r h_y e_z}{h(h+h_z)^2}(h_y\cos L - h_x\sin L) - \frac{h_y r v_r}{h} + \frac{h_y h_z r v_r}{h(h+h_z)} \tag{A.167}$$

$$= \frac{\mu r e_z}{h+h_z}\cos L - \frac{h_y r v_r}{h+h_z} \tag{A.168}$$

$$\frac{de'_y}{dv_h} = \frac{re_z}{h+h_z}\cos L - \frac{h_y r}{h(h+h_z)}(e'_x \sin L - e'_y \cos L) \quad \text{(A.169)}$$

$$= \frac{rh(h+h_z)e_z + h_y(h+h_z)e_y - h_y^2 e_z}{h(h+h_z)^2}\cos L - \frac{rh_y e'_x}{h(h+h_z)}\sin L \quad \text{(A.170)}$$

$$= -\frac{rh_x e'_x}{h(h+h_z)}\cos L - \frac{rh_y e'_x}{h(h+h_z)}\sin L \quad \text{(A.171)}$$

These are all of the orbital elements. However, the equations still contain terms that are not made by combining the basic orbital elements. They can be rewritten to fix this problem.

The basic equations (ignoring the zeros) are:

$$\frac{dh}{dv_t} = r \quad \text{(A.172)}$$

$$\frac{di_x}{dv_h} = \frac{r\cos L}{h+h_z} \quad \text{(A.173)}$$

$$\frac{di_y}{dv_h} = \frac{r\sin L}{h+h_z} \quad \text{(A.174)}$$

$$\mu\frac{de'_x}{dv_r} = h\sin L \quad \text{(A.175)}$$

$$\mu\frac{de'_x}{dv_t} = 2h\cos L + rv_r \sin L \quad \text{(A.176)}$$

$$\frac{de'_x}{dv_h} = \frac{re'_y}{h(h+h_z)}(h_x \cos L + h_y \sin L) \quad \text{(A.177)}$$

$$\mu\frac{de'_y}{dv_r} = -h\cos L \quad \text{(A.178)}$$

$$\mu\frac{de'_y}{dv_t} = 2h\sin L - rv_r \cos L \quad \text{(A.179)}$$

$$\frac{de'_y}{dv_h} = -\frac{re'_x}{h(h+h_z)}(h_x \cos L + h_y \sin L) \quad \text{(A.180)}$$

In order to have the equations be only in terms of orbital elements, it is necessary to make substitutions for r and v_r.

$$\xi = \frac{p}{r} \quad \text{(A.181)}$$

$$= 1 + e'_x \cos L + e'_y \sin L \quad \text{(A.182)}$$

$$p = \frac{h^2}{\mu} \quad \text{(A.183)}$$

$$r = \frac{h^2}{\mu\xi} \quad \text{(A.184)}$$

$$v_r = \frac{\mu}{h}(e'_x \sin L - e'_y \cos L) \quad \text{(A.185)}$$

$$rv_r = \frac{h}{\xi}(e'_x \sin L - e'_y \cos L) \quad \text{(A.186)}$$

$$\mu\frac{de'_x}{dv_t} = 2h\cos L + \frac{h}{\xi}(e'_x\sin L - e'_y\cos L)\sin L \tag{A.187}$$

$$= 2h\cos L + \frac{he'_x}{\xi} - \frac{h}{\xi}(1 + e'_x\cos L + e'_y\sin L - 1)\cos L \tag{A.188}$$

$$= \frac{2h\xi}{\xi}\cos L + \frac{he'_x}{\xi} + \frac{h}{\xi}(1-\xi)\cos L \tag{A.189}$$

$$= \frac{h}{\xi}[(\xi+1)\cos L + e'_x] \tag{A.190}$$

$$\mu\frac{de'_y}{dv_t} = 2h\sin L - \frac{h}{\xi}(e'_x\sin L - e'_y\cos L)\cos L \tag{A.191}$$

$$= 2h\sin L + \frac{he'_y}{\xi} - \frac{h}{\xi}(1 + e'_x\cos L + e'_y\sin L - 1)\sin L \tag{A.192}$$

$$= \frac{h}{\xi}[(\xi+1)\sin L + e'_y] \tag{A.193}$$

$$\frac{de'_x}{dv_h} = \frac{h^2 e'_y}{\mu\xi h(h+h_z)}(h_x\cos L + h_y\sin L) \tag{A.194}$$

$$= \frac{he'_y}{\mu\xi}\left(\frac{h_x}{h+h_z}\cos L + \frac{h_y}{h+h_z}\sin L\right) \tag{A.195}$$

$$\frac{de'_y}{dv_h} = -\frac{h^2 e'_x}{\mu\xi h(h+h_z)}(h_x\cos L + h_y\sin L) \tag{A.196}$$

$$= \frac{-he'_x}{\mu\xi}\left(\frac{h_x}{h+h_z}\cos L + \frac{h_y}{h+h_z}\sin L\right) \tag{A.197}$$

$$\frac{dh}{dv_t} = \frac{h^2}{\mu\xi} \tag{A.198}$$

$$\frac{di_x}{dv_h} = \frac{h^2\cos L}{\mu\xi(h+h_z)} \tag{A.199}$$

$$\frac{di_y}{dv_h} = \frac{h^2\sin L}{\mu\xi(h+h_z)} \tag{A.200}$$

This puts all of the equations in terms of the vector elements, but it is still necessary to eliminate h_x, h_y, and h_z

$$\phi = 1 + i_x^2 + i_y^2 \tag{A.201}$$

$$= \frac{2h}{h+h_z} \tag{A.202}$$

$$\frac{di_x}{dv_h} = \frac{h\phi\cos L}{2\mu\xi} \tag{A.203}$$

$$\frac{di_y}{dv_h} = \frac{h\phi \sin L}{2\mu\xi} \tag{A.204}$$

$$\eta = i_x \sin L - i_y \cos L \tag{A.205}$$

$$= \frac{-h_y}{h + h_z} \sin L - \frac{h_x}{h + h_z} \cos L \tag{A.206}$$

$$\frac{de'_x}{dv_h} = -\frac{he'_y \eta}{\mu\xi} \tag{A.207}$$

$$\frac{de'_y}{dv_h} = \frac{he'_x \eta}{\mu\xi} \tag{A.208}$$

The equations are now

$$\frac{dh}{dv_t} = \frac{h^2}{\mu\xi} \tag{A.209}$$

$$\frac{di_x}{dv_h} = \frac{h\phi}{2\mu\xi} \cos L \tag{A.210}$$

$$\frac{di_y}{dv_h} = \frac{h\phi}{2\mu\xi} \sin L \tag{A.211}$$

$$\frac{de'_x}{dv_r} = \frac{h}{\mu} \sin L \tag{A.212}$$

$$\frac{de'_x}{dv_t} = \frac{h}{\mu\xi}[(\xi + 1) \cos L + e'_x] \tag{A.213}$$

$$\frac{de'_x}{dv_h} = -\frac{he'_y \eta}{\mu\xi} \tag{A.214}$$

$$\frac{de'_y}{dv_r} = -\frac{h}{\mu} \cos L \tag{A.215}$$

$$\frac{de'_y}{dv_t} = \frac{h}{\mu\xi}[(\xi + 1) \sin L + e'_y] \tag{A.216}$$

$$\frac{de'_y}{dv_h} = \frac{he'_x \eta}{\mu\xi} \tag{A.217}$$

One more term that can be changed is replacing h/μ by h'. This will remove all the μ's from the equations.

$$\frac{dh'}{dv_t} = \frac{h'^2}{\xi} \tag{A.218}$$

$$\frac{di_x}{dv_h} = \frac{h'\phi}{2\xi} \cos L \tag{A.219}$$

$$\frac{di_y}{dv_h} = \frac{h'\phi}{2\xi} \sin L \tag{A.220}$$

$$\frac{de'_x}{dv_r} = h' \sin L \tag{A.221}$$

$$\frac{de'_x}{dv_t} = \frac{h'}{\xi}[(\xi + 1) \cos L + e'_x] \tag{A.222}$$

$$\frac{de'_x}{dv_h} = -\frac{h'e'_y \eta}{\xi} \tag{A.223}$$

$$\frac{de'_y}{dv_r} = -h' \cos L \tag{A.224}$$

$$\frac{de'_y}{dv_t} = \frac{h'}{\xi}[(\xi + 1) \sin L + e'_y] \tag{A.225}$$

$$\frac{de'_y}{dv_h} = \frac{h' e'_x \eta}{\xi} \tag{A.226}$$

Appendix B

Development of the Hamiltonian Method

The Hamiltonian method of control optimization is based on variational calculus. It is used to solve problems that have a cost function of the form

$$J = \zeta[\mathbf{X}(t_f), t_f] + \int_{t_0}^{t_f} g(\mathbf{X}, \mathbf{U}, t)dt \tag{B.1}$$

where $\mathbf{X}$ is the state vector and $\mathbf{U}$ is the vector of control variables. The state vector is constrained by

$$\dot{\mathbf{X}} = \mathbf{b}(\mathbf{X}, \mathbf{U}, t) \tag{B.2}$$

The optimization problem has t_0 and $\mathbf{X}(t_0)$ fixed[1].

The cost function can be augmented by adding the system dynamics multiplied by the costate:

$$J_a = \zeta[\mathbf{X}(t_f), t_f] + \int_{t_0}^{t_f} g(\mathbf{X}, \mathbf{U}, t) + \mathbf{p}^T[\mathbf{b}(\mathbf{X}, \mathbf{U}, t) - \dot{\mathbf{X}}]dt \tag{B.3}$$

The costate vector is a set of Lagrange multipliers. They are unknown functions of time. Adding the system dynamics in this manner does not actually change the cost function, because the added term is constrained to be 0 at all times.

Taking the first variation,

$$\begin{aligned} \delta J_a &= \frac{\partial \zeta}{\partial \mathbf{X}}(t_f)\delta\mathbf{X}_f + \frac{\partial \zeta}{\partial t}(t_f)\delta t_f + \left[g + \mathbf{p}^T(\mathbf{b} - \dot{\mathbf{X}})\right]_{t_f} \delta t_f + \\ &+ \int_{t_0}^{t_f} \left[\frac{\partial g}{\partial \mathbf{X}}\delta\mathbf{X} + \frac{\partial g}{\partial \mathbf{U}}\delta\mathbf{U} + \delta\mathbf{p}^T(\mathbf{b} - \dot{\mathbf{X}}) + \mathbf{p}^T\frac{\partial \mathbf{b}}{\partial \mathbf{X}}\delta\mathbf{X} + \mathbf{p}^T\frac{\partial \mathbf{b}}{\partial \mathbf{U}}\delta\mathbf{U} - \mathbf{p}^T\delta\dot{\mathbf{X}}\right] dt \end{aligned} \tag{B.4}$$

[1] This is not necessary for the Hamiltonian method, but simplifies things and is true for the problem considered here.

To simplify this, we define the Hamiltonian H

$$H(\mathbf{X}, \mathbf{U}, \mathbf{P}, t) = g(\mathbf{X}, \mathbf{U}, t) + \mathbf{p}^T \mathbf{b}(\mathbf{X}, \mathbf{U}, t) \tag{B.5}$$

which simplifies the augmented cost differential to

$$\begin{aligned} \delta J_a &= \frac{\partial \zeta}{\partial \mathbf{X}}(t_f)\delta \mathbf{X}_f + \left[H + \frac{\partial \zeta}{\partial t} - \mathbf{p}^T \dot{\mathbf{X}}\right]_{t_f} \delta t_f + \\ &+ \int_{t_0}^{t_f} \left[\frac{\partial H}{\partial \mathbf{X}}\delta \mathbf{X} + \frac{\partial H}{\partial \mathbf{U}}\delta \mathbf{U} + \delta \mathbf{p}^T(\mathbf{b} - \dot{\mathbf{X}}) - \mathbf{p}^T \delta \dot{\mathbf{X}}\right] dt \end{aligned} \tag{B.6}$$

The variations in $\delta \mathbf{X}$ and $\delta \dot{\mathbf{X}}$ are not independent, so they should be combined. This can be done by integrating the $\delta \dot{\mathbf{X}}$ terms. Using integration by parts:

$$\int_{t_0}^{t_f} \mathbf{p}^T \delta \dot{\mathbf{X}} dt = \mathbf{p}^T(t_f)\delta \mathbf{X}(t_f) - \mathbf{p}^T(t_0)\delta \mathbf{X}(t_0) - \int_{t_0}^{t_f} \dot{\mathbf{p}}^T \delta \mathbf{X} dt \tag{B.7}$$

Because the state is fixed at t_0, the second term is 0. Putting the rest of the terms into equation B.6 produces

$$\begin{aligned} \delta J_a &= \frac{\partial \zeta}{\partial \mathbf{X}}(t_f)\delta \mathbf{X}_f + \left[H + \frac{\partial \zeta}{\partial t} - \mathbf{p}^T \dot{\mathbf{X}}\right]_{t_f} \delta t_f - \mathbf{p}(t_f)\delta \mathbf{X}(t_f) + \\ &+ \int_{t_0}^{t_f} \left[\left(\frac{\partial H}{\partial \mathbf{X}} + \dot{\mathbf{p}}^T\right)\delta \mathbf{X} + \frac{\partial H}{\partial \mathbf{U}}\delta \mathbf{U} + \delta \mathbf{p}^T(\mathbf{b} - \dot{\mathbf{X}})\right] dt \end{aligned} \tag{B.8}$$

$\delta \mathbf{X}_f$ and $\delta \mathbf{X}(t_f)$ are related by

$$\delta \mathbf{X}(t_f) = \delta \mathbf{X}_f - \dot{\mathbf{X}}(t_f)\delta t_f \tag{B.9}$$

The final form of the first variation in the augmented general cost function is

$$\begin{aligned} \delta J_a &= \left[\frac{\partial \zeta}{\partial \mathbf{X}} - \mathbf{p}^T\right]_{t_f} \delta \mathbf{X}_f + \left[H + \frac{\partial \zeta}{\partial t}\right]_{t_f} \delta t_f + \\ &+ \int_{t_0}^{t_f} \left[\left(\frac{\partial H}{\partial \mathbf{X}} + \dot{\mathbf{p}}^T\right)\delta \mathbf{X} + \frac{\partial H}{\partial \mathbf{U}}\delta \mathbf{U} + \delta \mathbf{p}^T(\mathbf{b} - \dot{\mathbf{X}})\right] dt \end{aligned} \tag{B.10}$$

For the optimal solution, $\delta J_a = 0$. Since all of the variations are independent, this provides the following constraints for all optimization problems:

$$\dot{\mathbf{p}}^T = -\frac{\partial H}{\partial \mathbf{X}} \tag{B.11}$$

$$\frac{\partial H}{\partial \mathbf{U}} = 0 \tag{B.12}$$

$$\dot{\mathbf{X}} = \mathbf{b} \tag{B.13}$$

There are also 2 sets of transversality conditions. If the final time is not constrained

$$H(t_f) = -\frac{\partial \zeta}{\partial t}(t_f) \tag{B.14}$$

and if the final state is not constrained,

$$\mathbf{p}^T(t_f) = \frac{\partial \zeta}{\partial \mathbf{X}} \tag{B.15}$$

It is useful to note the following relationship between H and $\dot{\mathbf{X}}$:

$$\begin{aligned} H(\mathbf{X}, \mathbf{U}, \mathbf{p}, t) &= g(\mathbf{X}, \mathbf{U}, t) + \mathbf{p}^T \mathbf{b}(\mathbf{X}, \mathbf{U}, t) && \text{(B.16)} \\ \frac{\partial H(\mathbf{X}, \mathbf{U}, \mathbf{p}, t)}{\partial \mathbf{p}} &= 0 + \frac{\partial \mathbf{p}}{\partial \mathbf{p}}^T \mathbf{b}(\mathbf{X}, \mathbf{U}, t) + \mathbf{p}^T \mathbf{0} && \text{(B.17)} \\ &= \mathbf{b} && \text{(B.18)} \\ &= \dot{\mathbf{X}} && \text{(B.19)} \end{aligned}$$

B.1 Orbital Trajectory Optimization

For the specific problem of orbital trajectory optimization, the state and control vectors are

$$\mathbf{X}^T = [h \; e_x \; e_y \; i_x \; i_y \; L \; m] \tag{B.20}$$

$$\mathbf{U}^T = [\theta \; \psi \; F] \tag{B.21}$$

The cost function for minimum fuel use is

$$g(\mathbf{X}, \mathbf{U}, t) = \dot{m} = -\frac{F}{c} \tag{B.22}$$

$$\zeta[\mathbf{X}_{t_f}, t_f] = 0 \tag{B.23}$$

With this form of cost function, the cost should be maximized (which minimizes the magnitude).

When the engine can be switched on and off, there is a slight complication because the derivatives are no longer continuous. This is solved by using Pontryagin's maximum principle, which states that the control should be selected so as to maximize H at every point. If $H(\mathbf{U})$ is a continuous function, the first-order necessary condition is as given in equation B.12.

The transversality conditions are that h, e_x, e_y, i_x, and i_y all have initial and final values specified, so the corresponding elements of the costate are free. The final time is free, so

$$H(t_f) = 0 \tag{B.24}$$

The initial longitude and both the final mass and longitude are also free, which leads to

$$p_L(t_0) = 0 \tag{B.25}$$

$$p_L(t_f) = 0 \tag{B.26}$$

$$p_m(t_f) = 0 \tag{B.27}$$

The differential equation for p_L is very complicated. When the controls are optimized, the costate varies in such a way as to make H constant:

$$\frac{dH}{dt} = \frac{\partial H}{\partial \mathbf{X}}^T \dot{\mathbf{X}} + \frac{\partial H}{\partial \mathbf{U}}^T \dot{\mathbf{U}} + \frac{\partial H}{\partial \mathbf{p}}^T \dot{\mathbf{p}} \tag{B.28}$$

$$= -\dot{\mathbf{p}}^T \dot{\mathbf{X}} + 0 + \dot{\mathbf{X}}^T \dot{\mathbf{p}} \tag{B.29}$$

$$= 0 \tag{B.30}$$

Because the thrusting is small, the orbital elements do not change much, so they can be treated as constants over one orbital period. The mass will also not change significantly over one orbital period. The only terms that change within one orbit are the terms containing p_L and the terms containing L. The optimal control laws produce the following Hamiltonian:

$$H = -\frac{F(1+p_m)}{c} + \frac{FA}{m} + \frac{\xi^2}{\mu h^3} p_L \tag{B.31}$$

The first term is assumed to be constant over one orbit. The second term is periodic, so the third term must also be periodic. Both of them must vary with the same magnitude. Because the second term is divided by the mass, which is generally large, the variations will be small. Since the initial and final values of p_L are both zero and the variations in its magnitude are small, it can be approximated as 0 throught the entire transfer. This means that H is no longer constant, but that property is never used in the optimization anyway.

Appendix C

Differential Equations of Motion

The optimized equations of motion come from

$$\frac{d\mathbf{X}}{dt} = \frac{\partial H}{\partial \mathbf{p}} = \frac{F}{m}\left[\frac{1}{A}\left(A_t\frac{\partial A_t}{\partial \mathbf{p}} + A_r\frac{\partial A_r}{\partial \mathbf{p}} + A_n\frac{\partial A_n}{\partial \mathbf{p}}\right)\right] \tag{C.1}$$

$$\frac{d\mathbf{p}}{dt} = \frac{\partial H}{\partial \mathbf{X}} = -\frac{F}{m}\left[\frac{1}{A}\left(A_t\frac{\partial A_t}{\partial \mathbf{X}} + A_r\frac{\partial A_r}{\partial \mathbf{X}} + A_n\frac{\partial A_n}{\partial \mathbf{X}}\right)\right] \tag{C.2}$$

where

$$A_r = h(p_{e_x}\sin L - p_{e_y}\cos L) \tag{C.3}$$

$$A_t = \frac{h}{\xi}\{hp_h + [(\xi+1)\cos L + e_x]p_{e_x} + [(\xi+1)\sin L + e_y]p_{e_y}\} \tag{C.4}$$

$$A_n = \frac{h}{\xi}\left[\eta(e_x p_{e_y} - e_y p_{e_x}) + \frac{\phi}{2}(p_{i_x}\cos L + p_{i_y}\sin L) + \xi\eta p_L\right] \tag{C.5}$$

$$\mathbf{A} = A_r\mathbf{i}_r + A_t\mathbf{i}_t + A_n\mathbf{i}_n \tag{C.6}$$

$$A = \sqrt{A_r^2 + A_t^2 + A_n^2} \tag{C.7}$$

The partial derivatives are:

$$\frac{\partial A_r}{\partial h} = \frac{A_r}{h} \tag{C.8}$$

$$\frac{\partial A_r}{\partial p_{e_x}} = h\sin L \tag{C.9}$$

$$\frac{\partial A_r}{\partial p_{e_y}} = -h\cos L \tag{C.10}$$

$$\frac{\partial A_t}{\partial h} = \frac{hp_h}{\xi} + \frac{A_t}{h} \tag{C.11}$$

$$\frac{\partial A_t}{\partial e_x} = \frac{h}{\xi}[(1+\cos^2 L)p_{e_x} + p_{e_y}\cos L \sin L] - \frac{\cos L}{\xi}A_t \tag{C.12}$$

$$\frac{\partial A_t}{\partial e_y} = \frac{h}{\xi}[(1+\sin^2 L)p_{e_y} + p_{e_x}\cos L \sin L] - \frac{\sin L}{\xi}A_t \tag{C.13}$$

$$\frac{\partial A_t}{\partial p_h} = \frac{h^2}{\xi} \tag{C.14}$$

$$\frac{\partial A_t}{\partial p_{e_x}} = \frac{h(\xi+1)\cos L + he_x}{\xi} \tag{C.15}$$

$$\frac{\partial A_t}{\partial p_{e_y}} = \frac{h(\xi+1)\sin L + he_y}{\xi} \tag{C.16}$$

$$\frac{\partial A_n}{\partial h} = \frac{A_n}{h} \tag{C.17}$$

$$\frac{\partial A_n}{\partial e_x} = \frac{h\eta p_{e_y}}{\xi} - \frac{\cos L}{\xi}A_n \tag{C.18}$$

$$\frac{\partial A_n}{\partial e_y} = -\frac{h\eta p_{e_x}}{\xi} - \frac{\sin L}{\xi}A_n \tag{C.19}$$

$$\frac{\partial A_n}{\partial i_x} = \frac{h}{\xi}[(e_x p_{e_y} - e_y p_{e_x})\sin L + i_x(p_{i_x}\cos L + p_{i_y}\sin L)] \tag{C.20}$$

$$\frac{\partial A_n}{\partial i_y} = \frac{h}{\xi}[-(e_x p_{e_y} - e_y p_{e_x})\cos L + i_y(p_{i_x}\cos L + p_{i_y}\sin L)] \tag{C.21}$$

$$\frac{\partial A_n}{\partial p_{e_x}} = -\frac{h\eta e_y}{\xi} \tag{C.22}$$

$$\frac{\partial A_n}{\partial p_{e_y}} = \frac{h\eta e_x}{\xi} \tag{C.23}$$

$$\frac{\partial A_n}{\partial p_{i_x}} = \frac{h\phi}{2\xi}\cos L \tag{C.24}$$

$$\frac{\partial A_n}{\partial p_{i_y}} = \frac{h\phi}{2\xi}\sin L \tag{C.25}$$

$$\frac{dh}{dt} = \frac{FA_t}{mA}\frac{h^2}{\xi} \tag{C.26}$$

$$\frac{de_x}{dt} = \frac{Fh}{mA\xi}[A_r\xi\sin L - A_n\eta e_y + A_t\{(\xi+1)\cos L + e_x\}] \tag{C.27}$$

$$\frac{de_y}{dt} = \frac{Fh}{mA\xi}[-A_r\xi\cos L + A_n\eta e_x + A_t\{(\xi+1)\sin L + e_y\}] \tag{C.28}$$

$$\frac{di_x}{dt} = \frac{FA_n h\phi}{2mA\xi}\cos L \tag{C.29}$$

$$\frac{di_y}{dt} = \frac{FA_n h\phi}{2mA\xi}\sin L \tag{C.30}$$

(C.31)

$$\frac{dp_h}{dt} = -\frac{F}{m}\left[\frac{A_r^2 + A_t^2 + A_h^2}{Ah} + \frac{A_t h p_h}{\xi}\right] \tag{C.32}$$

$$= -\frac{F}{m}\left[\frac{A}{h} + \frac{A_t h p_h}{\xi}\right] \tag{C.33}$$

$$\frac{dp_{e_x}}{dt} = -\frac{F}{mA\xi}\left[h(p_{e_x} + p_{e_x}\cos^2 L + p_{e_y}\cos L \sin L)A_t + h\eta p_{e_y}A_n - (A_t^2 + A_n^2)\cos L\right] \quad \text{(C.34)}$$

$$\frac{dp_{e_y}}{dt} = -\frac{F}{mA\xi}\left[h(p_{e_y} + p_{e_y}\sin^2 L + p_{e_x}\cos L \sin L)A_t - h\eta p_{e_x}A_n - (A_t^2 + A_n^2)\sin L\right] \quad \text{(C.35)}$$

$$\frac{dp_{i_x}}{dt} = -\frac{FhA_n}{mA\xi}[(e_x p_{e_y} - e_y p_{e_x})\sin L + i_x(p_{i_x}\cos L + p_{i_y}\sin L)] \quad \text{(C.36)}$$

$$\frac{dp_{i_y}}{dt} = -\frac{FhA_n}{mA\xi}[-(e_x p_{e_y} - e_y p_{e_x})\cos L + i_y(p_{i_x}\cos L + p_{i_y}\sin L)] \quad \text{(C.37)}$$

For m and p_m, the optimal equations of motion come from

$$\frac{dm}{dt} = \frac{\partial H}{\partial p_m} \quad \text{(C.38)}$$

$$= -\frac{F}{c} \quad \text{(C.39)}$$

$$\frac{dp_m}{dt} = -\frac{\partial H}{\partial m} \quad \text{(C.40)}$$

$$= \frac{FA}{m^2} \quad \text{(C.41)}$$

Bibliography

[1] Richard H. Battin. *An Introduction to the Mathematics and Methods of Astrodynamics, Revised Edition.* American Institute of Aeronautics and Astronautics, Inc., 1999.

[2] Leon P Gefert and Kurt J Hack. Low-thrust control law development for transfer from low earth orbits to high energy elliptical parking orbits. In Kathleen C Howell, Felix R Hoots, Bernard Kaufman, and K Terry Alfriend, editors, *Astrodynamics 1999*, Advances in the Astronautical Sciences, pages 1695–1712, Girdwood, Alaska, August 1999. Advances in the Astronautical Sciences, Univelt, Incorporated. AAS 99-410.

[3] A. L. Herman and D. B. Spencer. Optimal, low-thrust leo to geo/heo trajectories. In Kathleen C Howell, Felix R Hoots, Bernard Kaufman, and K Terry Alfriend, editors, *Astrodynamics 1999*, Advances in the Astronautical Sciences, pages 1663–1680, Girdwood, Alaska, August 1999. Advances in the Astronautical Sciences, Univelt, Incorporated. AAS 99-408.

[4] Mark R. Ilgen. A hybrid method for computing optimal low thrust otv trajectories. In John E. Cochran, Jr., Charles D. Edwards, Jr., Stephen J. Hoffman, and Richard Holdaway, editors, *Spaceflight Mechanics 1994*, Advances in the Astronautical Sciences, pages 941–958, Cocoa Beach, Florida, February 1994. Advances in the Astronautical Sciences, Univelt, Incorporated. AAS 94-129.

[5] M Scott Kimbrel. Optimization of electric propulsion orbit raising. Master's thesis, Massachusetts Institute of Technology, June 2002.

[6] M. S. Konstantinov. Optimization of low thrust transfer between noncomplanar elliptic orbits. In *International Astronautical Federation Conference 48th Turin*, Turin, Italy, October 1997. International Astronautical Federation. IAF-97-A.6.06.

[7] John E. Prussing. Optimal impulsive linear systems: Sufficient conditions and maximum number of impulses. In John E. Cochran, Jr., Charles D. Edwards, Jr., Stephen J. Hoffman, and Richard Holdaway, editors, *Spaceflight Mechanics 1994*, Advances in the Astronautical Sciences, pages 1015–1023, Cocoa Beach, Florida, February 1994. Advances in the Astronautical Sciences, Univelt, Incorporated. AAS 94-174.

[8] Vyacheslav Ptukhov. Optimal multirevolution transfers between non-coplanar elliptical orbits.

[9] Gregory J. Whiffen and Jon A. Sims. Application of a novel optimal control algorithm to low-thrust trajectory optimization. In Louis A. D'Amario, Lester L. Sackett, Daniel J. Scheeres, and Bobby G. Williams, editors, *Spaceflight Mechanics 2001*, Advances in the Astronautical Sciences, pages 1525–1540, Santa Barbara, California, February 2001. Advances in the Astronautical Sciences, Univelt, Incorporated. AAS 01-209.